



Technische Universität München



Elite Master Course

Theoretical and Mathematical Physics

MASTER'S THESIS

Making Use of Quantum Trajectories for Numerical Purposes

Leopold Kellers

October 12, 2017

Advisor: Dirk-André Deckert

Co-advisor: Ward Struyve

Abstract

For quantum systems involving many particles, numerically integrating the time-dependent Schrödinger equation on a stationary lattice is hard, because the amount of memory required for the wave function samples scales exponentially in the number of degrees of freedom. Special algorithms have been designed, which use Bohmian trajectories as a tool in various ways in order to work around this problem. One part of this thesis analyzes the limitations of approaches, which for a speedup exploit the possibility to do away with explicitly integrating the probability density redundantly contained in Wyatt's algorithm on an adaptive Bohmian grid. This is done by comparing their results to explicit solutions of the Schrödinger equation in simple one-dimensional scenarios. Another part benchmarks the recent mixed quantum–classical Bohmian method against the traditional mean field backreaction approach for a kind of interaction missing in previous work by applying both to the hydrogen atom in the Jaynes–Cummings model, within and beyond the rotating wave approximation. Last but not least, Bohmian trajectories can be employed to compute time of arrival statistics. This is demonstrated here within the context of a double slit scenario in an actual two-dimensional setting without restricting to plane waves, as is common in the literature. The setting is further extended by letting one of the slits close dynamically while the wave packet is still passing through in order to determine how the time of arrival statistics differ from a semiclassical geometric optics estimate in the near field.

Contents

1	Motivation and Outline	1
2	Introduction to Bohmian Trajectories	5
2.1	Equations and Theorems for Numerics with Trajectories	5
2.2	Select Features of Bohmian Trajectories	8
3	Bohmian Trajectories and Time of Arrival Statistics	13
3.1	Theory	14
3.2	A dynamic double slit setup	18
3.3	Conclusions	32
4	Employing Bohmian Trajectories in Quantum Numerics	35
4.1	Overview over Adaptive-Grid Methods	36
4.2	Discussion of Results	49
4.3	Conclusions	68
5	Employing Bohmian Trajectories in Semiclassical Numerics	71
5.1	The Backreaction Problem	72
5.2	Application to Different Toy Models	76
5.3	Conclusions	103
6	Summary, Concluding Remarks and Future Directions	107
	Appendix	113

1 Motivation and Outline

Since the early days of quantum mechanics, solving the time-dependent Schrödinger equation for several interacting particles has proven to be a difficult task. With only a handful of explicit solutions known, the majority of results had to be obtained from numerical treatment. These have greatly contributed to the understanding of quantum phenomena, particularly in the field of theoretical chemistry.

The common approach to studying the dynamics of such a wave function is discretizing it and its Hamiltonian on a grid representing configuration space and to evolve those sampled values while keeping the grid fixed. Numerical methods for computing the time evolution on the grid, most notably the Crank-Nicolson method [1] and the split-step method based on Fourier transformation [2], have been developed and are mature. However, when increasing the number of particles, this approach features a very inconvenient scaling behavior. For n particles in d dimensions, the total number of wave function samples \mathcal{N} grows exponentially in the number of degrees of freedom nd , i.e. $\mathcal{N} = N^{nd}$. In this expression, N is the number of grid points desired in each component of configuration space, which in is \mathbb{R}^{nd} or a subspace of it. Thus, the computational expense quickly grows out of hand. For example, with $N = 1000$ only, 9 particles in three-dimensional space already constitute the very large number of 10^{81} wave function samples, which is the same order of magnitude as the estimated number of nucleons in the observable universe. Today's computers require more than a single atom per memory cell, so none of them could even come close to being able to handle this. This is in stark contrast to the numerical treatment of classical dynamics, where the number of variables to keep track of scales linearly in the number of degrees of freedom. With help of an ordinary computer, said 27 degrees of freedom under Newtonian time evolution thus pose an easy challenge.

To make things worse, the static grid needs to cover all parts of configuration space where the wave function significantly differs from zero at least once during its evolution. Usually this means that some parts of the grid do not actually carry useful information all of the time. To solve differential equations numerically, adaptive stepsize has long been a useful and heavily used feature in numerical analysis. Based on an error estimate calculated at each integration step, the time step can be chosen such that given accuracy requirements remain satisfied. This allows to quickly step through less challenging phases of the integration process while performing more precise calculations when the integrated quantities do change rapidly and require more careful evaluation. Further expanding on this idea, it would be useful to also have a self-adapting grid for the integration which is no longer fixed, but at each time is dense where the wave function has large modulus and sparse in regions where it almost vanishes anyway without changing much. Then, although the exponential scaling in the number of particles would not be remedied directly, at least the parameter N in N^{nd} could be reduced, resulting in a significant improvement in situations with many degrees of freedom.

A large part of this thesis will be about demonstrating how Bohmian trajectories can be employed as a tool to achieve this goal. For that reason, chapter 2 will introduce the general concept of Bohmian trajectories to the reader. Chapter 3 then highlights some of the central properties of these trajectories in an illustrative example, a dynamic double slit setup. It is in fact the first numerical computation of Bohmian trajectories guided through an actual two-dimensional double slit by a non-plane wave function that the author is aware of. In the literature the double slit is usually presented in an essentially one-dimensional fashion, which gives rise to a common misconception that the interference pattern is absolutely stationary also for a localized multidimensional wave packet passing through the slits before hitting the screen. That chapter will not only point out how this is incorrect, but also demonstrate how Bohmian trajectories can be used to visualize time of arrival statistics in quantum mechanics.

Faced with the aforementioned scaling problem, around the turn of the millennium quantum chemist R. Wyatt came up with a new computational method featuring exactly the desired adaptive grid property [3]. After a surge of interest in the theoretical chemistry community, the literature has grown rich with applications of this method since. Using an ensemble of Bohmian trajectories as the grid, on which the wave function is sampled, this so-called quantum trajectory method is very efficient for computing long time dynamics of wave functions that fulfill certain requirements. Recently M. Hall, D.-A. Deckert and H. Wiseman [4] have proposed a computationally even more efficient method. Their approach describes the evolution of an ensemble of trajectories, which approximate the Bohmian ones and from which the wave function can then be reconstructed. These two approaches together with a new algorithm, which can be viewed as a hybrid between them, will be benchmarked for simple and explicitly solvable quantum systems in chapter 4. An analysis of the problems encountered in these approaches when a wave function features nodes and the applicability of the known strategies around them to the new methods will be discussed in that chapter, too.

Another way to reduce the required computational effort is to directly tackle the scaling problem by reducing the number of degrees of freedom to be expanded onto the grid. Sometimes it might be possible to solve part of the system analytically or to expand part of the wave function into a complete orthogonal set of basis states. In the latter case, one then has to solve a linear combination of Schrödinger equations, which can work well, but for example fails, when it is necessary to deal with a continuous spectrum.

Alternatively, in some physical situations it might be possible to reduce the number of quantum degrees of freedom by treating some as classical particles and only the remaining ones quantum. In this approach, called mixed quantum–classical dynamics, it is not a priori clear how to incorporate the influence of the quantum subsystem onto the classical part. The Ehrenfest method, also known as mean field method, is typically used to deal with this issue. It has some limitations though, which can be overcome by another approach, which also makes use of Bohmian trajectories. It has been proposed independently by O. Prezhdo and C. Brooksby [5] as well as E. Gindensperger, C. Meier and J. Beswick [6]. Previous work has shown advantages of the Bohmian trajectory based method in some scattering situations. First, this intrinsic advantage of the Bohmian approach will be confirmed in another example of scattering in chapter 5. Following that, a comparison of the quality of the results obtained from semiclassically treating the Jaynes-Cummings model as a real world example will be carried out.

Note that the field of integrating the Schrödinger equation is vast and there are quite a few more trajectory methods, which will not be treated in this thesis. These include B. Poirier's wave function-free/trajectories-only quantum mechanics [7] as well as the complex trajectory method [8] for fully quantum treatment. Examples in the mixed quantum–classical case are phase space methods based on the Wigner distribution [9] or surface hopping techniques [10]. In fact, only such methods that make use of Bohmian trajectories have been selected here in order to provide a coherent picture despite the already large number of separate concepts analyzed in this thesis.

2 Introduction to Bohmian Trajectories

The purpose of this section is to acquaint the reader with the concept and features of Bohmian trajectories. It is by no means an exhaustive account of the topic. Most of the attention will be paid to those parts, which are relevant for carrying out the numerics dealt with in the following chapters, restricting coverage of the theory's physical interpretation to the degree required for understanding the concept itself. To this end, the pragmatic presentation will follow the description given by Dürr and Teufel [11] which they call Bell's route. For additional information and discussion of the interpretation [12] or [13] could be consulted for example. Also, for simplicity only a d -dimensional quantum system consisting of n scalar, distinguishable particles will be covered here. A more general exposition and a more elaborate derivation from first principles can also be found in [11].

2.1 Equations and Theorems for Numerics with Trajectories

Let $\Omega \subseteq \mathbb{R}^{nd}$ be the relevant configuration space¹ for a self-adjoint Hamiltonian with potential $V : \Omega \rightarrow \mathbb{R}$ and particle masses m_1, \dots, m_n . Then, starting from the non-stationary Schrödinger equation

$$i\hbar \frac{\partial \psi}{\partial t}(\mathbf{q}, t) = - \sum_{i=1}^n \frac{\hbar^2}{2m_i} \Delta_i \psi(\mathbf{q}, t) + V(\mathbf{q})\psi(\mathbf{q}, t) \quad (2.1)$$

for a normalized wave function $\psi : \Omega \times \mathbb{R} \rightarrow \mathbb{C}$ and its complex conjugate counterpart

$$-i\hbar \frac{\partial \bar{\psi}}{\partial t}(\mathbf{q}, t) = - \sum_{i=1}^n \frac{\hbar^2}{2m_i} \Delta_i \bar{\psi}(\mathbf{q}, t) + V(\mathbf{q})\bar{\psi}(\mathbf{q}, t) \quad (2.2)$$

multiplied by $\bar{\psi}$ or ψ resp. and subtracting the latter from the former followed by using the product rule, the quantum flux equation

$$i\hbar \frac{\partial |\psi|^2}{\partial t} = - \sum_{i=1}^n \frac{\hbar^2}{2m_i} \nabla_i \cdot (\bar{\psi} \nabla_i \psi - \psi \nabla_i \bar{\psi}) \quad (2.3)$$

is easily derived. It is commonly written down in the form of the continuity equation

$$\frac{\partial \rho^\psi}{\partial t} + \nabla \cdot \mathbf{j}^\psi = 0 \quad (2.4)$$

¹E.g. the complement of the set of singularities of V .

2.1 Equations and Theorems for Numerics with Trajectories

using Born's rule for the probability density ρ^ψ

$$\rho^\psi = |\psi|^2 \quad (2.5)$$

and the expression for the quantum flux \mathbf{j}^ψ associated with ψ

$$j_i^\psi = \frac{\hbar}{2im_i} \left(\bar{\psi} \nabla_i \psi - \psi \nabla_i \bar{\psi} \right) = \frac{\hbar}{m_i} \Im \left(\bar{\psi} \nabla_i \psi \right). \quad (2.6)$$

On a subset of configuration space Ω such that ψ is differentiable and nonzero on this subset, the velocity vector field \mathbf{v}^ψ can be defined via

$$\nabla \cdot \mathbf{j}^\psi = \nabla \cdot \left(\frac{\mathbf{j}^\psi}{|\psi|^2} |\psi|^2 \right) =: \nabla \cdot \left(\mathbf{v}^\psi \rho^\psi \right). \quad (2.7)$$

The continuity equation (2.4) together with (2.7) states that the probability density gets transported along the integral curves of the flow

$$\mathbf{v}^\psi(\mathbf{q}, t) = \frac{\mathbf{j}^\psi(\mathbf{q}, t)}{|\psi(\mathbf{q}, t)|^2} = \hbar m^{-1} \Im \frac{\nabla \psi}{\psi}(\mathbf{q}, t), \quad (2.8)$$

where the inverse of the mass matrix m appears in the last expression.

So far, neither Bohmian particles nor trajectories have shown up. Introducing them is the next step. To this end consider a collection of coordinates $\mathbf{x} := (\mathbf{x}_1, \dots, \mathbf{x}_n) \in \Omega$ and call it the *configuration* of the n -particle system. A Bohmian particle is exactly this, a point particle described by its position $\mathbf{x}_i \in \mathbb{R}^d$. *Only* by its position. Other properties that one might assign to a particle, charge for example, are just parameters to the Schrödinger equation (2.1) and thus impact the time evolution of ψ . The field in equation (2.8) is called the guiding field, i.e. the particles are transported by the flow of the velocity vector field \mathbf{v}^ψ :

$$\frac{d\mathbf{x}}{dt} = \mathbf{v}^\psi(\mathbf{x}, t). \quad (2.9)$$

This is called the guiding equation and sometimes also the Bohmian² law of motion. It is a first order differential equation and thus (given initial positions \mathbf{x}_0 at a time t_0) completely determines the time evolution of the particle ensemble under the evolution of ψ . So at any time t , the sole knowledge of $\psi(t)$ and $\mathbf{x}(t)$ suffices to describe the state of the system. This explains why \mathbf{x} is also called *world*. Similarly, $\mathbf{x}_t := (t \mapsto \mathbf{x}(t))_{t \in [t_0, \infty]}$, a solution of both (2.1) and (2.9) also carries the name *world trajectory*. It is a single trajectory on configuration space containing the trajectories of all particles. In particular, since the law of motion is first order, different solutions can never cross in configuration space. This is quite different from the situation in Newtonian mechanics, where trajectories can cross in configuration space and phase space represents all possible states that the n -particle system can be in at a specific point in time.

²In the modern sense. Originally it has been introduced by L. de Broglie, however.

2. Introduction to Bohmian Trajectories

There are two important theorems to be summarized. The first one is, that subject to some general conditions, unique solutions ψ_t and \mathbf{x}_t exist globally almost always [14]. This means that given an initial condition ψ_0 at time t_0 , the set of initial configurations, for which the world trajectory runs into nodes, reaches infinity in finite time or crosses the trajectory of another initial configuration, has measure zero with respect to the probability distribution (2.5). On top of that, a fundamental property called *equivariance* holds, which states that for an ensemble of initial configurations distributed according to $|\psi_0|^2$, the ensemble of configurations at time $t > t_0$ will remain distributed according to $|\psi_t|^2$ when from t_0 to t the wave function evolves under the Schrödinger equation and the trajectories are obtained from the Bohmian guiding law (2.9). A concise proof of the latter theorem can be found in the appendix of [15].

It is worth pointing out that the interpretation of Bohmian mechanics works in the following way. An actual physical quantum system with initial wave function ψ_0 at t_0 will be in some initial configuration \mathbf{x}_0 , but the exact values of \mathbf{x}_0 are unknown. The particles, of which the system consists, will travel along their particle trajectories, which are projections of \mathbf{x}_t onto the particle's subspace. Upon a measurement, one or more particle's locations can be revealed. The theory is completely deterministic, so that repeating the same experiment with the same initial configuration would yield identical measurement results. It is however not possible to create identical setups with the same initial configuration on purpose, since, as already stated, the exact initial configuration is not known. The best that can be done is to prepare copies of a quantum system in the lab, such that for a large number of instances of this system the initial configurations \mathbf{x}_0 of the particle ensemble are distributed according to ρ^{ψ_0} among the instances.

These copies will be called *identical initial setups*. Compatibility with textbook quantum mechanics is established in the following way. Prepare a large number of these identical initial setups and carry out the same measurement again and again at the same time t for precisely the same particle(s). Then, by equivariance the distribution of measurement results approaches the squared modulus of the appropriate projection of the probability density at t in agreement with Copenhagen style quantum mechanics. This is how the probabilistic nature of quantum theory is realized in Bohmian mechanics. It arises from the amount of knowledge about the initial state of the particle ensemble being limited to the information contained in the initial wave function.

As a side note, making a measurement simply reveals the past of Bohmian particles and does not collapse the wave function. There is no measurement problem in Bohmian mechanics. It is necessary to treat the measurement apparatus as a quantum system though, which becomes entangled with the system to be measured. See for example [12] or [13] for details.

From the Bohmian point of view, out of all the possible Bohmian trajectories, there is ultimately just a single one realized in the universe and guided by the universal wave function, hence the name world trajectory. For numerical purposes however, *ensembles of world trajectories* are employed to compute the evolution of a quantum (sub-)system instead. The numerical techniques to obtain the wave function time evolution presented in this thesis do not at all depend on the interpretation of Bohmian mechanics and some are even outright incompatible with it. Only for the subject of computing time of arrival statistics in chapter 3 the Bohmian interpreta-

2.2 Select Features of Bohmian Trajectories

tion will be fundamental, since that quantity cannot easily be obtained from Copenhagen style quantum theory. Bohmian mechanics is of advantage for this purpose since at the end of the day, it boils down to taking the concept of quantum particles seriously. This provides a physical interpretation of the quantum flux \mathbf{j}^ψ associated to each wave function ψ as the actual flux of actual particles. That in turn makes it possible to provide an answer to the question “*When will the detector click?*”, despite there not being any positive operator valued measure to extract information about the time of arrival of a particle at a detector from. The latter is the reason why the question is anything but trivial in Copenhagen style quantum mechanics. Time of arrival at the detector is nonetheless an important quantity and can in principle be measured in the lab without doubt. A more in-depth theoretical treatment of this issue together with the pitfalls that one can run into will be deferred to chapter 3.

Now the main ingredients needed to carry out numerical calculations using Bohmian trajectories in the scope of this thesis have been put together. Before continuing with some properties to aid understanding the nature of Bohmian trajectories in the next section, it should be mentioned, that Bohmian mechanics has been seen from an alternative point of view for a large part of history.

By differentiating the guiding equation (2.9) with respect to t and plugging the Schrödinger equations (2.1) and (2.2) into the resulting expressions followed by some calculus to rearrange the differential operators, it is possible to transform the Bohmian law of motion into a classical looking form, in components:

$$m_i \frac{d^2}{dt^2} x_i = -\nabla_i V - \nabla_i Q^\psi. \quad (2.10)$$

The last symbol represents what is called the *quantum potential*

$$Q^\psi = - \sum_{j=1}^n \frac{\hbar^2}{2m_j} \frac{\Delta_j |\psi|}{|\psi|}. \quad (2.11)$$

Its negative gradient is often referred to as *quantum force*. This formulation of Bohmian mechanics has traditionally been derived via an analogy to Hamilton-Jacobi theory. Despite equation (2.10) looking similar to Newtonian mechanics, it describes a type of mechanics very different from Newtonian motion. Also, there is only a single initial parameter to this equation, which is \mathbf{x}_0 , whereas the initial velocity is given by the initial wave function. Despite these caveats, this picture gives a nice intuition about the Bohmian trajectories converging towards classical ones in the limit where $\frac{\hbar^2}{m}$ becomes small and the contribution of the quantum force becomes negligible. Moreover, the concept of the quantum potential will be fundamental to the adaptive grid algorithms in chapter 4.

2.2 Select Features of Bohmian Trajectories

The first visualization of Bohmian trajectories was given in 1979 by Philippidis, Dewdney and Hiley [16], who calculated a set of possible trajectories of a Bohmian particle for what they call

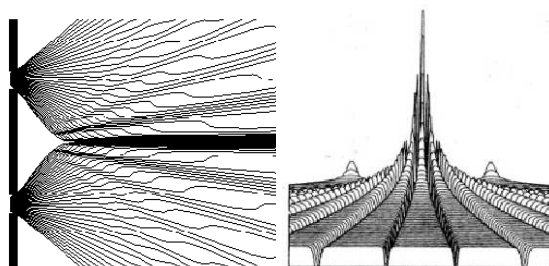


Figure 2.1: Philippidis', Dewdney's and Hiley's illustration of Bohmian mechanics in a double slit setup. Left: an ensemble of Bohmian trajectories, taken from [17]. Right: corresponding quantum potential, directly from [16] with kind permission of Società Italiana di Fisica.

the usual double slit setup from an explicitly known wave function. Their trajectory plot has widely been reproduced in the literature, and is also given in figure 2.1.

Their choice of wave function does not exactly describe a double slit setup in the way that one would imagine it to be built in the lab, but an approximation based on a proposal of Feynman and Hibbs [18]. One can think of it as a pair of slits with Gaussian shape through which a single electron, represented by a plane wave, passes. One could consider figure 2.1 as a stationary two-dimensional situation with spatial coordinates on both axes or equivalently as a one-dimensional picture with time labeling the abscissa. Both points of view are possible because for a plane wave time and spatial coordinate are linearly dependent and any global phase factor does not affect the Bohmian dynamics since it simply cancels in equation (2.6). Note that in any case the trajectories of the electron are precisely the world trajectories in configuration space. Thus the trajectory along which the particle travels cannot cross any other one of the possible trajectories. In particular, this implies that no trajectory can pass the axis of symmetry.

Trajectories starting at one of the slits are guided by the Bohmian law (2.9) in such a way that after initially spreading outward from each slit like a wavelet, an interference pattern emerges with the majority ending up in the center, sided by several maxima and minima. The plot of the quantum potential Q^ψ on the right hand side of figure 2.1 helps visualize the dynamics. Trajectories passing through regions, where the wave function is tiny, do so strongly accelerated, which is represented by grooves in Q^ψ , c.f. the “kinks” in the trajectories. On the other hand the initial wave function, which consists of two superposed Gaussians, creates potential bumps that push the trajectories outward at the beginning.

There is one thing to be aware of when looking at figure 2.1, though: a uniform distribution over each slit has been chosen as initial condition. Denote this distribution as $\tilde{\rho}(t=0)$ and recall $\rho^\psi = |\psi|^2$. Since the initial wave function consists of two superposed Gaussians, the principle of equivariance does not apply for this uniform distribution. So neither any intermediate nor the final distribution $\tilde{\rho}(t)$ match $\rho^\psi(t)$, regardless of how large t is chosen³. Their ratio however

³Typically there is however a relaxation of $\tilde{\rho}$ towards ρ^ψ on a coarse grained level for sufficiently complicated quantum systems. See [19] for details on the sense in which this is to be understood.

2.2 Select Features of Bohmian Trajectories

is preserved under Bohmian time evolution,

$$\frac{d}{dt} \frac{\tilde{\rho}}{\rho^\psi} = 0, \quad (2.12)$$

which enabled the authors of [16] to compare their data to experimental data collected by Jönsson [20] and report “agreement”⁴.

These caveats have led to considerable confusion in the past. For example, it has been claimed by P. Chen and H. Kleinert, that Bohmian trajectories were only approximately describing the laws by which nature behaves [21] and that the predictions of Bohmian mechanics were not equivalent to those of Copenhagen style quantum mechanics. To support their claim, they presented exactly figure 2.1 and stated that it was in contradiction to the distribution expected by Young’s formula in the Fraunhofer limit by counting the number of trajectories ending in the side maxima⁵ without accounting for equation (2.12). The aforementioned plane wave and Gaussian slit approximations were also neglected. Plots of numerical calculations with ρ^ψ -distributed initial conditions can be found in Holland’s book [12]. For the remainder of this thesis, within numerical limits all initial conditions will always be $|\psi|^2$ -distributed.

For the very wave function discussed so far, the velocity field is stationary. This is generally not the case. For example, chapter 3 will present a different double slit simulation with a wave packet that is an actual normalizable, two-dimensional Gaussian. There are however many quantum systems, for which the velocity field is not just constant in time, but actually zero. An example for the latter are ground states in bound potentials⁶. It might be surprising at first sight that an electron in the ground state (n=1, aka. 1s) of a Hydrogen atom should remain at place without moving at all. This is simply a consequence of the Bohmian law of motion, which creates dynamics that are very different from the intuition obtained from the study of Newtonian mechanics.

Furthermore, the guiding law (2.9) does not even constitute a unique choice for generating suitable trajectories [22]. In fact, it is possible to add upon the quantum flux \mathbf{j} in equation (2.8) another quantity $\tilde{\mathbf{j}}$ for which

$$\nabla \cdot \tilde{\mathbf{j}} = 0 \quad (2.13)$$

holds. Then the continuity equation (2.4) is still fulfilled. Letting $\tilde{\mathbf{j}}$ be a suitably crafted curl term can result in sets of trajectories that differ from the genuine Bohmian ones but still remain invariant under Galilei transformations. For the course of this thesis only the “simplest”⁷ kind of trajectories, i.e. the Bohmian ones will be dealt with.

It is already possible to have different Bohmian trajectories for the same quantum system depending on the choice of the orthonormal basis to work in. To see this, consider for example

⁴Unfortunately without specifying any precise details.

⁵For a plane wave hitting a screen on the right end of the left half of fig. 2.1, the intensity of the interference pattern is the projection of \mathbf{j}^ψ onto the direction orthogonal to the screen. In the plane wave scenario under consideration here however, this turns out to be proportional to $|\psi|^2$. See chapter 3 for more details.

⁶Ultimately this follows from the fact that it is always possible to find a positive ground state wave function, i.e. $\arg(\psi) = 0$ such that the imaginary part in equation (2.9) vanishes

⁷See [22] for the large amount of consideration required when designing a suitable $\tilde{\mathbf{j}}$.

2. Introduction to Bohmian Trajectories

the first excited state (2p, i.e. $n = 1, l = 1, m = 0$ or ± 1) of the hydrogen atom⁸. The orthonormal basis in which all three eigenfunctions ϕ_{11m} are real is popular in chemistry. The Bohmian particle in the field of the nucleus is thus stationary for all m , simply distributed according to $|\phi_{11m}|^2$ among different atoms, which, depending on the value of m , is one the three orthogonal dumbbell-shaped orbitals familiar from pictures in chemistry textbooks. Physicists however usually describe the hydrogen atom in terms of a complex basis where $\phi_{11m} \propto e^{im\varphi}$. For $m = 0$ nothing changes at all, but for $m = 1$ the shape is no longer dumbbell-like and the imaginary part in the Bohmian guiding law does not vanish, giving rise to a circular motion around the z-axis. For $m = -1$, the trajectories go the other way round. One simply arrives at the real eigenbasis by taking the superposition

$$(\phi_{111}, \phi_{110}, \phi_{11-1}) \mapsto \left(\frac{1}{\sqrt{2i}}(\phi_{111} + \phi_{11-1}), \phi_{110}, \frac{1}{\sqrt{2}}(\phi_{111} - \phi_{11-1}) \right), \quad (2.14)$$

i.e. the circular motions precisely cancel. Both choices of orthonormal basis set are equally satisfactory to work in⁹ [24], yet they display different sets of Bohmian trajectories.

Central to the birth of quantum mechanics was the question why the electron does not radiate off energy and spiral into the atom's nucleus. Sometimes this concern is also raised in the context of Bohmian mechanics [21]. A humorous reply would be that if nothing moves, nothing can radiate. But what about the absence of radiation damping for circular motion as in the complex $\phi_{11\pm 1}$ orbitals of hydrogen? The correct answer is of course what has already been said before, but because it is so important¹⁰ and frequently misunderstood, the actual reason will be stressed again to conclude this chapter. In the theory of Bohmian mechanics, particles themselves are not equipped with properties like charge (or spin). These only enter as parameters to the Hamiltonian in the Schrödinger equation, whose solution gives rise to the trajectories. Bohmian particles are passive in the sense that they do not influence the time evolution of the wave function. The trajectories will approach classical trajectories in regimes where classical mechanics is a good approximation [27, 11]. In general, the dynamics arising from the guiding equation (2.9) can be highly nonclassical.

⁸For now only consider the model system usually found in introductory textbooks to quantum mechanics of an electron in an external Coulomb potential, where the electron is assumed to be a spinless particle. To treat the electron as a spin- $\frac{1}{2}$ particle requires to add the Pauli flux to equation (2.8), which results in no states being stationary any longer [23].

⁹For numerical purposes, one might be more advantageous than the other though, depending on the precise target.

¹⁰In particular since this goes hand in hand with the explicit nonlocality contained in Bohmian theory, which has also caused considerable confusion in the past [25, 26].

3 Bohmian Trajectories and Time of Arrival Statistics

Bohmian mechanics makes the same predictions as Copenhagen style nonrelativistic quantum mechanics in the domain where the latter is unambiguous, testable and confirmed. But in his book, P. Holland raised the question whether that domain might be enlarged by Bohmian mechanics [12]. As an example of a fringe area of the orthodox theory, but where the Bohmian formalism is sharply formulated, he quoted the treatment of time in both theories. From the Bohmian point of view, it is totally clear how much time an individual particle spends within a certain region of space.

This comes in useful to answer a question put forward to the author and his advisors by H. Weinfurter at a meeting in fall 2016. With the usual “double slit” trajectory picture, the left part of fig. 2.1, in mind, the question was

Consider a double slit setup through which Bohmian particles pass and put a detector into the position of a certain side minimum. Then close the slit which is closer to the detector. At what time will a particle with a trajectory through the other slit (which remains open) be detected by this detector for the first time?

The question by itself is ill-posed in the way it is stated above, but it did spark interest to investigate how the time statistics of detector clicks in such a case would look like. Additional motivation arose from the sparseness of the literature regarding a numerical investigation of Bohmian trajectories in a double slit beyond the very simple case presented in previously in chapter 2. In particular, no works that treat the double slit experiment both from a Bohmian viewpoint and as an actual multi-dimensional system, be it a static slit arrangement or a dynamical one as described above, with localized wave packets instead of a plane wave is known to the author. Some research can be found in the literature however, which deals with interference arising from opening and closing a *single* slit as a function of time, referred to as temporal or time double slit. Also experiments on this topic have been carried out, see [28] and references therein. These slit arrangements do not a priori have a lot in common with the topic of this chapter.

This chapter deals with the question “When will the detector click?” and in the spirit of the Bohmian interpretation, the probability rate of detector clicks will be called *time of arrival statistics*. The theoretical framework will be implemented for a two-dimensional double slit setup, investigating the dynamical interference pattern of a single, spin-less electron passing through a set of Gaussian slits, which are initially open but can be closed dynamically. With the electron initially being described by a two-dimensional Gaussian wave packet, its time of arrival statistics at a screen on the opposite side of the slits and suitable aspects of the time

3.1 Theory

dependence of trajectories through each slit will illustrate what is going on in the Bohmian picture in the second half of this chapter.

In textbook quantum mechanics each observable quantity is intimately related to a self-adjoint operator. In that sense, time cannot be treated as an observable, because its conjugate, the Hamilton operator must be bounded from below as was already known to Pauli [29]. Ultimately, time only enters quantum theory as a classical parameter labeling the unitary evolution of the wave function, but there is no such thing as a “time operator”. So it is easy to predict the distribution of detector clicks over an array of detectors at a fixed time t , which is simply $|\psi(t)|^2$, but it is unclear how to obtain the detection statistics of a single, stationary detector over time. This is different with Bohmian mechanics, where the probability current is taken seriously and the time of arrival probability rate can be obtained from it. How this is done will be explained in the following section, followed by a numerical implementation of a simulation of the aforementioned dynamical double slit and a discussion of the resulting dynamics. So unlike the two chapters following this one, Bohmian mechanics is not turned into a tool for numeric calculations but uses a tool that Bohmian mechanics provides in order to illustrate the essence of Bohmian theory. Because following the Bohmian trajectories will turn out to be fundamental for the principles at work, it is still reasonable to call it a trajectory method.

3.1 Theory

Using clocks, all kinds of characteristic times can be measured. The quantity of interest in this chapter is the *time of arrival* of a quantum particle at a detector. Imagine some time-of-flight measurement, i.e. an experimental setup in a laboratory where particles are shot at the detector from a source with known characteristics, passing through some (or no) obstacles placed in between on their way. So prepare each quantum particle in a certain initial state and set a stopwatch to zero. At what time will the detector click¹? Of course, the stopwatch will show different readings every time the experiment is repeated. But how can the statistical distribution of detector clicks, the *time of arrival distribution* be calculated in quantum mechanics?

In the far-field, which is easily accessible to experiments, a semiclassical analysis based on the momentum operator can give sufficiently good approximate answers. But it would be unsatisfactory to restrict oneself to such regimes, effectively denying the possibility of developing more sophisticated detectors probing the near-field. Of course, the interaction of the particle to be measured with the measurement apparatus, for example an electron hitting a fluorescent or photographic screen, needs to be described quantum-mechanically in principle. However, depending on how complicated the measurement apparatus is, this might not be possible and, as will be shown, need not even be necessary.

Usually measurable quantities in quantum mechanics are described by positive operator valued measures. But one that gives the probability rate of the screen being hit by an electron, aka. its time of arrival statistics, does not exist [30]. So the statistics must be obtained in another way. It is possible to see how this works by following the analysis of N. Vona [30, 31, 32]. For the

¹Or, depending on the type of detector, signal in any other way that a detection event happened.

3. Bohmian Trajectories and Time of Arrival Statistics

course of discussion here, it is sufficient to think of the detector as being said screen, subject to some idealizations, thin with respect to the wave function, and of such shape that it divides configuration space into disjoint regions. The detector may completely surround the electron source or be infinitely large to fulfill that requirement. Call \mathcal{G} the region that contains the particle initially and on the region's boundary $\partial\mathcal{G}$ denote an infinitesimal area element by $d\mathbf{S}$ (which points away from the direction the electron is expected to arrive, orthogonally to the detector area). One fundamental assumption is, that when the particle leaves \mathcal{G} , it will be detected as some bright spot on $\partial\mathcal{G}$ with certainty, i.e. the idealized detector is considered to be of *hard* type². The other one is that the particle's wave function ψ vanishes outside of \mathcal{G} at initial time t_0 ³. Then the usual line of argument is that when "looking" where the particle is at time t , it will be found within \mathcal{G} with probability $\int_{\mathcal{G}} |\psi(\mathbf{q}, t)|^2 d\mathbf{q}$. Its derivative with respect to time gives the detection probability rate $\pi^\psi(t)$. Thus the probability of a detection event anywhere on the detector between t and $t + dt$ reads

$$\pi^\psi(t)dt = -\frac{d}{dt} \left(\int_{\mathcal{G}} |\psi(\mathbf{q}, t)|^2 d\mathbf{x} \right) dt = \left(\int_{\partial\mathcal{G}} \mathbf{j}^\psi(\mathbf{q}, t) \cdot d\mathbf{S} \right) dt \quad (3.1)$$

where the last step follows directly from the continuity equation and the fundamental theorem of calculus. Of course, if only the detection probability rate of some part of the detector is of interest, then the integration over $\partial\mathcal{G}$ can be restricted to that part.

There is a problem with interpreting this equation as giving the detection probability. Integration of the probability rate with respect to time should yield a monotonously increasing function, hence the right hand side must always be positive. This is called the *current positivity condition* [35]

$$\forall t > t_0 \text{ and } \forall \mathbf{q} \in \partial\mathcal{G} : \mathbf{j}^\psi(\mathbf{q}, t) \cdot d\mathbf{S} > 0. \quad (3.2)$$

It turns out that this is a pretty strong restriction of generality though, rendering the whole ansatz too naïve. Figure 3.1 gives a very simple example of the time evolution of flow lines of the flux for a superposition of two one-dimensional Gaussians for which the current positivity condition is violated. In a way, it looks similar to figure 2.1 in principle, but here the parameters of the initial Gaussians have been chosen purposefully to explicitly demonstrate forward- and backward-crossing of a detector. The detector simply is a dot in this case of course, the yellow line indicates that it remains at its place over time.

In particular, figure 3.1, in which $\langle \hat{p} \rangle_\psi = 0$ holds at all times, demonstrates that having a non-negative expectation value of the momentum operator does not suffice to guarantee $\mathbf{j}^\psi \cdot d\mathbf{S} \geq 0$. In fact, it is possible to construct examples of superposed, fast-traveling Gaussians with only positive momentum in the sense that the Fourier transform of the wave function is ridiculously small for negative momenta, $\tilde{\psi}(p \leq 0) \approx 0$, but still featuring backflow [32]. So equation (3.1) only holds for a subset of all possible wave functions, and even simple superpositions of freely evolving Gaussians need not be contained in this set.

²This actually opens a whole can of worms and requires the detector to be absorbing on its surface $\partial\mathcal{G}$. It will also alter the wave function time evolution in a certain way, but this will be assumed to be negligible here. See a recent prescription of R. Tumulka [33] for one way of dealing with this issue.

³It is sufficient for the scope of this thesis to simplify the problem in this way. It is not a general requirement [34].

3.1 Theory

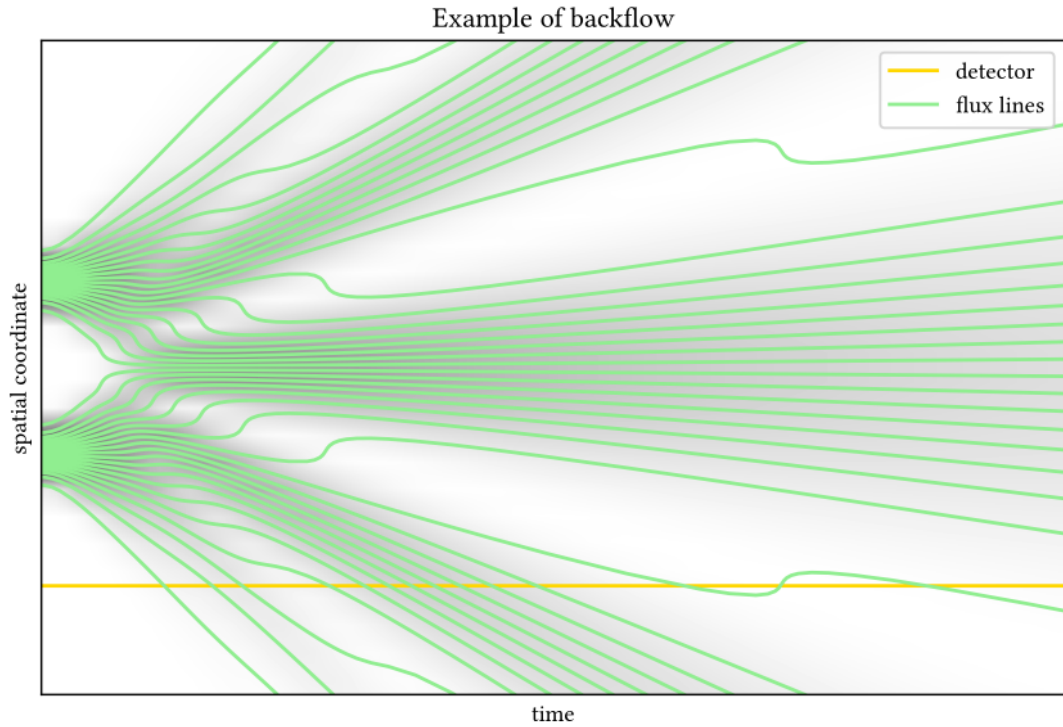


Figure 3.1: A $|\psi|^2$ -distributed set of flow lines (aka. Bohmian trajectories) displaying backflow, i.e. the flux \mathbf{j}^ψ through the detector is not positive at all times. Background shading $\propto |\psi|^2$. Wave function parameters same as in [30].

So how to deal with this problem? The Bohmian interpretation offers a way out. Recalling that the Bohmian trajectories are precisely given by the flow of the quantum flux, figure 3.1 can also be described using Bohmian language. The interpretation is straightforward then: in any physical realization there will be one Bohmian particle that follows one of the flow lines. Which one it is, is of course uncertain, and in particular it does not need to be one from the sample set in the plot but can also be any of the not depicted ones in between or, less likely, outside those.

An implicit assumption so far has been, that the measurement device, e.g. the aforementioned screen, does not interact in a long-range fashion with the wave function guiding the particle to be measured. Only when the particle ultimately arrives at the screen, the time evolution of the wave function will somehow be altered in the course of the measurement process. For the pathological trajectory in figure 3.1 this implies that the prediction of a second and third crossing of the detector is unlikely to be correct. One might even argue that it is pointless to talk about the dynamics after the first detector crossing, because the approximation of neglecting the measurement devices' presence and quantum nature breaks down. Recall that another assumption was that the detector will register the particle arriving on it with certainty, which

3. Bohmian Trajectories and Time of Arrival Statistics

requires the particle to be absorbed by the idealized hard detector⁴ [33]. This constitutes a rabbit hole that one can go down quite deep into but for the scope of this thesis these intricacies will not be covered. The above motivates to only consider the *time of first passage*. It can be described by the *truncated current* through the detector

$$\tilde{\mathbf{j}}^\psi(\mathbf{q}, t) = \begin{cases} \mathbf{j}^\psi(\mathbf{q}, t) & \text{if } \mathbf{q} \in \partial\mathcal{G} \text{ and } (\mathbf{q}, t) \text{ is a first exit from } \mathcal{G} \\ 0 & \text{otherwise} \end{cases}. \quad (3.3)$$

This is a quantity that has no respective counterpart in Copenhagen style quantum theory. To compute it in general situations, there is no way round integrating the time evolution of the flow lines, which need to be interpreted as Bohmian trajectories to make sense of the construction.

To obtain an expression for a time of arrival probability rate $\tilde{\pi}^\psi$ that works for any wave function ψ , substitute \mathbf{j}^ψ by $\tilde{\mathbf{j}}^\psi$ in equation (3.1) and recall that the setup was designed to be such that the particle's first arrival at the detector can never happen coming from the wrong direction. It is possible to define the truncated current without some of the simplifying restrictions applied here [34], but for the scope of this thesis that is not going to be needed. Finally, the probability $P_{\mathcal{D}}$ that a detection event on the area $\mathcal{D} \subseteq \partial\mathcal{G}$ occurs within the time interval $[t_1; t_2]$ can be computed by integrating over the probability rate

$$P_{\mathcal{D}}([t_1; t_2]) = \int_{t_1}^{t_2} \underbrace{\int_{\mathcal{D}} \tilde{\mathbf{j}}^\psi(\mathbf{q}, t) \cdot d\mathbf{S}}_{:= \tilde{\pi}^\psi} dt, \quad (3.4)$$

which is to be interpreted as only the first time a Bohmian particle comes into contact with the whole detector being of relevance.

So the upshot is that in Bohmian mechanics it is always possible to compute the time of arrival statistics. This works without referring to a positive operator valued measure. If the wave function is sufficiently nice, i.e. the current positivity condition (3.2) is fulfilled, then the quantity sought after is simply the quantum flux and in this case there is no need at all to invoke Bohmian mechanics – in that case textbook quantum mechanics perfectly works with equation (3.1). On the other hand though, if the wave function gives rise to a probability current that displays backflow through the detector, the situation is not that simple any more. In the Bohmian interpretation it is then still possible to refer to the time of first passage, which is given by the truncated current, while in Copenhagen style quantum mechanics it remains unclear how to deal with this situation. It is important to realize that the momentum of a particle as the expectation value of a quantum measurement outcome is conceptually different from the change in position of a Bohmian particle moving along the flow lines. The trajectories of Bohmian particles should hence not directly be associated with particle momentum. Only in the semiclassical limit it is that both notions happen to agree and as such, positive particle

⁴It will also change the Bohmian trajectories at least in the vicinity of the detector, but here it will be assumed that the amount is negligible.

3.2 A dynamic double slit setup

momentum does not suffice to guarantee the absence of backflow. A final note to keep in mind is that the Bohmian interpretation merely provides a computational tool here, that can provide an approximate answer to the question “When will the detector (figuratively) click?”. A fundamentally correct analysis would of course require the specification of the precise interaction between particle and measurement device and a fully quantum treatment of the latter, completely bypassing the backflow problem.

3.2 A dynamic double slit setup

Now it is time to return to the question that was formulated at the beginning of this chapter. The picture to have in mind is a double slit experiment, where a stream of electrons continuously passes from a source through the slits, producing an interference pattern with a main maximum in the middle and an alternating series of minima and maxima alongside on a screen, as usual. In particular, look closely at one of the minima of the interference pattern. At time t_0 , the one slit which is closer to this minimum is closed, so from now on particles can only pass through the opposite slit and the interference pattern changes. At what time can a particle that has passed through this leftover slit be detected in the previous minimum for the first time?

Of course, it is not possible to discern between a particle arriving through the leftover slit from one that had already slipped through the closing slit before it was closed and in the framework of Copenhagen style quantum theory this is a pointless question to deal with. One could rely on a semiclassical estimate based on the expected momentum of the incoming particle being deflected towards where it ultimately shows up in a measurement on the screen. But the question can be answered in the context of Bohmian mechanics, where each particle follows a distinct trajectory passing through one of the slits before arriving at the screen. Hence it is possible to compare the time of arrival statistics from Bohmian mechanics to the semiclassical estimate and that is what the remainder of this chapter is ultimately about.

Before jumping straight into the numerical investigation, a bit of simplification is needed, because as mentioned in the introduction already, it is hard to deal with high-dimensional configuration space when solving the Schrödinger equation. One helpful assumption is that the electronic current coming out of the source can be described by a product wave function of unentangled electrons, for example when the current is so low that at all times there is at most one electron expected to be between source and screen. It then suffices to restrict oneself to a single electron wave function and interference of the electron “only with itself”. Also when the slits in the lab are considered to be of significant length in one direction, the system can be treated as essentially two-dimensional and this will also be done. Lastly, only the case where the slit will be closed at the time when half of the wave packet representing the electron, a two-dimensional Gaussian in this case, has passed through the slits will be looked at. Then the semiclassical time of flight estimate should give the most accurate prediction. To compute the Bohmian time of arrival statistics to compare to the semiclassical prediction it seems to be reasonable to obtain the former from the truncated current of equation (3.3), because it is not a priori clear whether or not backflow might occur at the screen after the slit closes.

3. Bohmian Trajectories and Time of Arrival Statistics

A final word of warning should be that this would be a tremendously difficult experiment to perform [36]. In particular it is not ideal as a setup to experimentally check whether or not the truncated current produces the correct time of arrival statistics observed in nature. Other experiments have been proposed [32] which are better suited to test whether or not this Bohmian tool yields accurate predictions, but at the time of writing no one has been able to perform one yet. Here the main objective is to build intuition about what is going on from a Bohmian point of view in the simplified situation described above.

3.2.1 Implementation

Unlike the following chapters, which make use of Bohmian concepts for numerical computations of Schrödinger dynamics itself, the integration of the wave function time evolution in this chapter is carried out in a more traditional manner. Since there is no backreaction from the Bohmian particles, the velocity field can afterwards be derived from the wave function via equation (2.8) to obtain the trajectories in a second step. Integration of the Schrödinger equation requires solving a partial differential equation in principle. But discretizing the wave function and potential on a grid $\Lambda_{N_1 N_2} \subset [x_1^1; x_1^{N_1};] \times [x_2^1; x_2^{N_2};]$ of $N_1 \times N_2$ grid points with spacing $\Delta x_{1,2}$ between them,

$$\Lambda_{N_1 N_2} := \{(x_1^1 + i\Delta x_1; x_2^1 + j\Delta x_2)\}, \quad (3.5)$$

where $0 \leq i < N_1; 0 \leq j < N_2$, one can arrive at a set of quantities $\{\psi^{ij}\}$ without explicit spatial dependence. By using the finite difference expressions

$$\begin{aligned} \tilde{\nabla}_1 \psi^{ij}(t) &= \frac{\psi^{(i+1)j}(t) - \psi^{(i-1)j}(t)}{\Delta x_1} \\ \tilde{\nabla}_2 \psi^{ij}(t) &= \frac{\psi^{i(j+1)}(t) - \psi^{i(j-1)}(t)}{\Delta x_2}, \end{aligned} \quad (3.6)$$

to discretize the Laplacian $\tilde{\Delta} = \tilde{\nabla}^2$, the problem can be transformed into a coupled set of ordinary differential equations

$$\frac{d}{dt} \psi^{ij}(t) = -i \left(-\frac{1}{2} \tilde{\Delta} \psi^{ij}(t) + V^{ij}(t) \psi^{ij}(t) \right). \quad (3.7)$$

In these equations and from now on for the remainder of this thesis, all quantities and equations are given in (Hartree) atomic units where $\hbar = m_e = 1$ (and $e = 1$ and $\epsilon_0 = 4\pi$) for more concise expressions.

A commonly used algorithm for obtaining the wave function Schrödinger dynamics on a grid is the Crank-Nicolson method. Being a combination of the forward and backward Euler methods, it is an implicit scheme and thus a band-matrix needs to be inverted at each integration step, see e.g. [1]. In one dimension, that band-matrix is tridiagonal and an efficient⁵ inversion

⁵ $\mathcal{O}(N)$, i.e. the run time scales linearly in the number of grid points.

3.2 A dynamic double slit setup

algorithm exists. This feature and the fact that the algorithm's time evolution preserves the wave function's L^2 -norm are probably the reasons why the algorithm is so popular. But because the dynamic double slit simulation involves an explicitly time dependent Hamiltonian and in two dimensions the band-matrix is not invertible in the aforementioned efficient way, this algorithm's advantages cannot be exploited here.

Instead, it turns out to be totally sufficient to directly integrate equation (3.7) with a Runge–Kutta method, in particular the Dormand–Prince flavored one DOP853 [37]. Runge–Kutta integrators are a tough subject on their own and a detailed introduction to how they work is not in the scope of this thesis. The interested reader can find an exhaustive treatise in the book of E. Hairer, S. Nørsett and G. Wanner [38], from which the library providing the integrator used here originates.

The basic idea how Runge–Kutta methods integrate first order ordinary differential equations is as follows: for each time step $t \mapsto t + \Delta t$, estimates of the slope of the solution function at certain points within the interval $[t; t + \Delta t]$ are computed in a series of stages (here 10). Each stage refines the prediction by incorporating an estimate of the solution function's curvature from the previous stages. A certain, weighted sum of the values predicted in each stage then gives a pretty accurate prediction of the unknown function's value after one time step (with the error for each time step being of the order $\mathcal{O}((\Delta t)^8)$ here).

For some Runge–Kutta prescriptions it is possible to find a Dormand–Prince pair of coefficients which allows to, roughly speaking, recycle some of the results of the aforementioned stages into an embedded lower-order (order 5 for DOP853) prediction, yielding an estimate of a step's local error. In turn, this error estimate can be used to dynamically adapt the step size Δt depending on the dynamics of the differential equation. That means that, by imposing global tolerance restrictions, it is possible to “plough” through the time evolution in regimes where the solution function does not change much by increasing the step size, while spending more computational effort on time regimes where the integrated quantity rapidly changes. For additional stability, the error estimator of DOP853 is “stretched” [38, p. 254f] by an additional error estimator of order 3. Finally, the discovery of a particular Dormand–Prince pair enables DOP853 to produce dense output at order 7, which is useful for presenting the results graphically.

Now back to equation (3.6). Instead of the finite difference Hamiltonian with $\tilde{\Delta}$, it is also popular to numerically handle the Laplacian using a discrete Fourier transform. This has the advantage that the wave function globally contributes to the computation of the momentum, while in the finite differences approach the series expansion is truncated and only a few nearest neighbors contribute directly. However, because of the finite grid, usage of the Fourier series directly results in the necessity to impose periodic boundary conditions. These are somewhat undesirable for the purpose of obtaining arrival time statistics of a wave packet starting on one side of a slit setup, with the majority of it being reflected and only a small fraction actually arriving at the screen. Interference effects are thus best to be avoided by choosing boundary conditions that absorb the wave packet when it leaves the grid.

In fact, equation (3.6) is of course incomplete so far without a specification of the boundary conditions and only holds for values of i and j being not equal to 1 or $N_{1,2}$. For grid points that are on the fringe of the grid $\Lambda_{N_1 N_2}$, usage of the appropriate forward and backward differences

3. Bohmian Trajectories and Time of Arrival Statistics

instead of the central difference formula seems appropriate. One would expect a bit of reflection from the jump in derivative evaluation at the boundary, but small enough $\Delta x_{1,2}$ will make that amount negligible.

Finally, the introduction of the grid imposes an upper limit on the rate with which changes in phase or intensity of ψ can propagate during the simulation. This is due to the Nyquist theorem, which basically states that if the grid is too coarse, then aliasing artifacts may occur. For this reason the numbers of grid points in each direction, $N_{1,2}$, have to be chosen sufficiently large, i.e. the grid parameters need to match the problem under investigation.

Now that it is clear how to integrate the Schrödinger equation, it remains to discuss how the dynamic double slit can be implemented. Figure 3.2 contains a plot of the initial potential on the grid. It consists of a potential wall as a barrier. Its height and width should be chosen such, that (without the slits in it) the incoming wave packet is almost⁶ completely reflected. The apertures in the wall are modeled to have Gaussian shape, which minimizes the near field effects typically observed at slits with sharp edges. The plot also shows where the screen would be located. In particular, the screen is not modeled in the expression of the potential, only the time of arrival statistics are gathered in that place. In view of this, the term *time of first passage*

⁶A Gamow factor below 10^{-4} seems sufficient.

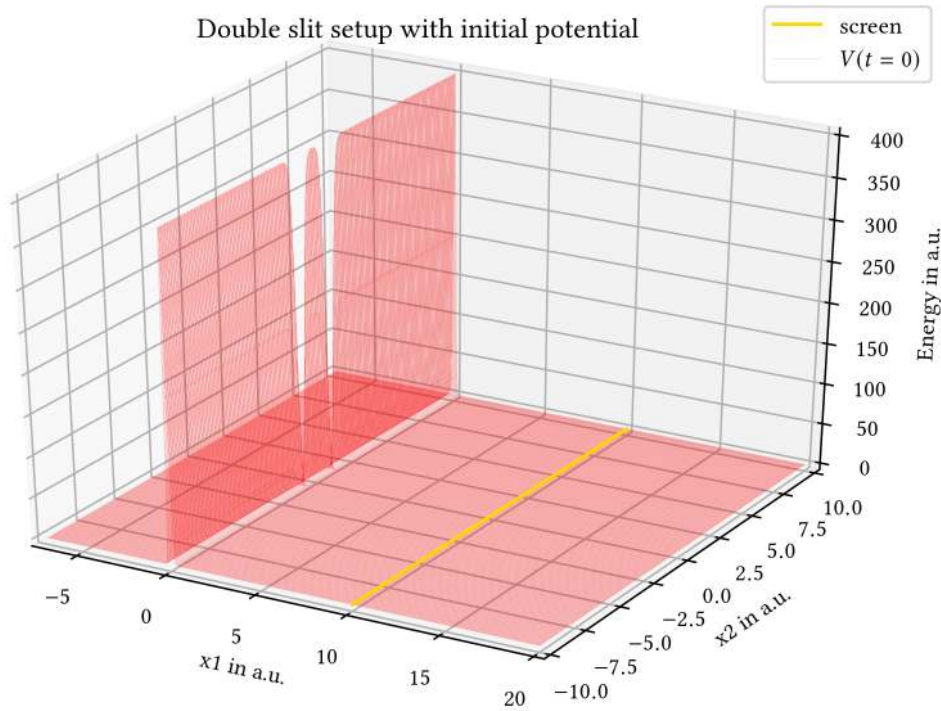


Figure 3.2: The dynamical double slit setup, modeled via a potential wall with two Gaussian shaped slits in it at $t = 0$. One of the slits can be closed by smoothly deforming it into the wall.

3.2 A dynamic double slit setup

statistics would actually be a more appropriate name for the quantity sought after. But to avoid confusion, the statistics will continue to be denoted time of arrival statistics.

The potential is given by the expression

$$V(x_1, x_2, t) = V_0 \exp\left(-\frac{x_1^2}{2\sigma_{V1}^2}\right) \left(1 - \exp\left(-\frac{(x_2 - \frac{d}{2})^2}{2\sigma_{V2}^2}\right) - f_\tau(t) \exp\left(-\frac{(x_2 + \frac{d}{2})^2}{2\sigma_{V2}^2}\right)\right) \quad (3.8)$$

where V_0 is the height of the potential wall, σ_{V1} the width of the wall and σ_{V2} the width of the slits. The slits are separated by distance d . The factor

$$f_\tau(t) := \frac{1}{2} \left(1 + \tanh\left(\frac{t_c - t}{\tau}\right)\right) \quad (3.9)$$

is the slit closing function that closes the bottom⁷ slit at time t_c . It contains the closing parameter τ , which provides control over the timescale on which the slit closes. The reason for using such a smooth function is, that it is challenging to numerically integrate differential equations with discontinuities. The initial wave packet

$$\psi(x_1, x_2, t = 0) = \frac{1}{\sqrt{2\pi\sigma_1\sigma_2}} \exp(ik(x_1 - x_{0,1})) \exp\left(-\frac{(x_1 - x_0)^2}{4\sigma_1^2} - \frac{x_2^2}{4\sigma_2^2}\right). \quad (3.10)$$

is a two-dimensional, normalized Gaussian traveling with group velocity k (in atomic units) and starting at position x_0 before the slits.

3.2.2 Results and Discussion

Let's start with having a look at the Schrödinger dynamics of the static, two-dimensional double slit, i.e. letting $f_\tau \equiv 1$ so that no slit ever closes. A grid consisting of 2053×1521 points on the interval $[-7; 20] \times [-10; 10]$ together with the parameters to equations (3.10) and (3.8) contained in table 3.1 on page 26 gives satisfactory results. Integrating from time zero to 1.75 a.u. suffices to capture the interesting dynamics. Running the integrator on a toy potential, in particular the two-dimensional harmonic oscillator potential and an initial wave function consisting of a superposition of eigenstates chosen such that the resulting dynamics are comparable with or even more complex than the dynamics for the choice of parameters here yields excellent agreement with the analytic time evolution. This establishes trust into the correct implementation of the numerical codes.

Figure 3.3 presents a few snapshots of $|\psi|^2$ at different times, while figure 3.4 contains magnitude and phase of ψ . The former shows that there is some reflection at the boundary of the domain of integration as expected from the implementation of the boundary conditions. But it only becomes visible in the last snapshot and is only of issue for the reflected part of the wave packet, so there is no need to bother about it. A striking observation is that, unlike the case

⁷The slit at negative x_2 -position will from now on be called the lower or the bottom slit.

3. Bohmian Trajectories and Time of Arrival Statistics

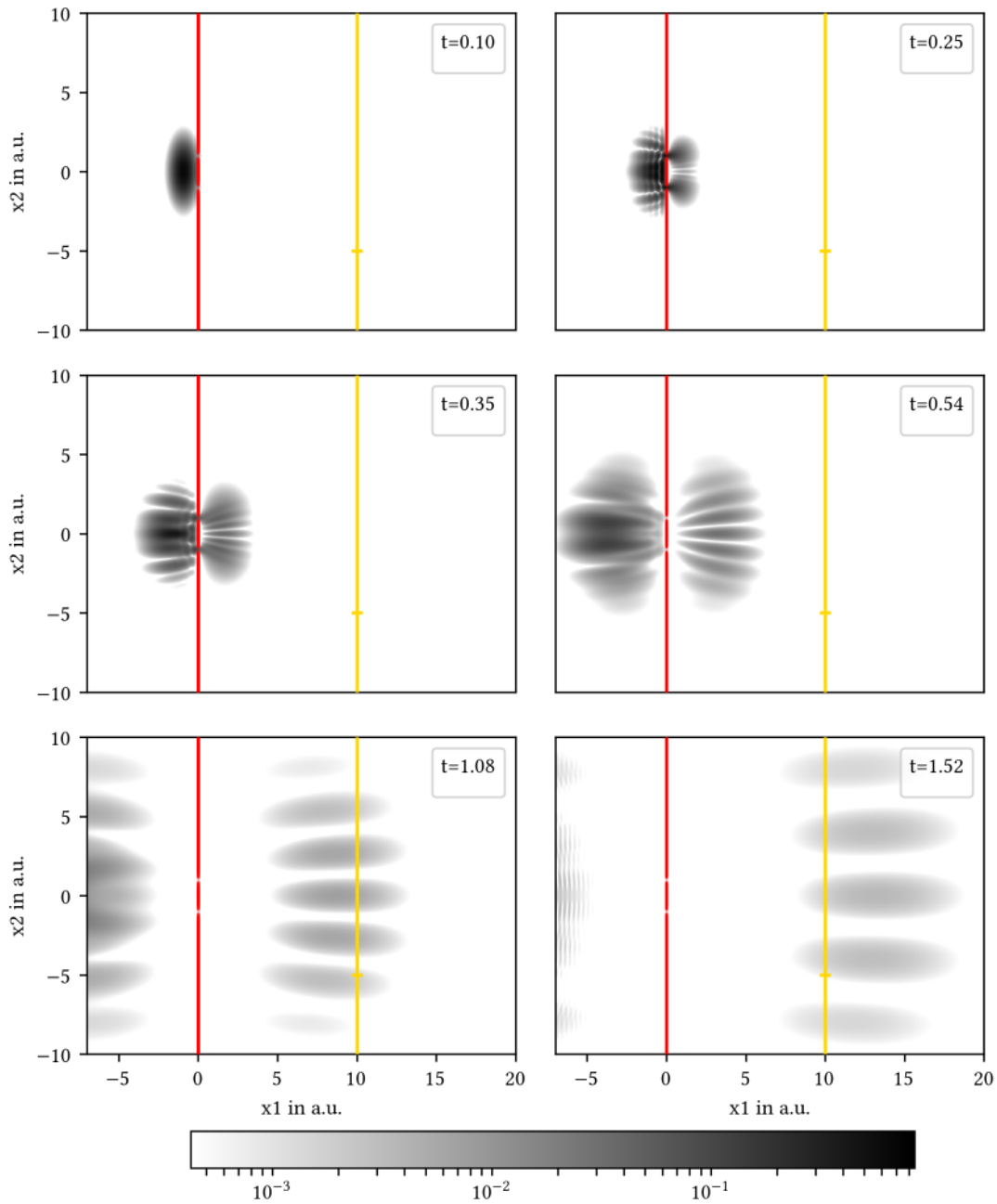


Figure 3.3: Samples from the time evolution of the probability density $|\psi|^2$ for both slits constantly open. Logarithmic scale in the intensity, same scale in all snapshots. The vertical red line is the double slit, the yellow one indicates where the screen might be placed. A particular position on the screen is marked for later reference.

3.2 A dynamic double slit setup

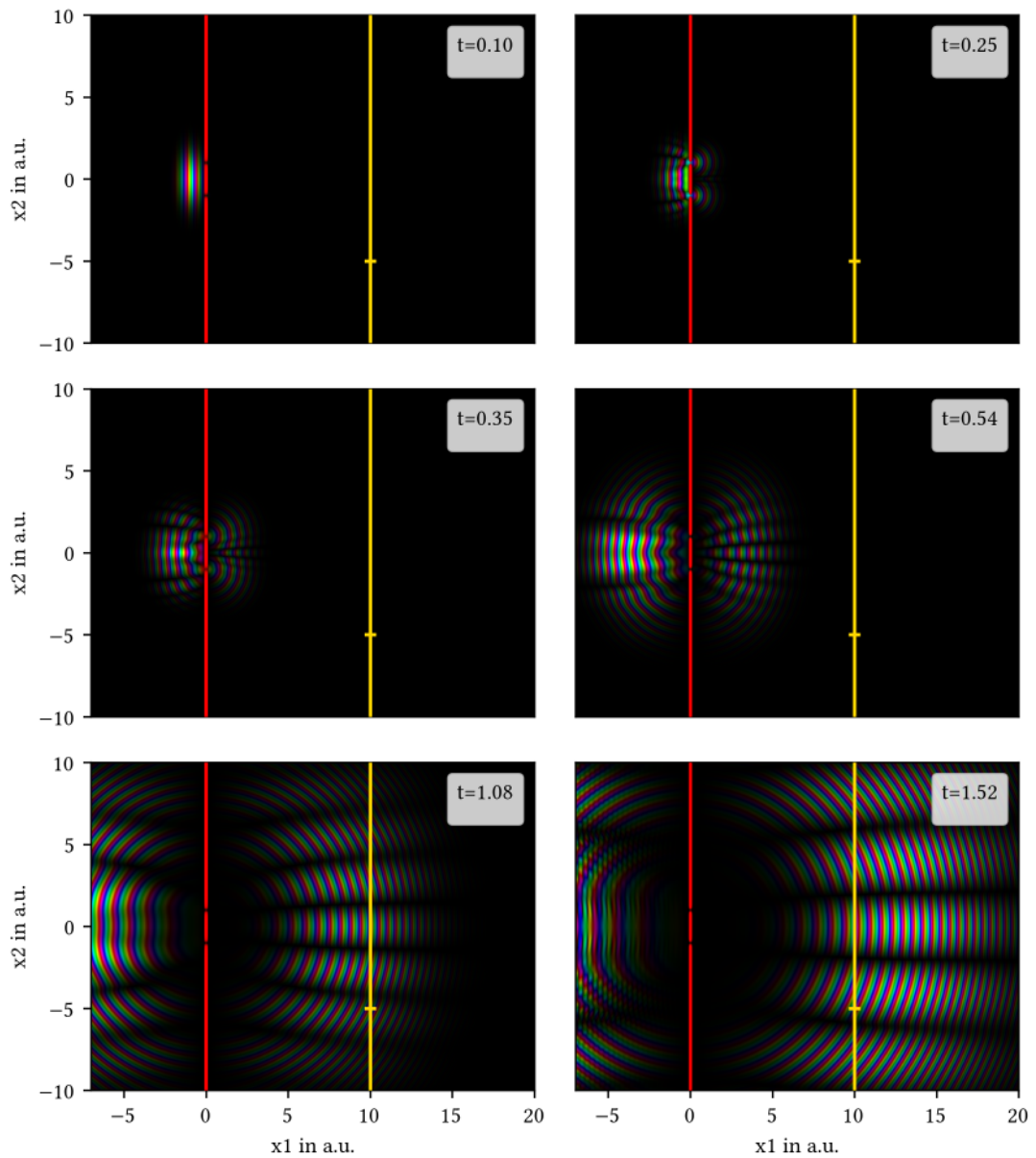


Figure 3.4: Samples from the time evolution of the wave function ψ for both slits constantly open. The color of each pixel represents the phase while the brightness is a measure for the amplitude $|\psi|$ on a linear scale. Unlike figure 3.3, the amplitude is normalized to its maximum value in each snapshot. Again, the vertical red line is the double slit, the yellow one indicates where the screen might be placed. A particular position on the screen is marked for later reference.

3. Bohmian Trajectories and Time of Arrival Statistics

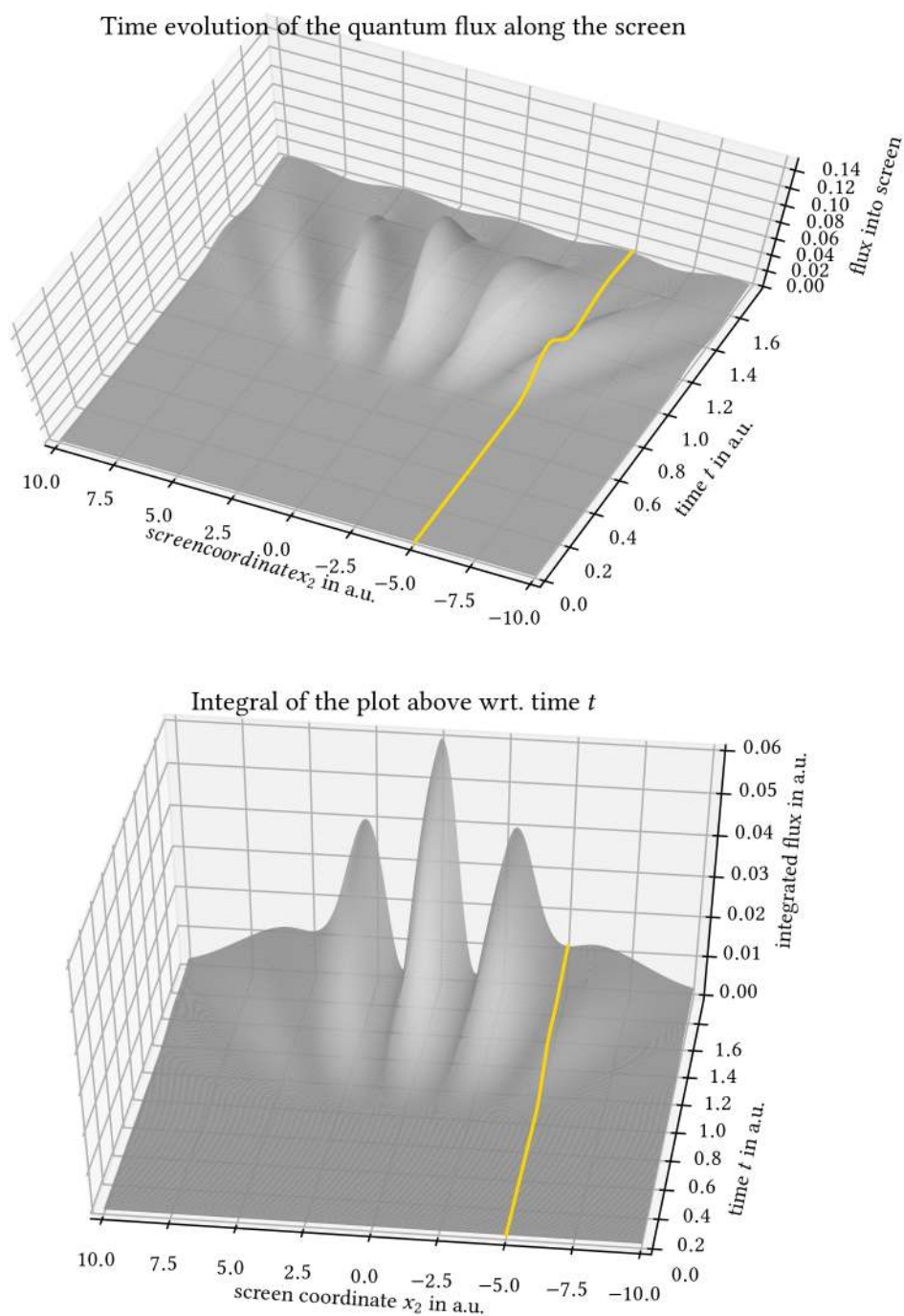


Figure 3.5: Top: the probability current $\mathbf{j}^\psi \cdot \mathbf{e}_1$ into the screen. Bottom: Integrated flux $\int_0^t \mathbf{j}(t')^\psi \cdot \mathbf{e}_1 dt'$ into the screen. The marked position is indicated by the yellow line.

3.2 A dynamic double slit setup

parameters of equation (3.10)		parameters of equation (3.8)	
k	10.5	V_0	400
x_0	-2	σ_{V1}	0.075
σ_1	0.25	σ_{V2}	0.25
σ_2	0.75	d	2

Table 3.1: Chosen values of the parameters in the equations above. All numbers given in a.u.

of an incoming plane wave, the positions of the minima between the bumps of the interfering wave packets are subject to dispersion, rather than staying at fixed positions over time. This effect will lead to a washed out interference pattern on the screen, and there is no reason why it should be expected to go away by going further to the far-field.

Figure 3.5 contains a plot of the probability current along the screen as a function of time in the top half and its cumulative time integral in the bottom half. Because it turns out that the projected flux $\mathbf{j}^\psi \cdot \mathbf{e}_1$ never becomes negative at the position of the screen, the bottom plot would be proportional to the interference pattern approximately expected to be observed on the screen when repeating the single particle experiment many times and when neglecting the interaction between screen and wave function. So this plot confirms the conclusion drawn from the dispersion of the interfering wave packet bumps, namely that even the two minima beside the main maximum will not be entirely dark on the screen. They are nonetheless much darker than their neighboring maxima of course. In view of the absence of any other pronounced minima for the parameters of table 3.1, the discussion of the closing slit time of arrival statistics will not revolve around a minimum position at which to place the detector, like it was formulated in the original question of H. Weinfurter at the very beginning of the chapter. Instead, the illustrations in the following will refer to the spot on the screen that is closest to the closing screen and also comes closest to being a minimum, but that will not change much of the essence. The spot had already been marked in figures 3.3 and 3.4 and is also present as the yellow line in figure 3.5.

Before turning to a closing lower slit, take a look at figure 3.6, which contains a sample of Bohmian trajectories from the initial wave packet through the slits and through the screen position. The initial conditions have been chosen randomly and then symmetrized. The majority of trajectories is being reflected backwards, but these are not plotted. Only about 20% make it through the slits. Trajectories still never cross the axis of symmetry and do not cross other trajectories at the same time. But unlike the plane-wave examples of figures 2.1 and 3.1, where the trajectory graphs were disjoint sets in configuration space, the trajectories do now overlap in the plot. A later particle from the rear of the wave packet can pass through spots where a particle from the front of the wave packet would have been previously. Of course, in a three-dimensional plot with time on the third axis there would be no trajectory crossings, just like when interpreting figures 2.1 and 3.1 as having one-dimensional configuration space. Also there are more than two nicely pronounced minima in figure 3.6. This is however only because the plot is not cluttered with more trajectories for clarity. Drawing more samples for the parameters of table 3.1 would only leave the two minima in the middle empty of trajectories.

3. Bohmian Trajectories and Time of Arrival Statistics

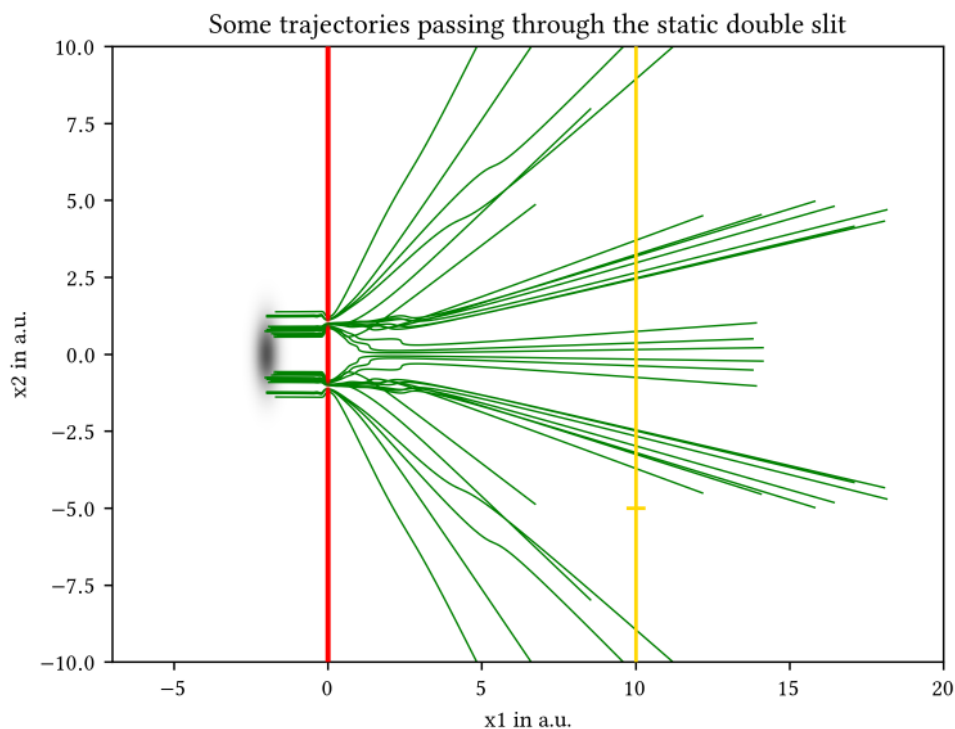


Figure 3.6: A set of some Bohmian trajectories passing through the constantly opened double slit. The majority of trajectories are reflected backwards (not shown). Symmetrized initial positions, but otherwise randomly sampled from the initial probability density of the wave function (shaded). Trajectories never cross the axis of symmetry and cannot cross other trajectories at the same time. A particle from the rear of the wave packet can however pass through places where a particle from the front of the wave packet would have been previously.

Now the discussion has finally come to the point where the double slit becomes dynamic. Recall that the closing function f_τ is a shifted inverse hyperbolic tangent so that discontinuities in the potential do not mess with the numerical integration. The closing parameter τ controls how fast the bottom slit is closed. To investigate also the dependence on the slit's closing speed, the results will be compared for two values of τ . For $\tau = 0.01$ the slit rapidly closes, while for $\tau = 0.05$ closing takes more time. Figure 3.7 compares the two processes. In both cases the closing time t_c at which $f_\tau(t_c) = 0.5$ is 0.25 a.u. This time corresponds to the incoming wave packet having passed about halfway through the slits as can be confirmed by visual inspection of figure 3.3.

Figure 3.8 contains the time of arrival statistics at the marked screen position for the two cases where the slits are being closed at different speeds and for the bottom slit never closing at all. For an interval Δl of width 0.013 around that spot there are plots of both the probability rate with which an incoming particle is detected on the screen at any time t and also its time integral, i.e. the probability that a particle has already been detected before t . Comparing the

3.2 A dynamic double slit setup

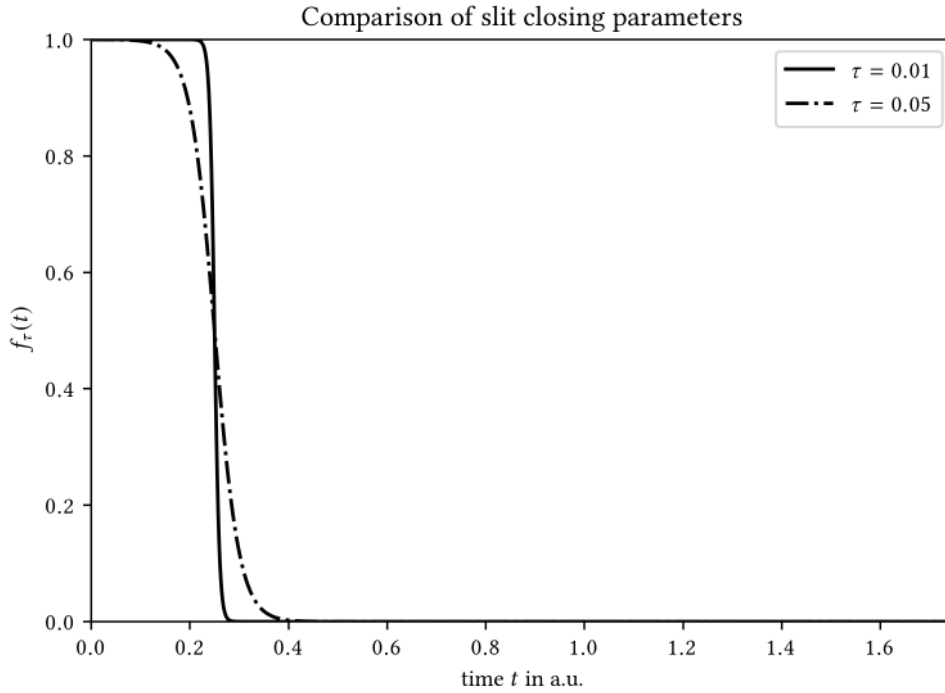


Figure 3.7: The closing function f_τ for the two different values of τ . A value of 1 means that the bottom slit is completely open while 0 indicates that the slit is fully closed.

different cases in the upper plot of figure 3.8, the most striking observation is that there is some kind of double peak structure. It arises from the two neighboring bumps in the interference pattern slightly touching the marked spot while they are dispersing as was seen in figure 3.4.

Now look at how closing the bottom slit affects the green curve of keeping the bottom slit open. Qualitatively at least, the first peak still remains, but the interference pattern changes such that it becomes larger. Next, in those cases where the bottom slit closes, there is a probability to detect a particle already ahead of time compared to the static double slit and this part of the probability rate is oscillatory in time. This effect is most pronounced when the slit closes rapidly, but it can also be observed in the slowly closing case. It arises from the closing slit producing a wave packet that has been cut off and is thus effectively more curved. The Schrödinger equation makes narrow wave packets, that are more strongly bent, expand more quickly than relaxed, wider ones. This expansion leads to part of the wave packet eventually overtaking the uncut part of the wave packet and propagating ahead of it with the sharp cutoff being responsible for the transient oscillations.

In fact, one can just run the simulation with the same closing parameters for a single slit instead of a double slit and compare the two on the time interval before interference in the double slit case takes place. Then, the exact same effect is observed in the closing single slit setup, so the conclusion must be that it exclusively arises from the closing procedure.

3. Bohmian Trajectories and Time of Arrival Statistics

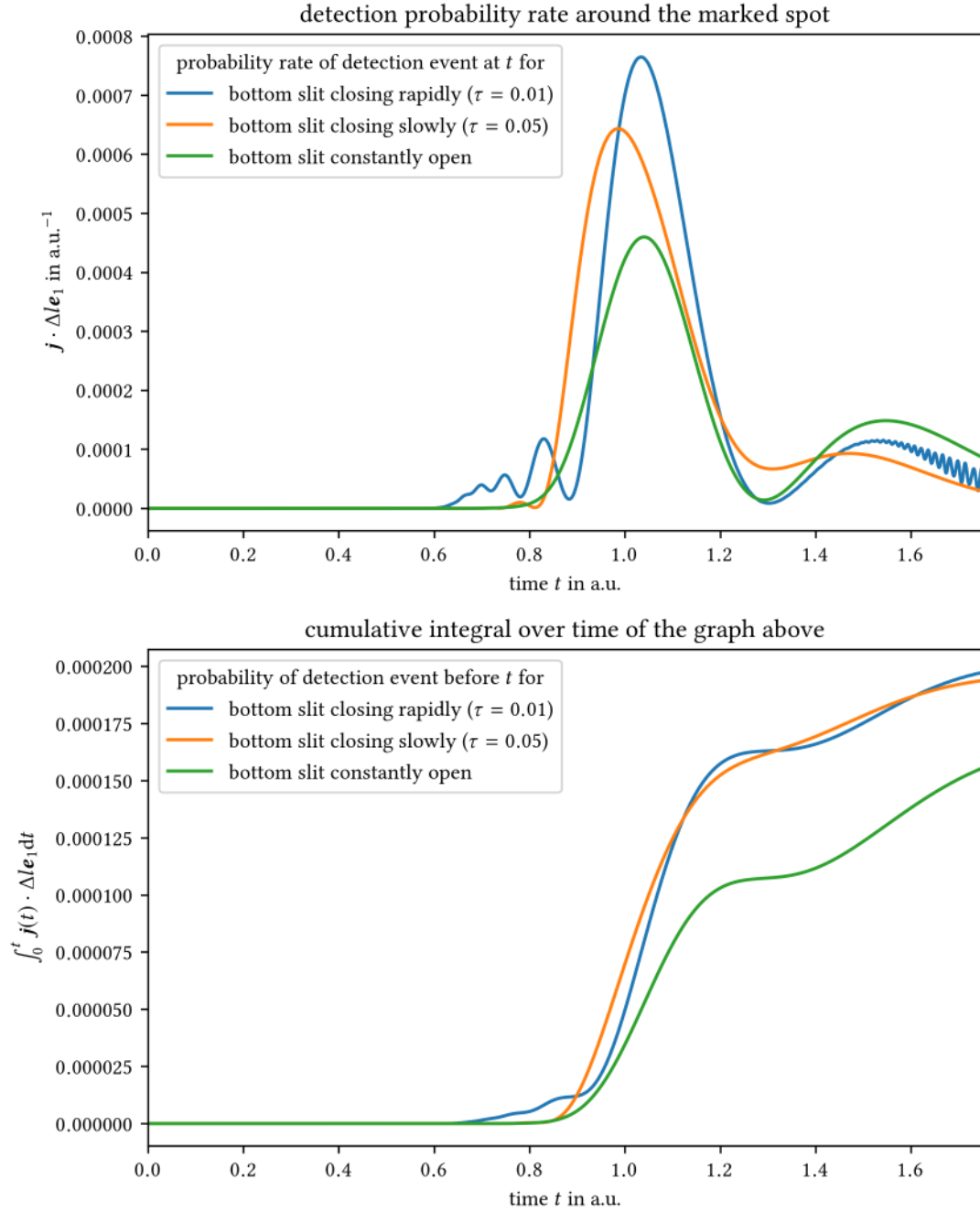


Figure 3.8: Comparison of the detection probability in an interval of length $\Delta l = 0.013$ a.u. around the spot marked on the screen for three different cases of double slit setups. Top: the probability rate of a particle being detected at this part of the screen at time t . Bottom: the probability that a detection of the particle occurs before time t , which is simply obtained by integrating over the probability rate until t .

3.2 A dynamic double slit setup

Finally, despite the biggest fraction of this quickly forward moving part of the wave function being absorbed at the boundary of the domain of integration, there is a small reflected part in the rapidly closing case that is fast enough to arrive at the screen from behind. It causes some ripples that can be seen in the blue graph from $t = 1.5$ a.u. onward. This artifact does not create any further problems though.

The bottom plot shows how the cumulative probability $P_{\Delta t}([0; t])$ evolves with t . As can be seen, for times at which one may observe a detection event in the static case, i.e. for $t \gtrsim 1.0$ a.u., the probability is already a lot bigger in the closing cases, but does not differ much among them. Where the curves do differ however is at the onset of detection, where the blue graph representing the rapidly closing slit rises away from zero earlier than the orange one of the slowly closing case.

Because ultimately the probability current turns out to be positive at all times in all three cases, it was not required to invoke the Bohmian interpretation in form of truncated trajectories for plotting the probability rate. This is purely a coincidence arising from the set of parameters used here and there was no a priori guarantee for expecting that. The functions depicted in figure 3.8 are thus basically scaled versions of cuts along the yellow lines in figure 3.5 for the static double slit setup and figures A.3 and A.6 in the appendix for the dynamic double slits, respectively.

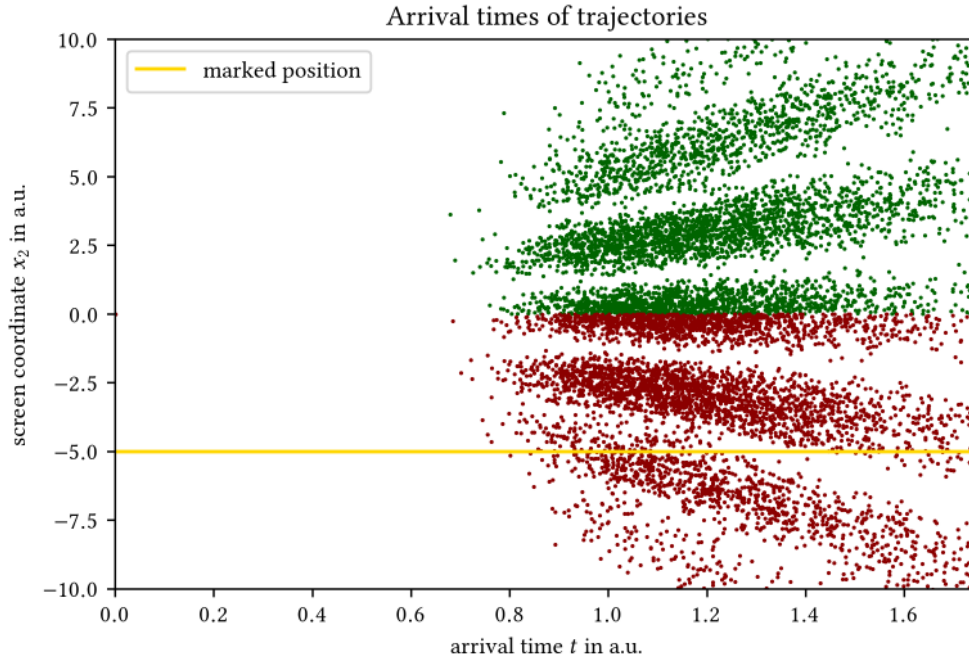


Figure 3.9: Scatter plot of trajectories arriving at the screen over time for the static double slit setup. Colors indicate whether the respective trajectory passed through the top (green) or bottom slit (red).

3. Bohmian Trajectories and Time of Arrival Statistics

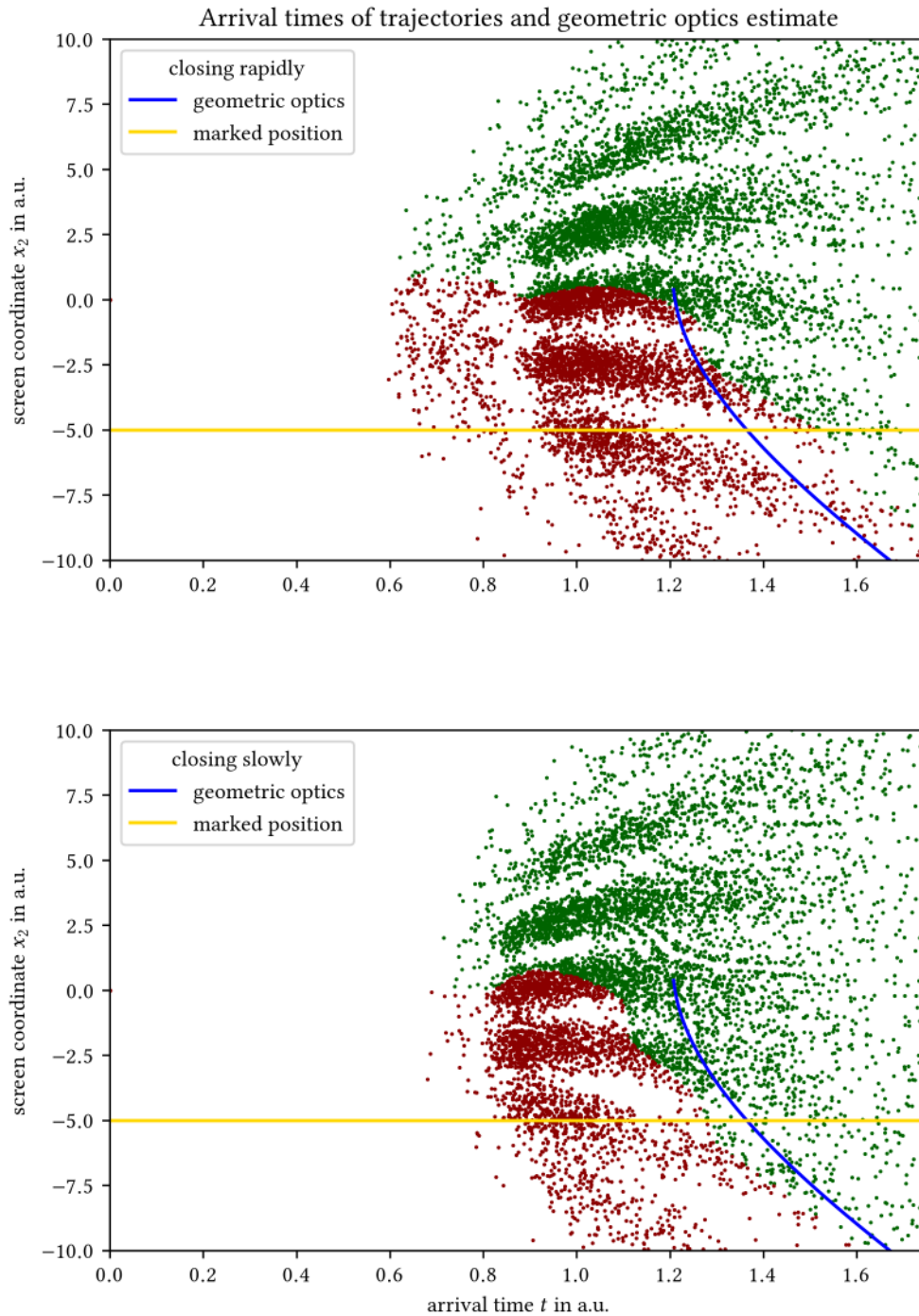


Figure 3.10: Scatter plots of trajectories arriving at the screen over time for the setup where the bottom slit closes rapidly (top) or slowly (bottom). Colors indicate whether a trajectory passed through the top (green) or bottom slit (red). The blue line gives the time of arrival of an elementary wave starting from the top slit at $t = 0.25$ a.u., at which the events of bottom slit halfway closed and wave packet having passed halfway through the slits coincide.

3.3 Conclusions

Nonetheless the times of first⁸ arrival of the trajectories on the screen can be plotted and this has been done in figure 3.9 for the static double slit. The dark red and green colors encode which slit a trajectory has passed through. As expected, the picture is perfectly symmetric up to the random sampling of initial conditions. Also, the interference picture on the screen is not entirely static, but moves outward over time as the bumps forming the maxima disperse, as has already been discussed in the context of figure 3.5 on page 25.

For completeness, the precise time evolution of the dynamical setups, i.e. the counterparts of figures 3.3, 3.4 and 3.5 are given in the appendix starting from page 114, but most interesting are the dynamic versions of figure 3.9, which are plotted in figure 3.10 above. The plots there also contain an estimate, based on semiclassical geometric optics, of when a particle that starts at the top slit at time t_c , i.e. when the bottom one has closed halfway, would arrive at the screen assuming the expectation value of initial momentum is deflected straight into the direction of where it would arrive eventually. This prediction is given by the real solutions of

$$x_{2,g}(t) = \frac{d}{2} - \sqrt{(t - t_c)^2 k^2 - L^2} \quad (3.11)$$

and is motivated by H. Weinfurter's original question.

From the plots it is clear that the accuracy of this prediction heavily depends on the slit closing parameters. For the rapidly closing bottom slit, particles originating from it keep arriving beyond the time predicted by equation (3.11) while in the slowly closing case particles from the top slit already arrive before they are supposed to according to the estimate. Interestingly also, in the closing slit scenario there are some trajectories passing through the bottom slit that penetrate into the previously forbidden region of positive x_2 -coordinates. From an experimental point of view it is of course moot to ask for the arrival times from a certain slit, because a detector cannot discriminate between detection events with a Bohmian trajectory through the upper or lower slit, c.f. also [26].

Finally, the original question on page 13 can be answered to a certain extent by comparing figure 3.10 to figure 3.9. The interference pattern in the former plot starts emerging around $t = 0.8$ a.u., while the closing slit accelerates some particles which can be detected before that time in the latter ones. So when placing a detector in an interference pattern minimum, then the first detection event after closing the slit will typically not indicate that a particle from the slit which remains open has arrived. Instead the distribution of particles detected at this position in an experimental setup like the proposed one would, again, mainly be governed by the slit closing characteristics.

3.3 Conclusions

Besides illustrating the nature and general features of Bohmian trajectories in preparing the reader for the following chapters, it was examined how Bohmian trajectories can be used as a tool for predicting time of arrival statistics in an investigation of the dynamics in a double

⁸And due to the lack of backflow in this case of course only arrival on the screen.

3. Bohmian Trajectories and Time of Arrival Statistics

slit experiment. Since an actual two-dimensional numeric treatment of a double slit from a Bohmian point of view elsewhere in the literature is not known to the author, it was instructive to see the trajectories in this case. They differ from the usual textbook pictures by the fact that trajectories become, as expected, no longer disjoint graphs on configuration space when going beyond the plane wave treatment. Also, for a wave packet of finite size passing through the slits, the interference pattern on a screen is not stationary but moves outwards due to dispersion in free space.

With one slit of the double slit setup becoming time-dependent, the choice of parameters turned out to still result in a quantum flux purely flowing into the screen, never out of it, thus rendering it unnecessary to invoke the Bohmian interpretation for obtaining the time of arrival statistics. As a consequence, barring effects resulting from neglecting an interaction between electron and screen, which would have to be described as a quantum system in principle, the integrated flux into the screen is directly proportional to the intensity pattern that would be observed in such an experiment. Unlike when solely relying on Copenhagen style quantum mechanics, by employing the truncated current it would have been possible in principle to deal with a wave function, whose current violates the positivity condition. That doing so was not necessary is simply a coincidence resulting from the choice of parameters here. With the dynamically closing slits stirring up the wave function dynamics, there would have been no reason to expect this a priori.

Having a closer look at the first and only time of arrival of the Bohmian particles at the screen elucidated on the predictive quality of the arrival times estimated via geometric optics in the near field behind the slits. Qualitatively the estimate yields a correct time evolution of how particles with Bohmian trajectories having passed through either one of the slits are distributed. But quantitatively the precise procedure of how the slit is being closed turned out to be very important. This is because essentially cutting the wave packet off at the closing slit results in a genuinely quantum effect, which manifests in part of the wave packet overtaking the interfering bumps and thus accelerating a Bohmian particle that had already passed through the slit before closing. This effect is not contained in the semiclassical equation and explains for the discrepancy. Closing the slit is a dynamic process, and by varying the closing parameter the entire range between both slits always opened and one slit closing instantly can be interpolated. An approximation which does not reflect this can of course not provide reliable results, when the actual outcomes depend on the exact way, in which the slit is closed. The lesson learned is thus, that geometric optics may provide sufficiently accurate predictions of arrival times in the far-field, but in the near-field the estimate becomes imprecise for the scenario discussed here.

With the parameters chosen here in a way, such that it would not be easy to build an actual experiment, the results are mainly of academic interest. Nonetheless, it should be possible to scale the setup towards a more realistic domain where integration on the grid would still be feasible. Even better with respect to experimental realizability would of course be to redo the whole calculation with photons instead of electrons.

Also, one could produce arrival time statistics for the slit closing at different times so that different proportions of the initial wave packets have already passed through the slit before it closes in order to form a statistical mixture. But whether that would be worth the effort is

3.3 Conclusions

questionable, because it is not possible to detect in an experiment which path a Bohmian particle has actually taken. This together with the aforementioned overtaking of part of the wave function, which moreover is sensitive to the precise way the slit closes, leads to the following conclusion: The original statement of the question that initially motivated the investigation needs to be reformulated because the underlying assumption is incorrect. Putting a detector into a minimum position of the static interference pattern and recording the time of detection events after closing one of the slits will not produce an estimate of the time of arrival of a particle from the slit that remained open as may have been the initial intention. Instead, a change of the guiding wave function affects the motion of Bohmian particles wherever they are, and as such, closing the slit behind a particle that has already passed through the slit, while its wave function has not yet, may consequently accelerate or deflect that particle in Bohmian mechanics.

4 Employing Bohmian Trajectories in Quantum Numerics

The underlying physical laws necessary for the mathematical theory of a large part of physics and the whole of chemistry are thus completely known, and the difficulty is only that the exact application of these laws leads to equations much too complicated to be soluble. It therefore becomes desirable that approximate practical methods of applying quantum mechanics should be developed, which can lead to an explanation of the main features of complex atomic systems without too much computation.

(P. Dirac, 1929 [39])

The above quote sets the frame for this chapter and the one following afterwards. Both chapter 5 and this one will deal with the “approximate practical methods” that Dirac had in mind. However, the methods discussed in the next chapter are fundamentally different from the ones here. While chapter 5 treats part of the system classically in order to reduce the number of quantum degrees of freedom, a system here is regarded to be fully quantum and “too much computation” is circumvented by making an approximation to the *exact*¹ numerical method of Wyatt, which, despite some issues, is already an efficient approach on its own.

Many methods for solving the Schrödinger equation have been put forward in the past. One way is to decompose the wave function into a superposition of eigenstates and to evolve these, but that approach does not work when part of the spectrum is continuous. In the latter case, the typical way of doing it is approximating the continuum of Fourier modes by integrating the wave function on a stationary grid. This approach runs exactly into the problem addressed by Dirac, because the required number of grid points scales exponentially in the number of degrees of freedom nd , with n being the number of particles and d the number of dimensions. Although the algorithms for solving the time dependent Schrödinger equation presented in this chapter do not necessarily overcome the exponential scaling, they do have at least the potential to make the basis in the scaling law significantly smaller.

Only about 20 years ago, people started to employ Bohmian trajectories as a numerical tool for this purpose in a serious way. In 2014, the Many Interacting Worlds approach was put forward by M. Hall, D.-A. Deckert and H. Wiseman [4], with a seemingly promising application to quantum numerics. This chapter quickly reviews the original method developed by R. Wyatt, which has already been laid out in his book [3] to great extent, and then compares how well the new, computationally simpler approach can keep up with it. Also this chapter explores

¹In principle. Discretization of the wave function and finite numerical precision are of course inevitable.

4.1 Overview over Adaptive-Grid Methods

whether and how both methods can be combined into a hybrid algorithm in order to overcome the difficulties that are inherent to the current approaches.

Wyatt coined the term *synthetic approach* in his book to emphasize the difference of this approach to the usual way of doing Bohmian mechanics, which he calls the *analytic approach*. In the usual way, as done in the previous chapter for example, the Schrödinger equation is solved first and then the Bohmian trajectories are obtained from the guiding wave function in a second step. In particular, the Bohmian trajectories do not have any effect on the wave function time evolution. Now, as Wyatt first discovered, for numerics it is possible to actually compute both at the same time by making use of the trajectories to calculate the wave function time evolution on the fly. In this context, Bohmian trajectories basically become a *numerical tool* for solving the Schrödinger equation on a special grid, in particular a grid whose density of grid points automatically adapts to the main features of the evolving wave function. Methods in the category of this paradigm are called *adaptive grid methods* and some particular instances will be introduced to the reader in the following section.

4.1 Overview over Adaptive-Grid Methods

As already stressed introductorily, integrating the Schrödinger equation on the lattice quickly runs into limitations in terms of computational resources. The method is not optimal in the sense that a fixed grid needs to cover all of configuration space at all times, or at least those parts of it, on which the wave function behavior is eventually of interest. In many cases this means that at times loads of computations are carried out in regions of the grid, where the wave function almost vanishes and does not significantly change at all. So computational budget is wasted without leading to better accuracy. An example would be the double slit simulation in the previous chapter. Once the interference pattern has detached from the slits, propagating the wave function's time evolution in this (now empty) area becomes unnecessary baggage. Conversely, the whole area around the screen is completely irrelevant for the dynamics before the wave packet has even started passing through the slits.

In such a situation, using an adaptive grid, i.e. a grid which dynamically adapts to the time evolution of the wave function being integrated, would be of advantage. Bohmian trajectories constitute one possible candidate to construct such an adaptive, also called *comoving* grid from. The equivariance principle guarantees that the density of the flux lines, which precisely form the possible Bohmian trajectories, always remains distributed with respect to the probability density $\rho^\psi = |\psi|^2$, which makes them appear particularly promising.

Using $N = 34$ grid points, figure 4.1 illustrates the difference between a fixed grid and the adaptive grid consisting of a set of Bohmian trajectories. Different aspects of the same one-dimensional wave function, a superposition of two Gaussians, which interfere while dispersing over time, are shown in all four plots. In the plots on the right hand side, the analytic expression is coarse-grained in space to the number of grid points. One case shows a stationary grid of uniform spacing, while in the other case at each point in time the Bohmian trajectories divide configuration space into regions that are filled with constant values. The trajectories are distributed such that the cumulative probability density $\int_{-\infty}^{\infty} |\psi(q)|^2 dq$ is divided into intervals

4. Employing Bohmian Trajectories in Quantum Numerics

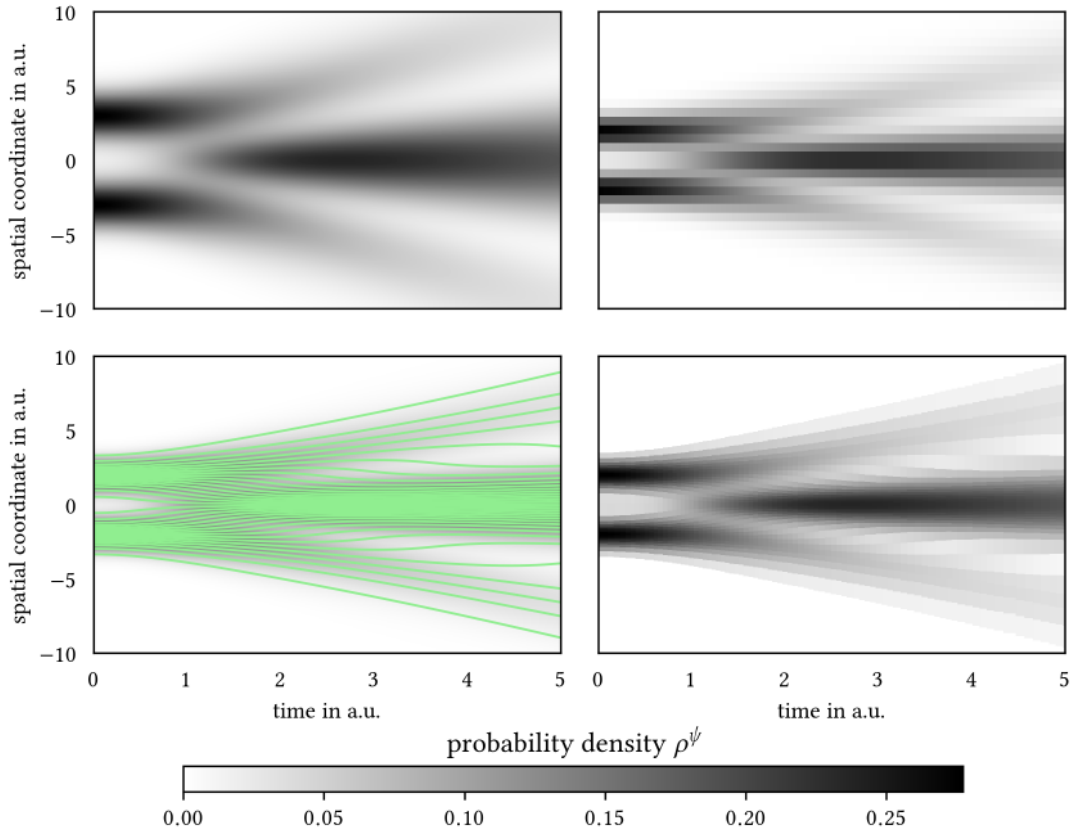


Figure 4.1: Comparison of a static to an adaptive grid for a superposition of two one-dimensional Gaussians. *Top left:* exact time evolution of the wave function’s probability density. *Top right:* discretization onto a static grid. *Bottom left:* Bohmian trajectories for this wave function, same number as grid points in top right. *Bottom right:* discretization onto the nearest Bohmian trajectories, forming the adaptive grid for this wave function, same number of grid points as above it.

of equal size. Compared to the discretization onto the static grid, the shapes of the two initial peaks and of the central main bump forming after a while are resolved much more clearly on the comoving grid. For the static grid, in order to obtain a similar resolution in this domain of interest, many more grid points need to be added to the initially almost completely white region as well. Especially for long-time simulations, such as in scattering scenarios, this quickly becomes a huge problem in particular if many degrees of freedom are involved due to the exponential scaling of configuration space’s dimension.

Leading the way out of this dilemma without continuously refining the grid by hand in regions of physical interest, this section will first introduce Wyatt’s method, which makes use of such an adaptive Bohmian grid to integrate the Schrödinger equation. It is then followed by an approximation to those dynamics deduced from the many interacting worlds paradigm, which makes it possible to carry out trajectory calculations in a much more efficient way. Before

4.1 Overview over Adaptive-Grid Methods

testing these methods against each other, some hybrid methods in between those two extremes will be introduced. They also try to exploit a redundancy of information contained in Wyatt's approach in order to enable more efficient and possibly more robust calculations. As before, the Bohmian trajectory describing the simultaneous motion of all n particles in an n -particle system is denoted by \mathbf{x}_t and, as motivated in chapter 2, the term *world* will in some contexts be used for a point \mathbf{x} in nd -dimensional configuration space.

The adaptive grids used for numeric calculations in this chapter rely on ensembles of trajectories. So at a time t , a grid of size N is described by $\{\mathbf{x}^k\}_{k=1,\dots,N}$. As has been pointed out [40], for a Bohmian grid the computational algorithms present a shift of paradigm compared to the description of nature by Bohmian theory. They do not refer to the wave function per se when evolving the trajectories, since the purpose is to *find* the wave function. The Bohmian theory of quantum mechanics on the other hand supposes that nature by itself solves the Schrödinger equation for the wave function independently of any trajectories or particles and then only one single world trajectory is guided by the solution wave function. This discrepancy reflects in the expression *hydrodynamic approach* to quantum mechanics, which is used in the context of Wyatt's algorithm every now and then.

4.1.1 Wyatt's Quantum Trajectory Method

Following what is called the *Bohmian route* by R. Wyatt himself, the starting point for deriving the numerical scheme is a polar decomposition of the wave function

$$\psi(\mathbf{q}, t) =: R(\mathbf{q}, t)e^{iS(\mathbf{q}, t)} \quad (4.1)$$

into a nonnegative amplitude term $R \geq 0$ and a suitably normalized phase S with values in \mathbb{R} . The idea of using this decomposition can actually be traced back to E. Madelung in the early days of quantum mechanics [41]. To be precise, one should consider S as a representative of the equivalence class generated by the shift $S \mapsto S + 2\pi k\hbar$ for integer $k \in \mathbb{Z}$ and the quotient topology needs to be considered when taking derivatives of S . Pulling out a factor of \hbar from S is the usual convention, but this is merely indicated in equation (4.1) for completeness. Using atomic units, $\hbar = 1$ of course holds.

For simplicity of the equations, only a single particle of mass m is considered from now on. But owing to the linearity of the Schrödinger equation, the generalization to n particles can of course be carried out in the usual, straightforward way. First, not that decomposing the wave function according to equation (4.1) leads to a simplified version of the guidance law,

$$\frac{d\mathbf{x}}{dt} = \frac{1}{m} \nabla S(\mathbf{q}, t) \Big|_{\mathbf{q}=\mathbf{x}(t)}. \quad (4.2)$$

After substituting the polar wave function wherever it is non-zero into the time dependent Schrödinger equation (2.1), real and imaginary parts can be separated to yield two coupled

4. Employing Bohmian Trajectories in Quantum Numerics

equations,

$$\frac{\partial R(\mathbf{q}, t)}{\partial t} = -\frac{1}{2R(\mathbf{q}, t)} \nabla \left((R(\mathbf{q}, t))^2 \frac{1}{m} \nabla S(\mathbf{q}, t) \right), \quad (4.3)$$

$$\frac{\partial S(\mathbf{q}, t)}{\partial t} = -\frac{1}{2m} (\nabla S(\mathbf{q}, t))^2 - V(\mathbf{q}) + \underbrace{\frac{1}{2m} \frac{\Delta R(\mathbf{q}, t)}{R(\mathbf{q}, t)}}_{=-Q^\psi(\mathbf{q}, t)}. \quad (4.4)$$

The first one, as can be seen from using $\rho^\psi = R^2$ and suitable rearrangement, simply is the well-known continuity equation (2.4). The other one can be recognized as a quantum variant of the Hamilton-Jacobi equation known from classical mechanics, where the quantum potential Q^ψ of equation (2.11) is added to the potential term V . $\hbar = 1$ holds in atomic units still used in equations (4.2) to (4.4), but in different units this quantity would solely show up inside the quantum potential.

So far, these equations still feature arguments which are points in configuration space, so no advantage when it comes to numeric integration has been achieved yet. The step which replaces this dependency is the usage of the chain rule when evaluating R and S along a Bohmian trajectory, i.e.

$$\frac{dR(\mathbf{x}(t), t)}{dt} = \frac{\partial R(\mathbf{x}(t), t)}{\partial t} + \nabla R(\mathbf{q}, t) \Big|_{\mathbf{q}=\mathbf{x}(t)} \frac{d\mathbf{x}}{dt} \quad (4.5)$$

and analogously for S . Plugging the equations together results in

$$\frac{dR(\mathbf{x}, t)}{dt} = -\frac{1}{2} R(\mathbf{x}, t) \frac{1}{m} \Delta S(\mathbf{x}, t), \quad (4.6)$$

$$\frac{dS(\mathbf{x}, t)}{dt} = \frac{1}{2m} (\nabla S(\mathbf{x}, t))^2 - V(\mathbf{x}) - Q^\psi(\mathbf{x}, t) \quad (4.7)$$

which can in principle be integrated together with equation (4.2) by using any proven off-the-shelf ode-solver like the Runge-Kutta integrator described in the previous chapter. The computations are sped up a bit however, when integrating the logarithm of R ,

$$C(\mathbf{x}, t) := \ln R(\mathbf{x}, t), \quad (4.8)$$

which is called *C-amplitude* by Wyatt [3]. Equation (4.6) then reduces to

$$\frac{dC(\mathbf{x}, t)}{dt} = -\frac{1}{2m} \Delta S(\mathbf{x}, t), \quad (4.9)$$

while the quantum potential can be evaluated as

$$Q^\psi(\mathbf{x}, t) = -\frac{1}{2m} \left((\nabla C(\mathbf{x}, t))^2 - \Delta C(\mathbf{x}, t) \right). \quad (4.10)$$

The working equations of Wyatt's plain algorithm are thus equations (4.2), (4.7) with (4.10) and (4.9). It is of course not possible, to just integrate these along a single Bohmian trajectory, because information about the derivatives of the wave function is required. To obtain it,

4.1 Overview over Adaptive-Grid Methods

a whole ensemble of Bohmian trajectories needs to be followed simultaneously. In principle, the ensemble does not need to be distributed according to the associated probability density, as that is only relevant for keeping the number of grid points low. At each time step, the Bohmian positions $\{\mathbf{x}^k(t)\}_{k=1,\dots,N}$ constitute the grid, albeit an unstructured one. Finally, an interpolation of S and C around each element of the trajectory ensemble can be computed at each time step. This is the sense in which “solving the Schrödinger equation” is to be understood. After integration up to a final time, using equations (4.1) and (4.8) the wave function can be reassembled from an interpolation of C and S between the sampled points.

Here, unlike with a uniformly spaced grid, it is not possible to use the finite difference formula between neighboring grid points, as was done in section 3.2. For the course of this chapter, it is sufficient to restrict the treatment to only one spatial dimension. Algorithms for the general case can for example be found in Wyatt’s book [3, chap. 8] or in a report of successful application of the method to up to hundreds of degrees of freedom [42] and references therein. In one dimension, at any time t the Bohmian grid $\{x^k\}_{k=1,\dots,N}$ is basically a set of real numbers which can be sorted in ascending order of the x^k . Because Bohmian dynamics forbids trajectories to cross one another, this order is preserved over time and an observation of crossing trajectories indicates numerical failure.

At each grid point x^k the values of C and S are known. The commonly used method for evaluating the derivatives on an unstructured grid is to interpolate the functions in between those sample points via least squares fitting. This is not done globally, but within a moving window, i.e. for each grid point, a polynomial of sufficient degree is constructed by taking into account a number of neighbors. It is then trivial to obtain the derivatives from the fitted polynomials.

Least square fitting is popular, because it is able to average out certain numerical inaccuracies. However, as demonstrated by D.-A. Deckert, D. Dürr and P. Pickl [43], at least for evaluating the derivatives of the probability density inside the quantum potential term (4.10), the method is less than ideal, because the repulsive nature of Q^ψ is not taken into account. Because of this, the usage of least square fitting does not prevent trajectories from crossing. The better approach is to use polynomial interpolation, which correctly captures the consequences of two trajectories coming closer towards each other than they should by equivariance. From the calculations in their publication it becomes clear, however, that this approach can also lead to problems at the wave function’s tails. The best results were achieved from a hybrid approach, combining polynomial interpolation at the inner grid points with moving least squares toward the boundary ones. Its implementation has been published in source code [44].

For completeness, it should be mentioned that both, the usual stationary grids and Bohmian comoving grids are only two extreme special cases of a more general concept, the *arbitrary Lagrangian–Eulerian* grids. This concept originates from numerical hydrodynamics. One can actually use any velocity field $\mathbf{u}(\mathbf{q}, t)$ for guiding grid points $\tilde{\mathbf{x}}(t)$ in equation (4.5) instead of the Bohmian one. Usage of the chain rule then results in

$$\frac{dR(\tilde{\mathbf{x}}, t)}{dt} = \left(\mathbf{u}(\tilde{\mathbf{x}}, t) - \frac{1}{m} \nabla S(\tilde{\mathbf{x}}, t) \right) \cdot \nabla R(\tilde{\mathbf{x}}, t) - \frac{1}{2} R(\tilde{\mathbf{x}}, t) \frac{1}{m} \Delta S(\tilde{\mathbf{x}}, t), \quad (4.11)$$

$$\frac{dS(\tilde{\mathbf{x}}, t)}{dt} = \left(\mathbf{u}(\tilde{\mathbf{x}}, t) - \frac{1}{m} \nabla S(\tilde{\mathbf{x}}, t) \right) \cdot \nabla S(\tilde{\mathbf{x}}, t) + \frac{1}{2m} (\nabla S(\mathbf{x}, t))^2 - V(\tilde{\mathbf{x}}) - Q^\psi(\tilde{\mathbf{x}}, t), \quad (4.12)$$

which reduce to equations (4.6) and (4.7) when $\mathbf{u}(\mathbf{q}, t)$ equals the Bohmian velocity (4.2). This is called the *Lagrangian* case. $\mathbf{u}(\mathbf{q}, t) = 0$ on the other hand is the traditional *Eulerian* case, where the grid points are frozen in space as described by equations (4.3) and (4.4). In Wyatt's framework it is thus possible to design completely custom dynamic grids to integrate the Schrödinger equation on. For the sake of comparing this approach to the following two methods, the numerics in this chapter only cover the case of Lagrangian, a.k.a. Bohmian grids, though.

4.1.2 The Many Interacting Worlds Method

Evaluation of the derivatives of the wave function components R and S on the unstructured grid is a laborious process in Wyatt's algorithm and usually amounts to the major fraction of computation time. The sole quantity that is of relevance when making predictions about an observable's measurement outcome is the squared modulus of the wave function $|\psi|^2$ interpreted as a probability density, though. Also, in Bohm's original, Newtonian-looking formulation of the guiding law (2.10), the quantum force term as the negative gradient of the quantum potential (2.11) only depends on $|\psi| = \sqrt{\rho^\psi}$. In fact, as long as

$$\dot{\mathbf{x}}(t_0) = \nabla S(\mathbf{x}(t_0), t_0) \tag{4.13}$$

holds for the second initial condition of a Bohmian particle at initial time t_0 , the dynamical law guarantees, that this relation holds at all future times.

With these things in the back of the mind, one might wonder, whether a quantum mechanics framework exists, in which the wave function is only a secondary object giving rise to initial conditions but with the dynamics realized in a different way. Surprisingly such a wave function-free framework does not only exist, but it even has an application to numerical calculations within its paradigm. Furthermore, these calculations are similar to Wyatt's method in terms of using a Bohmian grid, but the involved process of taking derivatives of a decomposition of the complex wave function on an unstructured grid is not required.

Few years ago, interest in a description of quantum mechanics in exclusively mechanical terms started to gain momentum. While J. Schiff and B. Poirier initially required a continuum of parallel worlds [45], an arbitrarily accurate description that works with a sufficiently large, but finite number of worlds was provided by C. Sebens [46]. Another one was proposed independently by M. Hall, D.-A. Deckert and H. Wiseman [4]. This section will build on the last one, because there a concrete model is proposed together with instructions on how to implement the idea for numeric purposes in the simplest possible case of a single, one-dimensional particle. In fact, here the focus will be only on those parts of the paradigm which are required for solving the time dependent Schrödinger equation. It should be mentioned though, that a rich range of general quantum effects can easily be demonstrated within the theory. A numerical scheme for computing bound ground states and their energies is also presented in the paper, while a more detailed analysis of this scheme has been carried out in H. Herrmann's masters thesis [15].

4.1 Overview over Adaptive-Grid Methods

Doing away with the wave function in this approach comes at the cost of introducing many parallel worlds. World here means an entire universe containing some number of particles and each world parallel to it is a copy of that universe in the sense that it has exactly the same particles, but in a different configuration. Each world by itself is governed by the same set of Newtonian equations of motion, too. Quantum effects then arise as a consequence of an interaction between these worlds, which enters the equations as a potential term. The limiting dynamics in the limit of infinitely many worlds is Bohmian mechanics. If only a finite number is considered, the resulting dynamics are only an approximation, but one which can in theory be made arbitrarily precise by increasing that number. Leaving the physical interpretation aside, the idea, which is central to the numerical scheme, is the following.

For a finite number N of worlds, a quantity U_N , whose gradient approximates the quantum force term in Bohm's original formulation of Bohmian mechanics (2.10), can be inferred from the configurations $\{\mathbf{x}^i\}_{i=1,\dots,N}$ of the worlds. The general dynamical law within the many interacting worlds concept is a system of Nnd coupled second order differential equations, which in analogy to Bohm's traditional law of motion reads

$$m_i \frac{d}{dt} \mathbf{x}_i^k(t) = -\nabla_{\mathbf{q}_i} V(\mathbf{q})|_{\mathbf{q}=\mathbf{x}^k(t)} - \nabla_{\mathbf{x}_i^k} U_N(\mathbf{x}^1(t), \dots, \mathbf{x}^N(t)) \quad (4.14)$$

in components. Here $i = 1, \dots, n$ subscripts the particle contained inside a particular world, while $k = 1, \dots, N$ selects a world from the ensemble of worlds, so \mathbf{x}_i^k is a vector in \mathbb{R}^d , denoting the position of a particle with mass m_i . The *interworld interaction potential* U depends on all the configurations of all worlds. Like the original quantum potential its negative gradient is supposed to result in a repulsive force between worlds that have similar configuration, i.e. are close within \mathbb{R}^{nd} .

Fundamental to the construction of the many interacting worlds theory is the requirement that the configuration space expectation values of an observable ϕ should of course coincide with the predictions of textbook quantum mechanics

$$\langle \phi \rangle_\psi = \int |\psi(\mathbf{q})|^2 \phi(\mathbf{q}) d\mathbf{q} \quad (4.15)$$

$$\stackrel{!}{=} \lim_{N \rightarrow \infty} \frac{1}{N} \sum_{k=1}^N \phi(\mathbf{x}^k) \underset{N \text{ large}}{\approx} \frac{1}{N} \sum_{k=1}^N \phi(\mathbf{x}^k) \quad (4.16)$$

which holds if the worlds $\{\mathbf{x}^k\}_{k=1,\dots,N}$ are $|\psi|^2$ -distributed. This means that in the many interacting worlds framework all worlds contribute to any expectation value with equal weight. Quantum statistics then simply arise from the lack of knowledge, which world the observer occupies.

So far it remains unclear how U should be constructed. By choosing the observable ϕ to be energy and comparing the average quantum energy as of equation (4.15) to the average energy per world (4.16), one can deduce the expression

$$U_N(\mathbf{x}^1, \dots, \mathbf{x}^N) = \sum_{k=1}^N \sum_{i=1}^n \frac{\hbar^2}{8m_i} \left(\frac{\nabla_{\mathbf{q}_i} P(\mathbf{q})|_{\mathbf{q}=\mathbf{x}^k(t)}}{P(\mathbf{x}^k)} \right)^2. \quad (4.17)$$

4. Employing Bohmian Trajectories in Quantum Numerics

See [4, p. 6] or [15, p. 16f] for the detailed rearrangement of terms necessary to derive it. P here simply stands for the probability density $|\psi|^2$. To get entirely rid of the reliance on the wave function, the actual P needs to be replaced by an estimate derived from the configuration of the ensemble of worlds.

By suggesting one such estimate P_N for a single particle of mass m in one spatial dimension, the following toy implementation of the interworld interaction potential has been put forward [4] for, among others, numerical purposes by the proponents of many interacting worlds. When $n = d = 1$, the world coordinates simply become real numbers and the ensemble of worlds can be ordered such that $x^1 < x^2 < \dots < x^N$. Furthermore define $x^k = -\infty$ if $k \leq 0$ and $x^k = \infty$ if $k > N$. Continuing from equation (4.16), one can observe that for any smooth interpolation P_N of the empirical density of the N worlds

$$\frac{1}{N} \sum_{k=1}^N \phi(x_k) \approx \int_{-\infty}^{\infty} P_N(q; x^1, \dots, x^N) \phi(q) dq \quad (4.18)$$

$$\approx \sum_{k=2}^N \int_{x_{k-1}}^{x^k} P_N(x^k; x^1, \dots, x^N) \phi(x^k) dq \quad (4.19)$$

$$= \sum_{k=2}^N (x^k - x^{k-1}) P_N(x^k; x^1, \dots, x^N) \phi(x^k) \quad (4.20)$$

must hold for sufficiently large N and a sufficiently slowly varying function ϕ . This motivates an ansatz for the values of P_N evaluated at each world position x^k ,

$$P_N(x^k; x^1, \dots, x^N) = \frac{1}{N(x^k - x^{k-1})} \approx \frac{1}{N(x^{k+1} - x^k)} \quad (4.21)$$

which relies on the assumption that the interworld separation is also slowly varying. It turns out, that even without specifying how P_N should interpolate the density in between these points, this is already sufficient for deriving one possible choice of the interworld potential. For N still large enough, the derivative of P_N at a world position x^k can be approximated by

$$P'_N(x^k; x^1, \dots, x^N) \approx \frac{P_N(x^{k+1}; x^1, \dots, x^N) - P_N(x^k; x^1, \dots, x^N)}{x^{k+1} - x^k}, \quad (4.22)$$

so that $\frac{\nabla P}{P}$ in equation (4.17) is approximated by

$$\frac{P'_N(x^k; x^1, \dots, x^N)}{P_N(x^k; x^1, \dots, x^N)} \approx N \left(P_N(x^{k+1}; x^1, \dots, x^N) - P_N(x^k; x^1, \dots, x^N) \right) \quad (4.23)$$

$$\approx \frac{1}{x^{k+1} - x^k} - \frac{1}{x^k - x^{k-1}}. \quad (4.24)$$

Plugging this in gives an expression for the interworld potential

$$U_N(x^1, \dots, x^N) = \frac{\hbar^2}{8m} \sum_{k=1}^N \left(\frac{1}{x^{k+1} - x^k} - \frac{1}{x^k - x^{k-1}} \right)^2. \quad (4.25)$$

4.1 Overview over Adaptive-Grid Methods

Finally, evaluating equation (4.14) with this toy potential for a single, one-dimensional particle per world yields

$$m \frac{d}{dt} x^k(t) = -\nabla_q V(q)|_{q=x^k(t)} + \frac{1}{4m} \left(\theta^{k+1}(x^1, \dots, x^N) - \theta^k(x^1, \dots, x^N) \right) \quad (4.26)$$

as the equation of motion in atomic units for each world particle, where

$$\theta^k(x^1, \dots, x^N) = \frac{1}{(x^k - x^{k-1})^2} \left(\frac{1}{x^{k+1} - x^k} - \frac{2}{x^k - x^{k-1}} + \frac{1}{x^{k-1} - x^{k-2}} \right). \quad (4.27)$$

This coupled set of equations of motion approximately reproduces the trajectories of Bohmian theory, provided that initially the worlds are $|\psi|^2$ -distributed and each one has an initial velocity according to equation (4.13). To keep the worlds distributed with respect to $|\psi|^2$ at later times, the previously mentioned requirements need to be fulfilled sufficiently well. In such a case the wave function can then be reconstructed from the ensemble of worlds. Recalling the polar decomposition of Madelung (4.1), the modulus R can be estimated from the distribution of worlds in configuration space with statistical methods, for example Gaussian kernel density estimation, which is described in section 4.1.3. S on the other hand can be obtained from equation (4.2) by integration of the worlds' velocities.

This sense of solving the Schrödinger equation is different from Wyatt's approach, where at each grid point, i.e. for each trajectory, explicit values of R and S are known. By calculating similar information on the fly from the distribution of worlds instead of carrying it along, the numerical scheme can be evaluated much more easily within the many interacting worlds paradigm. The computational efficiency is a consequence of having the equations of motion coupled through the positions of neighboring worlds within the potential here rather than a coupling through the evaluation of derivatives on the unstructured grid as in Wyatt's algorithm. Because the potential U at each world's position involves both² neighboring worlds, the positions of five worlds altogether enter into the equation of motion for each world, its own one and its two neighbors on each side.

The interworld interaction force term in equation (4.26) is of such nature, that two worlds approaching each other in terms of configuration space coordinates are repelled from each other. This can be seen more easily from the expression of the potential U in equation (4.25), which diverges in such a case. Thus a preservation of the ordering of worlds $x^1 < x^2 < \dots < x^N$ is always ensured. The concept of the interworld interaction potential per se is not necessarily easy to grasp at first glance, particularly with the introduction here being more on the concise side. The reader can find more exhaustive treatments elsewhere [4, 15]. Important to keep in mind however, is that U_N itself does not constitute an approximation to the quantum potential Q^ψ . Only their gradients happen to coincide approximately for large N .

²One can think of inserting worlds at negative and positive infinity, so the terms in equations (4.25) and (4.27) are trimmed suitably for the worlds x^1 and x^N .

4.1.3 New Density Estimation Based Hybrid Methods

In summary, the many interacting worlds method is numerically much more efficient than Wyatt's method. This is because the computationally involved process of calculating the second derivatives of the two wave function components R and S on an unstructured grid can be avoided. They are replaced by an equation, which approximates the dynamics of a Bohmian particle instead. It is however unsatisfactory, that there is no guarantee for the quality of that approximation. Instead, the accuracy of the outcome depends on a number of assumptions about certain quantities varying sufficiently slowly.

It is almost self-suggesting to combine the advantages of the two approaches into a hybrid algorithm. On the one hand, at the heart of the many interacting worlds algorithm is the idea of using the distribution of the Bohmian grid's grid points to obtain an estimate of the probability density $|\psi|^2$ and to process it on the fly. This information is available redundantly when using Wyatt's approach on a Bohmian grid, where R is known explicitly at each grid point and the grid points are R^2 -distributed. On the other hand, with Wyatt's method it is always guaranteed that the particles move with the correct velocity given by equation (4.2) – provided that S is accurately computed. This aspect is not only obfuscated in the many interacting worlds law of motion, but since the number of worlds N must be finite for any numerical application, the proofs that the limiting dynamics reproduce Bohmian mechanics are not applicable to the numerics.

The hybrid scheme works as follows: if a smooth function P , which approximates $|\psi|^2$ sufficiently well, is known at each time t , then \sqrt{P} can be plugged into equation (2.11) to obtain an approximation \hat{Q} to the quantum potential. The system of working equations in Wyatt's algorithm simplifies significantly, when P can be determined from the configurations at t . Only equations (4.2) and (4.7) remain in that case, because with \hat{Q} available externally there is no need to keep track of the C -amplitudes and equations (4.9) and (4.10) can be dropped. The resulting algorithm then also has the nice property, that at most one first derivative, ∇S , needs to be evaluated on the non-uniform grid. All the others, ΔS , ∇C and ΔC are only needed for computing the quantum potential.

The task now is to find an expression for the probability density function P at each step of the integration, so that P can be used to obtain \hat{Q} . This means that the hybrid algorithm must have a mapping M

$$M: \mathbb{R}^{Nd} \rightarrow \mathcal{C}(\mathbb{R}^{nd}, \mathbb{R}_0^+) \quad (4.28)$$

$$\{\mathbf{x}^k\}_{k=1,\dots,N} \mapsto P = M(\{\mathbf{x}^k\}_{k=1,\dots,N}) \quad (4.29)$$

at its disposal, which transforms an ensemble of configuration space coordinates into a continuous, positive and normalized function from configuration space to positive numbers. Because P is to approximate $|\psi|^2$, $P(\mathbf{q})$ should be nonzero at any \mathbf{x}^k and P should be differentiable at least twice around these points.

Restricting again to the one-dimensional single particle case $n = d = 1$, one possible way of implementing M will be described here. It is essentially one of the most promising methods

4.1 Overview over Adaptive-Grid Methods

analyzed by H. Herrmann in his master's thesis on numerically obtaining ground states using many interacting worlds [15]. In his work the approach is described both more generally and in more detail than the scope of this chapter permits.

Constructing a density estimate from an empirical distribution without knowing anything about its functional form is a problem commonly encountered in statistics and goes by the name of *non-parametric density estimation*. As such, many techniques to tackle this problem have been developed. One of these is making use of a *kernel density estimator*, which assigns a kernel function K to each point of the data set

$$P(q) = M\left(\{x^k\}_{k=1,\dots,N}\right)(q) = \frac{1}{Nh} \sum_{k=1}^N K\left(\frac{x^k - q}{h}\right), \quad (4.30)$$

where h is called *bandwidth parameter*. In principle, the kernel function K itself can be any positive, normalized function in order to make P a probability density function. In addition, the hybrid algorithm here requires K to be differentiable at least twice. For the course of this chapter, K is taken to be a normalized Gaussian,

$$K(x) = \frac{e^{-\frac{1}{2}x^2}}{\sqrt{2\pi}}. \quad (4.31)$$

For this kernel the bandwidth h then basically is a normal distribution's standard deviation.

Two limitations with the approach so far should be pointed out however, before explaining how to perform the remaining crucial step of determining the bandwidth parameter h from the data. The first is that taking the same Gaussian at every data point limits the achievable accuracy of the resulting estimate P . A better approach is to adapt each one separately by using N different h_k s. Secondly, to reflect the repulsiveness of the quantum potential when two Bohmian world particles approach each other, it is preferable to place the Gaussian into the center between two of them instead of on top of one. Because in this one-dimensional single particle scenario the ensemble $\{x^k\}_{k=1,\dots,N}$ is sorted, the notation $x^{k+\frac{1}{2}}$ can be used to abbreviate $\frac{1}{2}(x^{k+1} + x^k)$ expressing this in-between position. All this turns equation (4.30) into

$$P(q) = M\left(\{x^k\}_{k=1,\dots,N}\right)(q) = \frac{1}{(N-1)\sqrt{2\pi}} \sum_{k=1}^{N-1} \frac{1}{h_{k+\frac{1}{2}}} \exp\left(-\frac{\left(x^{k+\frac{1}{2}} - q\right)^2}{2h_{k+\frac{1}{2}}^2}\right), \quad (4.32)$$

This scheme can now be called *adaptive Gaussian kernel density estimation*.

Determining the now $N - 1$ bandwidth parameters requires additional input. If for each $x^{k+\frac{1}{2}}$ the probability density were known to be $p_{k+\frac{1}{2}}$, then the system of equations

$$P\left(x^{k+\frac{1}{2}}\right) \stackrel{!}{=} p_{k+\frac{1}{2}} \quad (4.33)$$

could still not be solved explicitly, but numerically a set of recursive relations like

$$h_{k+\frac{1}{2}} \leftarrow h_{k+\frac{1}{2}} \frac{P\left(x^{k+\frac{1}{2}}\right)}{p_{k+\frac{1}{2}}} \quad (4.34)$$

4. Employing Bohmian Trajectories in Quantum Numerics

or

$$h_{k+\frac{1}{2}}^{-1} \leftarrow h_{k+\frac{1}{2}}^{-1} - c \left(P(x^{k+\frac{1}{2}}) - p_{k+\frac{1}{2}} \right) \quad (4.35)$$

would provide a way to find appropriate values for the bandwidth parameters. In equation (4.34), the recursion will always converge and can be stopped for example, when for all $h_{k+\frac{1}{2}}$ the difference between consecutive values is less than $\varepsilon_a + \varepsilon_r h_{k+\frac{1}{2}}$ for given absolute and relative tolerances $\varepsilon_{a,r}$. For a value of c between 2 and 15, equation (4.35) seems to work well and is faster. As a first guess, the bandwidths can be taken as $h_{k+\frac{1}{2}}^{-1} = p_{k+\frac{1}{2}}$ initially.

The values of $p_{k+\frac{1}{2}}$ are the last missing ingredient to the hybrid algorithm. This is where the many interacting worlds density estimate P_N finally enters the stage. Following the same reasoning which led to equation (4.21), one can see that

$$p_{k+\frac{1}{2}} = \frac{1}{N(x^{k+1} - x^k)} \quad (4.36)$$

provides a suitable value. With this, the Gaussian kernel density estimation ultimately boils down to a smooth interpolation between the values given by a variant of the many interacting worlds density estimate. But unlike before, it is now no longer true that only some neighbors on the grid interact with each other. Rather, through the recursion relation (4.35), each x^k is coupled to each other one in principle. Because the tails of a Gaussian curve fall off rapidly however, here also mainly neighboring ones affect each other in practice. Figure 4.2 shows an example distribution and its estimate P , together with the single Gaussians that P consists of. The approximation looks very good almost everywhere.

The last equation needed for the hybrid algorithm follows from applying the chain rule to equation (2.11). Substituting $|\psi|$ by \sqrt{P} results in the approximate quantum potential

$$\hat{Q} = \frac{2P''P - P'^2}{4P^2}. \quad (4.37)$$

Summing up, the working equations are (4.2), (4.7) with Q^ψ replaced by \hat{Q} and (4.32) with (4.35) and (4.36) to compute \hat{Q} in equation (4.37). Because with each integration step, the estimated density changes only little, the set of bandwidths from the previous step can be reused in the recursion relation (4.35) and only if the values fail to converge after a large number of steps, the $h_{k+\frac{1}{2}}$ need to be reinitialized. This saves a significant amount of computation time.

In fact, the idea of fitting the empirical density with Gaussian functions has already shown up in the literature some time ago. One such quantum trajectory algorithm has been proposed by E. Bittner and J. Maddox [47], another one by S. Garashchuk and V. Rassolov [48]. The former one uses Bayesian statistics to fit a parametrized density estimate and hence differs quite a bit from the non-parametric approach here. The latter one however is very similar to the algorithm proposed above. Even though the authors there start off from a completely different point of view the “approximate quantum potential” resulting from their concept is essentially obtained in the same way. They rely on the density within a volume element being a conserved quantity, which in essence is what equation (4.36) stands for. The only difference between the algorithm

4.1 Overview over Adaptive-Grid Methods

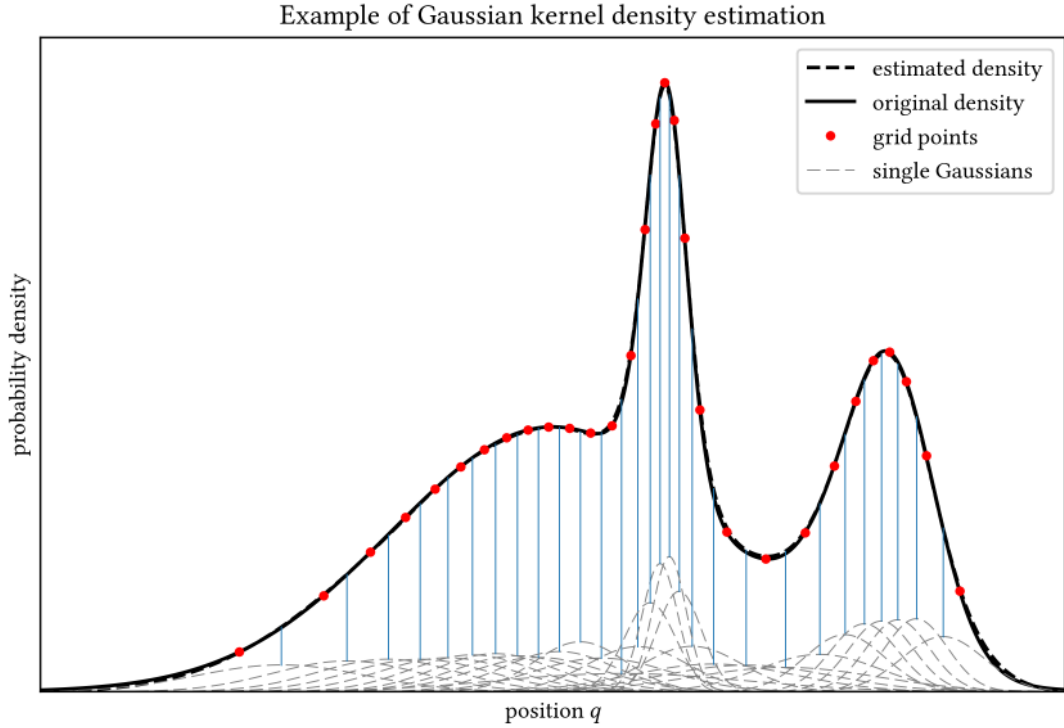


Figure 4.2: The original probability density compared to a density estimated from a distribution of 30 points using the adaptive Gaussian kernel density estimator. The center between two adjacent grid points is associated to one of the small gray Gaussians at the bottom. These sum up to the estimated density. Recursion terminated for $\varepsilon_a = 10^{-3}$ and $\varepsilon_r = 10^{-4}$.

there and the one here is that they use another minimization procedure to fit a variable number of Gaussians to density. Also that number of Gaussians can automatically adapt to the problem at hand.

The hybrid algorithm described above can be altered to improve its numerical results. The variant now proposed in the remainder of this chapter is completely new, at least to the author's knowledge. It is based on an idea originally brought up by H. Herrmann [49]. In both, Wyatt's original and the hybrid method, S is integrated in equations (4.2) and (4.7). By using the chain rule, these can be rewritten to integrate the complex quantity

$$\tilde{S} := e^{iS} \quad (4.38)$$

instead of S , resulting in

$$\frac{dx}{dt} = \frac{\overline{i\tilde{S}(x, t)}}{m} \nabla S(q, t) \Big|_{q=x(t)}. \quad (4.39)$$

as the analogue of equation (4.2) while

$$\frac{d\tilde{S}(x, t)}{dt} = i\tilde{S}(x, t) \left(\frac{1}{2m} |\nabla \tilde{S}(x, t)|^2 - V(x) - Q^\psi(x, t) \right) \quad (4.40)$$

4. Employing Bohmian Trajectories in Quantum Numerics

is the counterpart to equation (4.7). All other equations of the original hybrid method remain unchanged. The decomposition of the wave function $\psi = R\tilde{S}$ still maintains some similarity with Madelung's one (4.1). R remains the same, while \tilde{S} is now a complex-valued function with $|\tilde{S}| = 1$. In analogy to the *complex trajectory method* [8], this algorithm will be referred to as the *complex phase hybrid method*, but otherwise has nothing to do with that one.

One may ask why to even bother integrating the phase in this way. Not only do the equations look more complicated than before, also integrating a complex function \tilde{S} instead of the real-valued S demands more memory and computation time. The reason is that integrating equation (4.7) is numerically subtle when the wave function has a node, i.e. $\psi = 0$ somewhere between grid points. At a node, the value of S jumps to a value $S \pm \pi$. This is problematic when evaluating derivatives of S around such a point, as will be seen from the numeric analysis in the second half of this chapter. When integrating the complex phase, this discontinuity does of course not go away, but the magnitude between going from \tilde{S} to $-\tilde{S}$ is smaller, namely 2. It will be interesting to see how this reduction of the jump in the phase by about a third changes the impact of a node onto the numeric time evolution.

A last point to mention is that it is not straightforwardly possible to directly modify Wyatt's original algorithm into a complex phase variant. The reason is, that the expression

$$\Delta S = -i \left(|\nabla \tilde{S}|^2 + \bar{\tilde{S}} \Delta \tilde{S} \right) \quad (4.41)$$

inserted into equation (4.9) accumulates numerical errors³ so quickly that it results in extremely unstable dynamics. So only after getting rid of this equation in the hybrid approach, the transformation from real into complex phase becomes feasible.

4.2 Discussion of Results

For each of the adaptive-grid methods described above, the working equations can readily be integrated using a Runge–Kutta integrator. The numerical data presented in this section has been obtained from the same library as the one superficially described in chapter 3. Proper initial conditions must be given of course. Here, the initial grid is generated by dividing the image of the cumulative distribution function into N equispaced intervals. The x^k at time t_0 are then taken to be the preimage of the points at the center of these intervals. This means that for $k = 1, \dots, N$

$$\int_{-\infty}^{x^k} |\psi(q, t_0)|^2 dq \stackrel{!}{=} \frac{1}{N} \left(k - \frac{1}{2} \right) \quad (4.42)$$

holds.

When comparing the numeric results of the trajectory methods to the explicit solutions for some simple wave functions, as done below, the appropriate measure of accuracy would be the

³This can already be seen from $|\nabla \tilde{S}|^2$ having to cancel the real part of $\bar{\tilde{S}} \Delta \tilde{S}$ in order to have equation (4.41) result in a real quantity. This will not be the case unless the derivatives are evaluated with extreme accuracy.

4.2 Discussion of Results

L^2 -norm of their difference. For Wyatt's algorithm, R and S must be interpolated from a number of discrete samples of these functions in order to obtain ψ . In case of the many interacting worlds and hybrid methods, R is not even part of the whole concept and a reconstruction from the trajectory density is necessary. The exact way in which the reconstruction and interpolation are performed for each individual method will of course have an impact on any deviation in the L^2 -norm. To avoid such an effect and because approximating the Bohmian dynamics is an intrinsic property that all the approaches here share, the benchmark is instead carried out in terms of how well the dynamics of the adaptive grid reproduce the genuine Bohmian trajectories.

Doing this graphically also makes it possible to observe, in which part of configuration space the velocity constraint (2.9) is violated first in case the dynamics break down⁴ at some point. In Bohm's original formulation of Bohmian mechanics in terms of equation (2.10) with the quantum potential Q^ψ evaluated from an already known solution of the Schrödinger equation, this constraint is automatically fulfilled as long as it is fulfilled initially. As S. Goldstein and W. Struyve have pointed out [50], a violation can have severe consequences by means of trajectories being able to escape from their wave packet. In numeric applications, where the wave function is computed along with the trajectories, finite precision inherently limits the achievable accuracy and errors can accumulate, so this issue is something particularly important to keep an eye on.

4.2.1 Dispersion of a Gaussian Wave Packet

The nonlinear de Broglie dispersion relation gives rise to one of the most fundamental phenomena of quantum mechanics. Unless being held together by a suitably shaped external potential, any non-plane wave solution of the Schrödinger equation disperses over time. This provides the first test cases for the numerical methods of this chapter. For a Gaussian initial wave packet representing a one-dimensional single particle, both the dispersion in free space and the time evolution of a so-called coherent state in a harmonic oscillator potential will be checked here.

The analytic time-dependent wave function in the former case is given by

$$\psi(t, q) = \frac{\sqrt{\sigma}\sqrt{\sigma^2 - it}}{\sqrt[4]{\pi}\sqrt{\sigma^4 + t^2}} e^{-\frac{q^2(\sigma^2 - it)}{2\sigma^4 + 2t^2}}. \quad (4.43)$$

Here the width parameter σ^2 is defined to be *twice* the variance of the probability density for notational simplicity of the equations which will follow later and describe interference. Starting with zero velocity and the parameters of table 4.1 at $t = 0$, figures 4.3 and 4.4 show the dispersion of such a wave packet.

Within the wave packet, the density in Wyatt's algorithm was interpolated by a polynomial of order 6 from a sliding window of 3 neighbors on each side. Towards the boundary, the window size remained constant but the maximum degree was reduced linearly down to two, as suggested by the findings of [44]. For the hybrid methods, using the nearest neighbor on each side

⁴For example, a crossing of two trajectories in the one-dimensional single particle case indicates numerical failure, because a proper quantum potential would always prevent this from happening.

4. Employing Bohmian Trajectories in Quantum Numerics

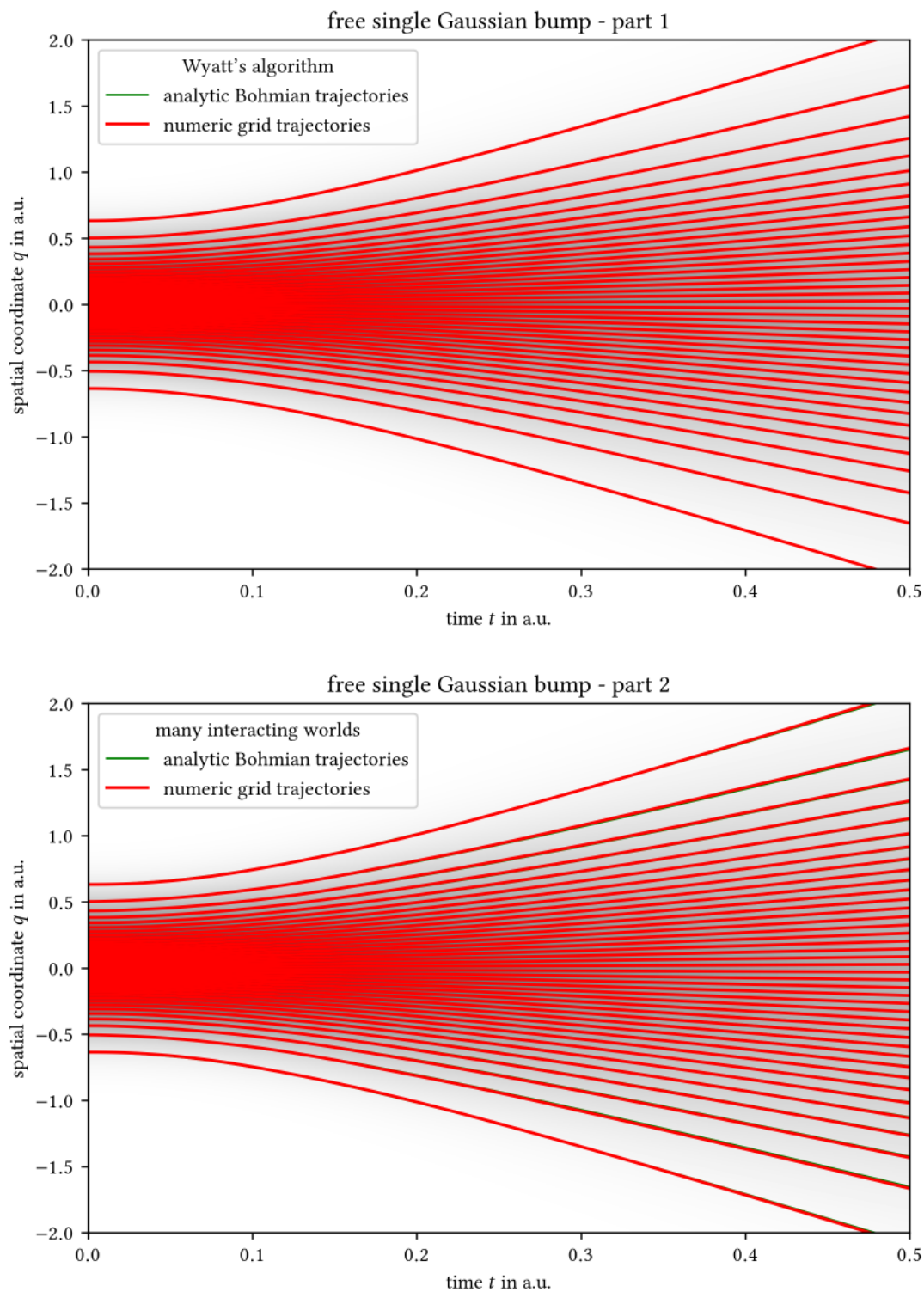


Figure 4.3: Comparison of the time evolution obtained from Wyatt's (top) and the many interacting worlds method (bottom) for a dispersive single Gaussian wave function. Background shaded with the probability density of the analytic solution.

4.2 Discussion of Results

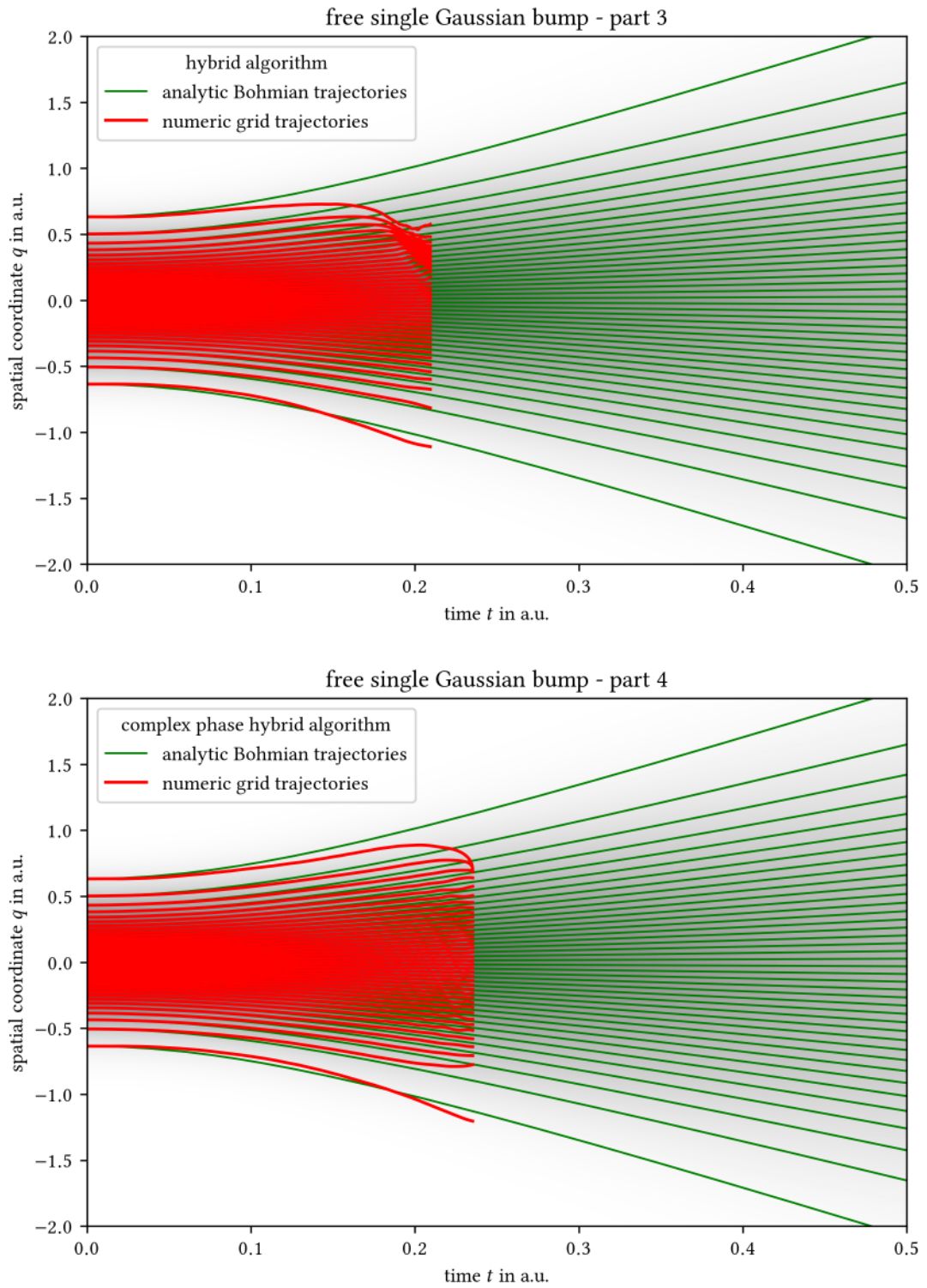


Figure 4.4: Comparison of the time evolution obtained from the hybrid algorithm (top) and its complex phase variant (bottom) for a dispersive single Gaussian wave function. Background shaded with the probability density of the analytic solution.

4. Employing Bohmian Trajectories in Quantum Numerics

general parameters to all methods		additional parameters to the hybrid methods	
N	40	ε_a	$2.5 \cdot 10^{-3}$
σ	0.4	ε_r	$2.5 \cdot 10^{-6}$

Table 4.1: Parameters used to compute figures 4.3 to 4.14. All quantities are given in their respective atomic units.

to interpolate the phase with a quadratic polynomial turned out to give the most stable results. The hybrid algorithms are, however, still not stable at all, quite the contrary is actually true. Both, the straightforward hybrid algorithm with Gaussian kernel density estimation and its complex phase variant feature trajectories on the fringe of the wave packet, whose dynamics deviate and start running towards their neighbors. Instead of being repelled by those neighbors, the deviation is reinforced until the dynamics break down. The grid dynamics of Wyatt's method on the other hand perfectly agree with the Bohmian trajectories that were obtained from letting the analytic wave function (4.43) guide the ensemble. The world trajectories of the many interacting worlds approach do not cover the Bohmian trajectories to the same extent, but the agreement is still excellent.

On time scales a hundred times larger, the results of these two methods still agree very well with the correct trajectories, as figure 4.5 shows. In the elementary case here, the limiting dynamics is very simple, after a short while the world particle just moves with constant velocity. Nonetheless, the picture exemplifies the main advantage of the adaptive grid methods over the traditional approach on a fixed lattice, where a humongous number of grid points is required to both resolve the wave function initially and to capture it in its entirety after a long time. The adaptive Bohmian grid can consist of even less than 40 trajectories instead.

The article originally proposing the many interacting worlds algorithm [4] also contains an investigation of how well the numerics work out. It deserves attention that the authors there did not distribute the initial world positions according to equation (4.42), which yields the convincing results above. Instead, their initial distribution is such that

$$\int_{-\infty}^{x^k} |\psi(q, t_0)|^2 dq \stackrel{!}{=} \frac{k}{N+1} \tag{4.44}$$

holds, which places the worlds slightly more towards the center. For the outermost worlds, the approximate quantum force in the many interacting worlds approach seems to be very sensitive to such a difference in the initial distribution. Figure 4.6 contains the dynamics of such an ensemble of worlds. Clearly, the worlds, particularly the ones in the Gaussian's tails, disperse more than expected from the guidance by the wave function. The same defect is also visible in the original numerical data [4, fig. 6] of two interfering Gaussians and can easily be fixed without introducing any new problems by distributing according to equation (4.42) instead. In fact, the symmetry and the regularity of the initial distribution are very important properties for the algorithm to produce acceptable results. Using for example Monte Carlo sampling to obtain a $|\psi(t=0)|^2$ -distribution of worlds requires such an absurdly large number of them to make the many interacting worlds method work, that any advantage of the adaptive

4.2 Discussion of Results

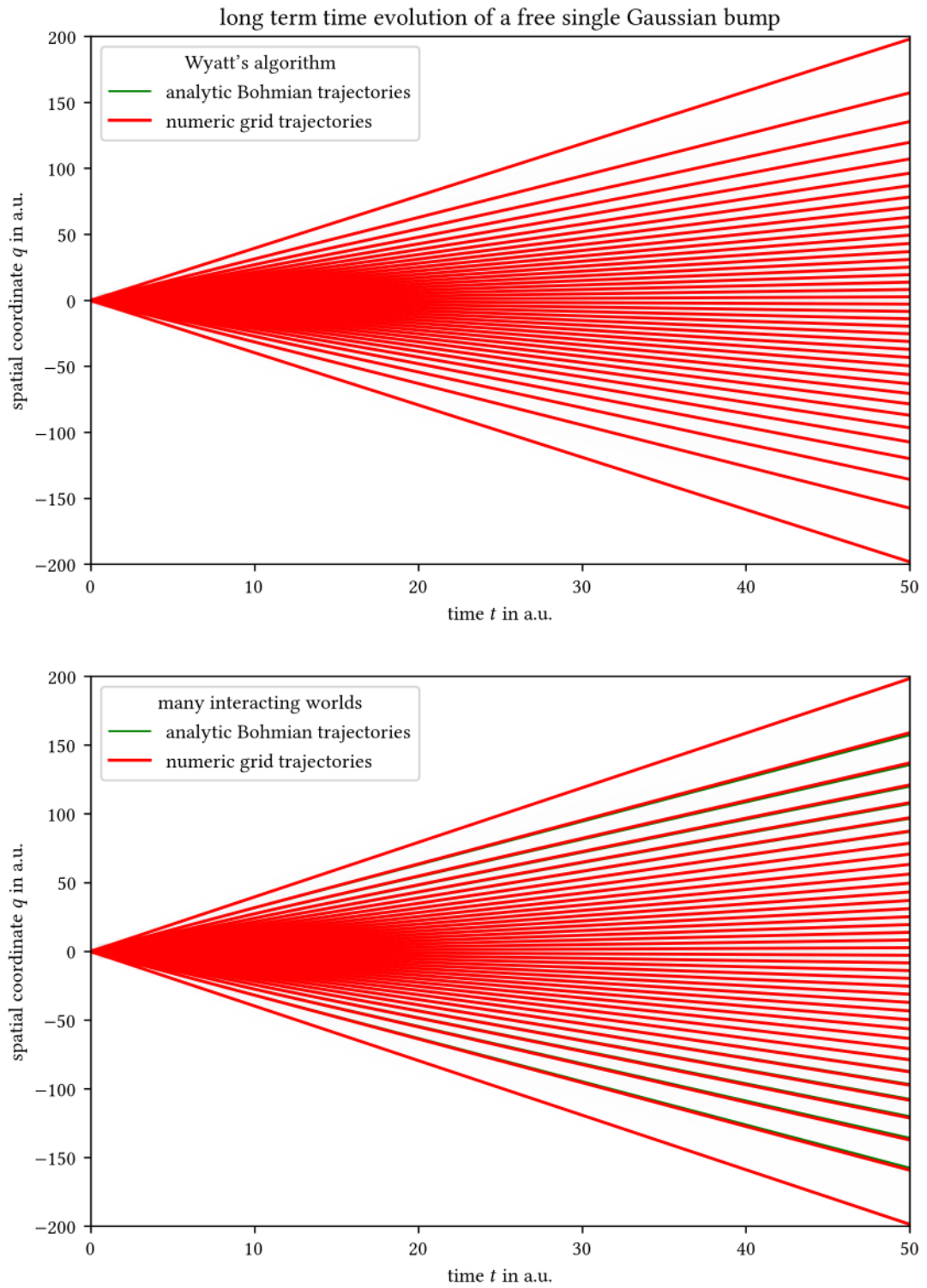


Figure 4.5: Same as figure 4.3, but with much longer time scales.

4. Employing Bohmian Trajectories in Quantum Numerics

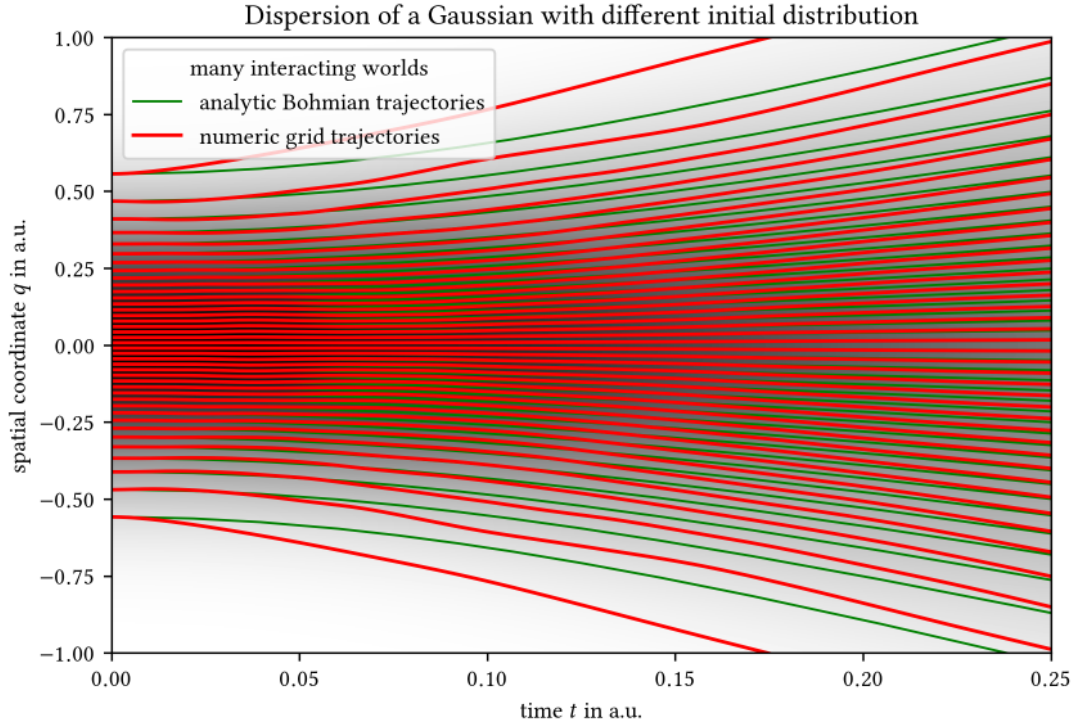


Figure 4.6: Initial dispersion of a Gaussian bump using the many interacting worlds method when distributing the worlds initially according to equation (4.44) as in [4].

grid in terms of grid point reduction is completely lost. Note that with Wyatt's method there are no such issues, since it is much more tolerant when it comes to the initial distribution in configuration space deviating from the density.

The next test case is rather the opposite of wave packet dispersion. As already discovered by Schrödinger himself [51], for a harmonic potential

$$V(q) = \frac{\omega^2}{2} q^2 \quad (4.45)$$

with parameter ω , the Schrödinger equation has a solution

$$\psi(t, q) = \frac{e^{-\frac{\mu^2}{4}}}{\sqrt[4]{\pi}} \exp\left(\frac{i\omega}{2} - \frac{\mu^2}{4} e^{2i\omega t} + \mu q e^{i\omega t} - \frac{q^2}{2}\right), \quad (4.46)$$

which describes a Gaussian that is initially displaced from the center of the potential by a distance μ and moves back and forth in the potential without changing its shape. On page 87, Chapter 5 provides more details about this wave function, which is called a *coherent state* in the context of photons trapped inside a cavity. But here none of that will be needed as only the time evolution of the wave packet in the potential is of interest.

4.2 Discussion of Results

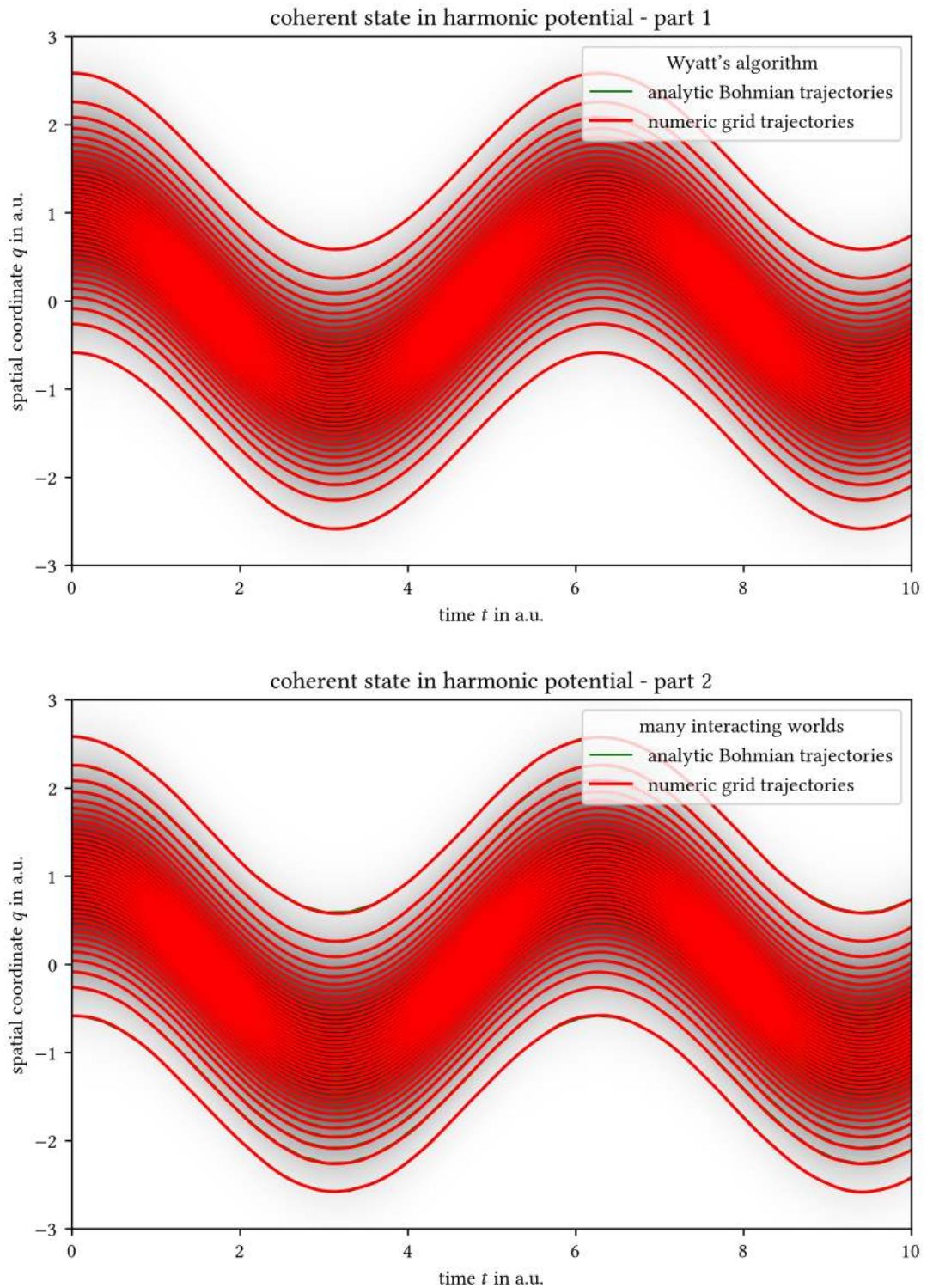


Figure 4.7: Comparison of the time evolution obtained from Wyatt's (top) and the many interacting worlds method (bottom) for a coherent state in a harmonic potential. Background again shaded with the probability density of the analytic solution.

4. Employing Bohmian Trajectories in Quantum Numerics

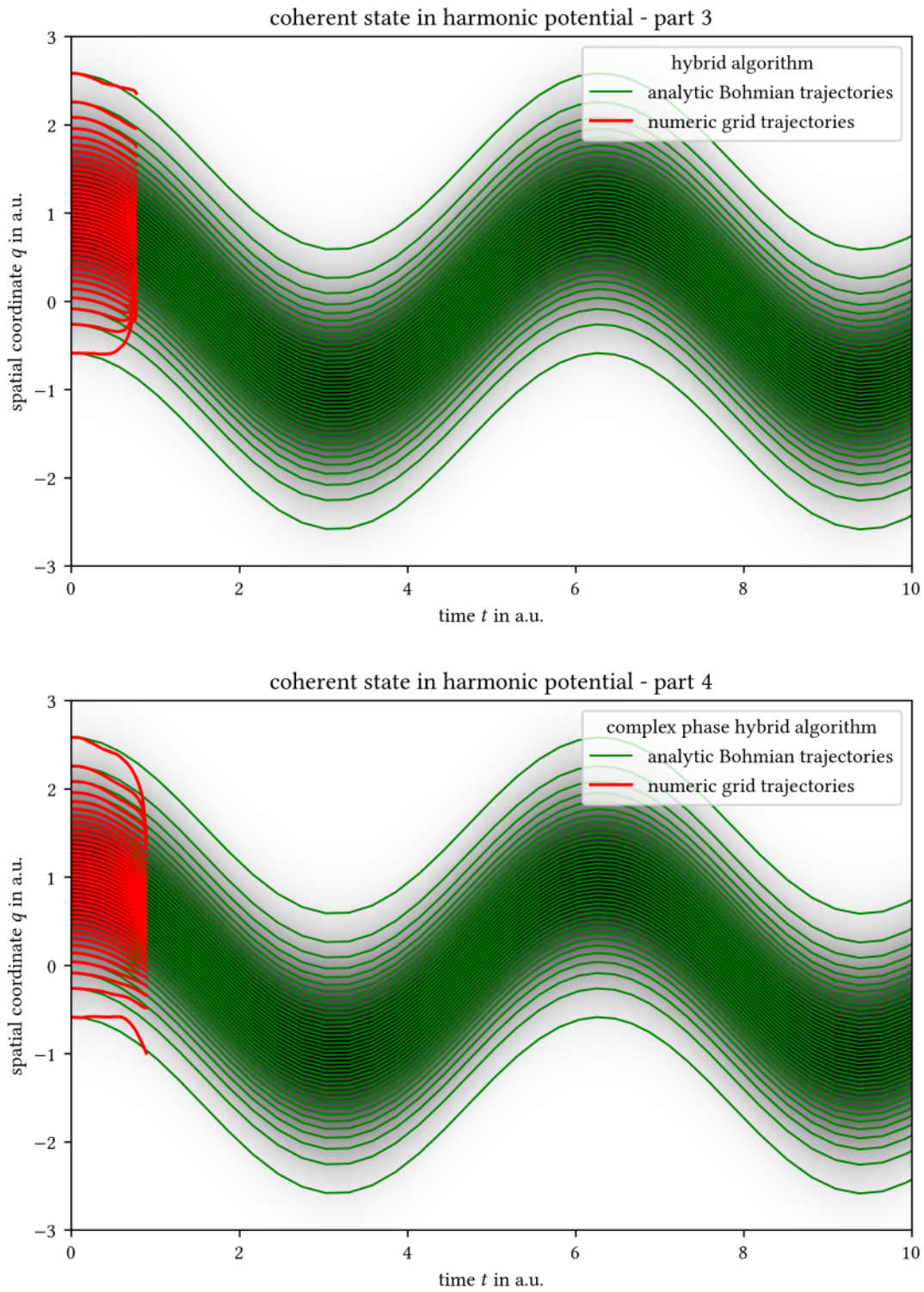


Figure 4.8: Comparison of the time evolution obtained from the hybrid algorithm (top) and its complex phase variant (bottom) for a coherent state in a harmonic potential. Background again shaded with the probability density of the analytic solution.

4.2 Discussion of Results

With the values of ω and μ both chosen to be unity in atomic units in addition to the parameters of table 4.1, figures 4.3 and 4.4 contain the results from all four methods again. As before, Wyatt's and the many interacting worlds algorithm produce trajectories in excellent agreement with the analytic Bohmian ones. Directly estimating the density using Gaussian kernels proves to be problematic again, though, even for a wave function that just translates in space without changing shape.

To understand the nature of this problem, it is instructive to look at figure 4.9. It contains the density P estimated from the ensemble of grid points at initial time and compares it to the density ρ^ψ associated with the explicit solution ψ . Despite both functions not differing visibly, the difference becomes apparent when subtracting one from the other. At the center of the grid, the approximation is very good with a relative deviation of the estimate from the analytic density being less than half a percent. The fringes of the grid however, feature a deviation of almost three percent, which is about an order of magnitude larger. This is probably a consequence of the tails of the single Gaussians, which P is composed of, adding up. The denominator in equation (4.37) being too small then leads to an estimated quantum potential \hat{Q} which is too big and thus the outermost grid points do not move away as fast as they should. This then leads to an even bigger deviation for those grid points, and the process self-enhances

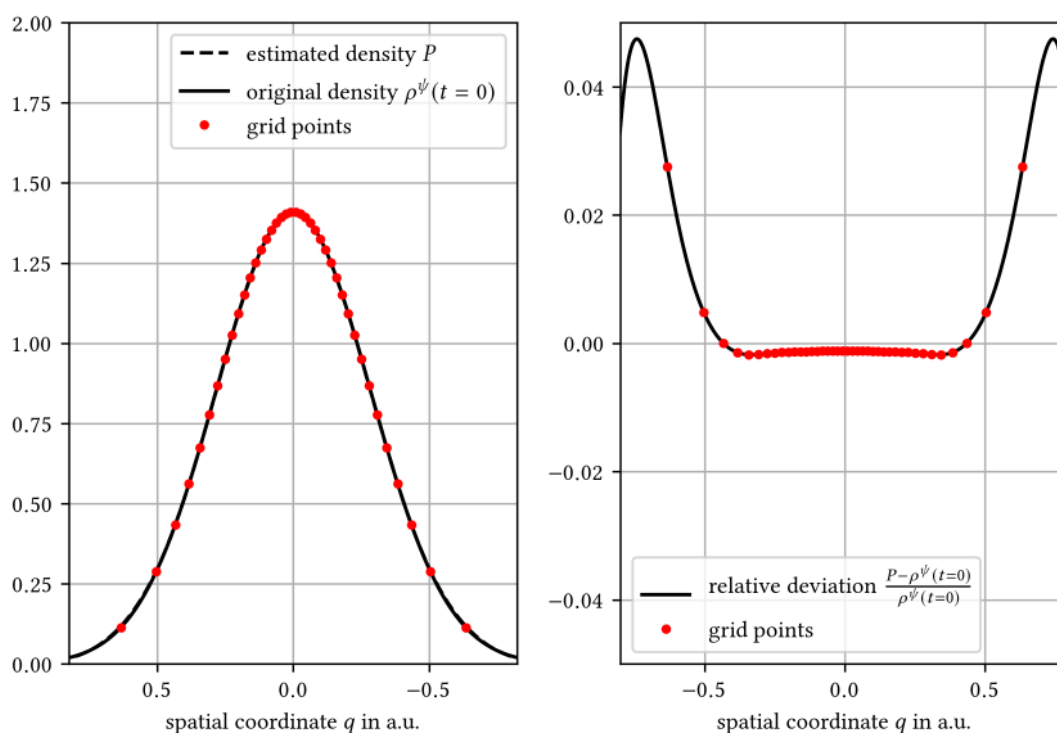


Figure 4.9: Comparison of the result of Gaussian kernel density estimation to the original density. Left: P and ρ^ψ on top of each other. Right: difference between them. Tolerance parameters as in table 4.1

until the whole grid becomes affected. Imposing stricter tolerances ϵ_a and ϵ_r reduces the effect in principle, but unfortunately when doing so, the recursion formula (4.35) quickly runs into convergence problems.

4.2.2 Superpositions of Gaussian Wave Packets

Apart from dispersion, the other fundamental effect in quantum mechanics is interference of wave packets. By superposing two one-dimensional Gaussians with same or opposite signs separated by a distance d , the wave functions ψ_+ and ψ_- given by

$$\psi_{\pm}(q, t) = \frac{\sqrt{\sigma}\sqrt{\sigma^2 - it}}{\sqrt[4]{\pi}\sqrt{\sigma^4 + t^2}\sqrt{2 \pm 2e^{-\frac{d^2}{4\sigma^2}}}} \left(e^{-\frac{(\sigma^2 - it)(\frac{d}{2} + q)^2}{2\sigma^4 + 2it^2}} \pm e^{-\frac{(\sigma^2 - it)(-\frac{d}{2} + q)^2}{2\sigma^4 + 2it^2}} \right) \quad (4.47)$$

display patterns of constructive or destructive interference.

To obtain the numerical data below from these wave functions, a separation of $d = 2$ a.u. is to be added to the parameters in table 4.1 on page 53. The previous subsection already demonstrated that the hybrid methods suffer from inaccuracies originating at the fringe of the grid which ultimately impact the stability of numeric solutions. To still draw meaningful conclusions about how well these approaches can deal with interference effects, this issue is fixed below by having the wave functions (4.47) directly guide the four outermost trajectories. Of course it is unsatisfactory to require the explicit solution in order to numerically solve for the same wave function, but this is only done here for the sake of being able to benchmark the method. In practice there should be no problem with having those trajectories guided by the interworld interaction force for example. Not only does the many interacting worlds algorithm seem to yield robust results at the wave packet fringes, as can also be seen from the figures below, it has even been shown [4] that an inverse-square scaling law of precisely the same form as the one in quantum mechanics holds in this theory.

The results for two constructively interfering Gaussians are presented in figures 4.10 and 4.11. Again, the adaptive grid in Wyatt's algorithm is quantitatively very close to the actual Bohmian trajectories, while the many interacting worlds give rise to trajectories with good agreement, but they deviate slightly when looking closely. Furthermore, when world trajectories come close together, they begin to display a slight wiggleness with worlds moving back and forth. This is then passed on to neighboring trajectories subsequently, ultimately pushing them from the main maximum into the minima beside it. With the four outermost trajectories externally fixed, the hybrid algorithms still do not perform well when it comes to constructively interfering wave packets. As can be seen on page 61, the straightforward kernel density algorithm again suffers from instability and the evolution breaks down quickly. The alternative one, which integrates the complex phase, on the other hand remains stable, but fails to reproduce the interference pattern correctly. Instead, both the maximum and the minima are covered more or less uniformly by the adaptive grid after a while, thus preventing a successful continuation of the algorithm because the quantum potential can no longer be estimated adequately.

4.2 Discussion of Results

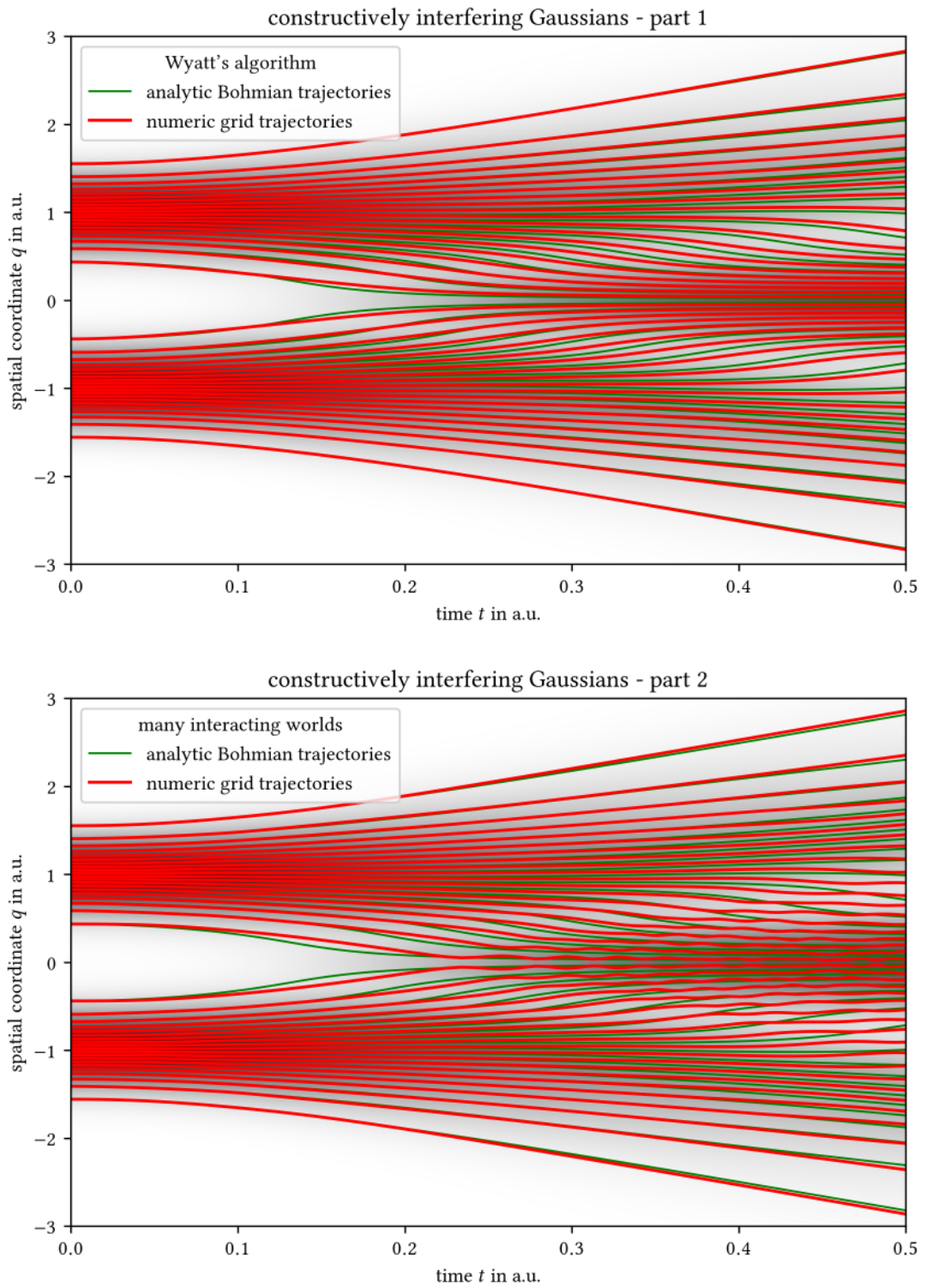


Figure 4.10: Comparison of the time evolution obtained from Wyatt's (top) and the many interacting worlds method (bottom) for two constructively interfering Gaussian wave functions. Background again shaded with the probability density of the analytic solution.

4. Employing Bohmian Trajectories in Quantum Numerics

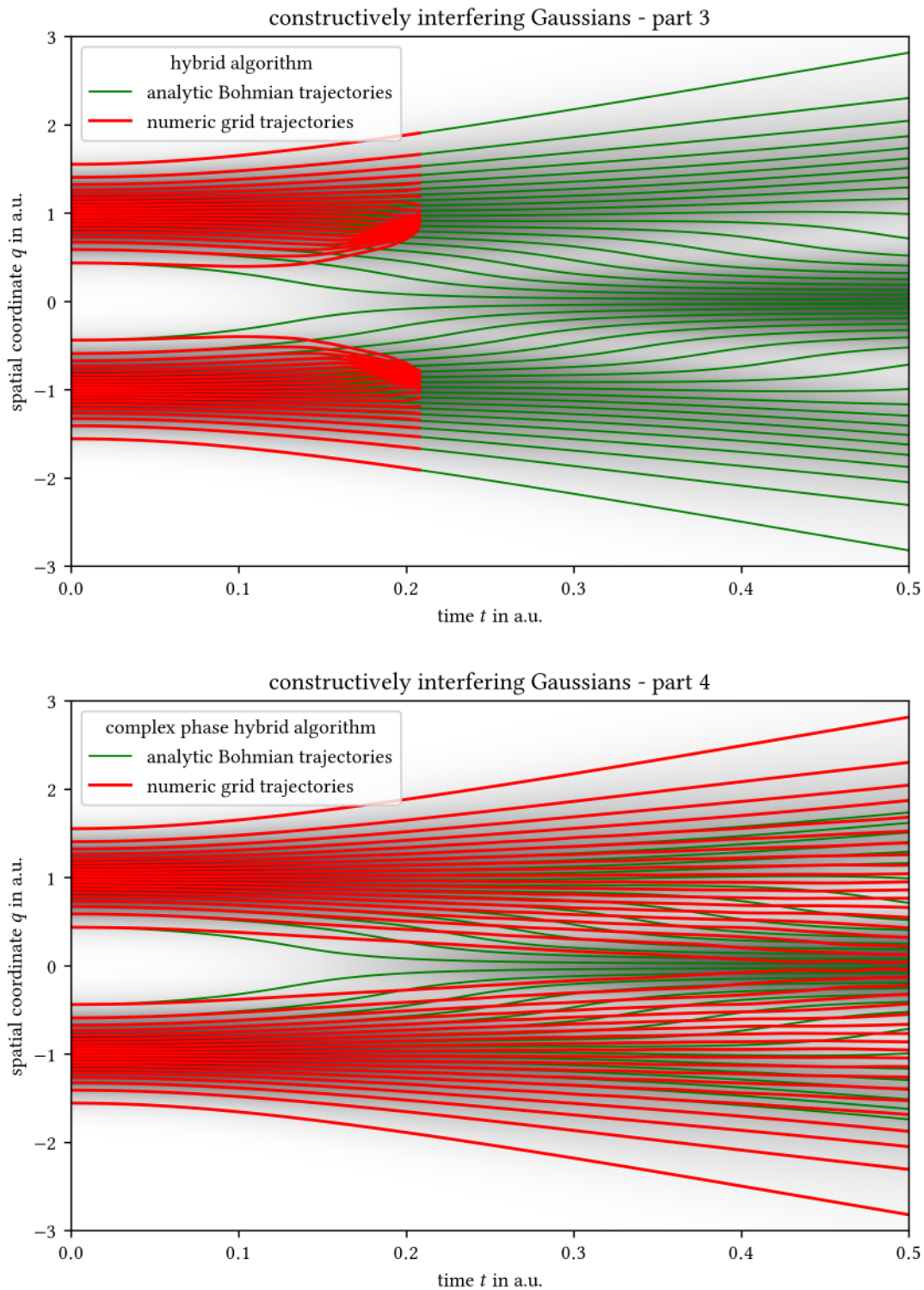


Figure 4.11: Comparison of the time evolution obtained from the hybrid algorithm (top) and its complex phase variant (bottom) for two constructively interfering Gaussian wave functions. Background again shaded with the probability density of the analytic solution.

4.2 Discussion of Results

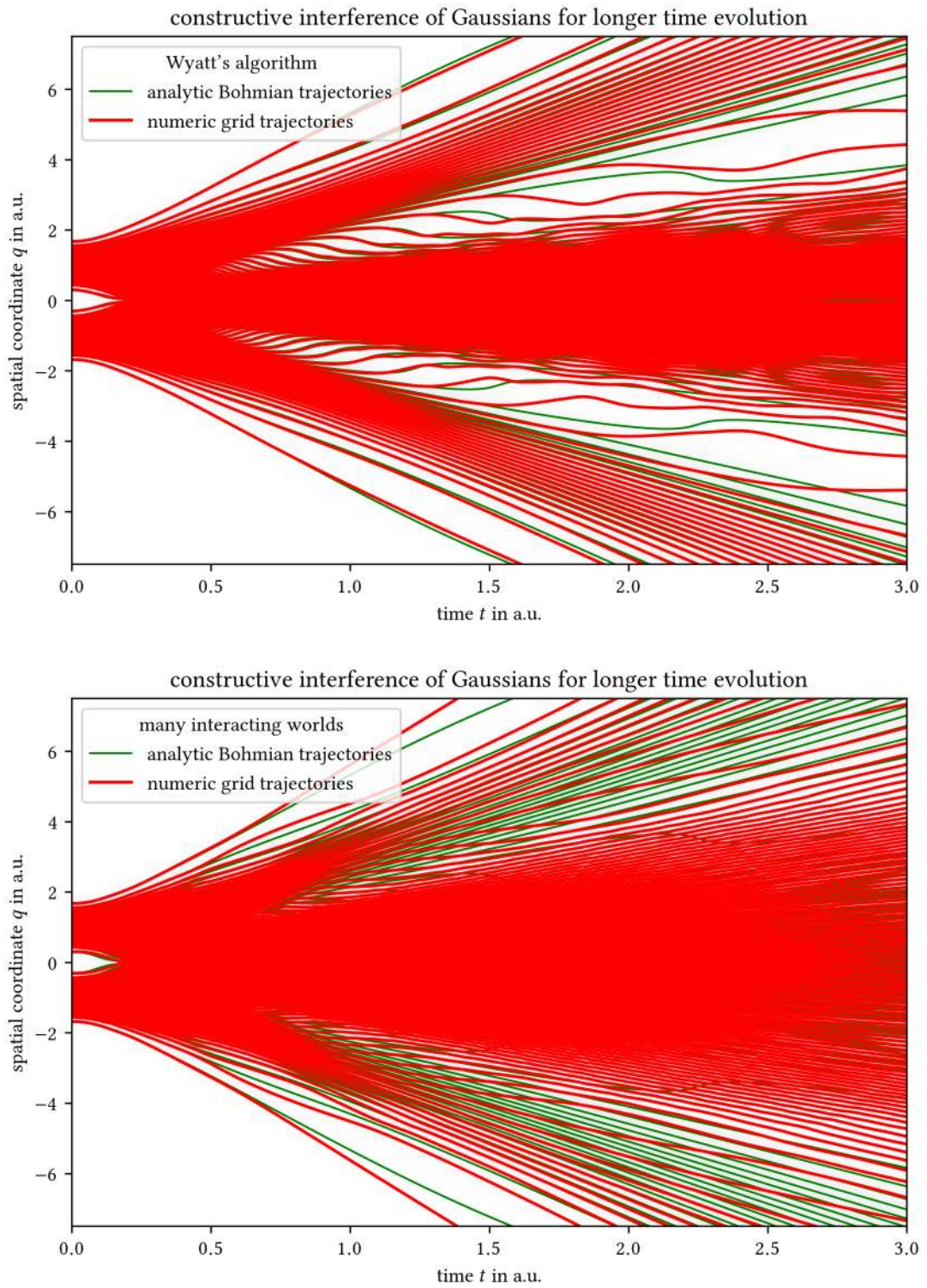


Figure 4.12: Same as figure 4.10, but with longer time scales and more trajectories.

4. Employing Bohmian Trajectories in Quantum Numerics

It is worth having a second look at the evolution of the two more successful approaches for longer times. This can be done in figure 4.12, where the ensemble size N has been raised to a value of 120. Now, a significant difference between the two methods is easily spotted. With the many interacting worlds method, the interference picture is considerably distorted. The main maximum consists of too many trajectories while the minima are much less pronounced and have been shifted outwards. Further increasing N does not fix this mismatch between numerical results and analytic prediction. This is in contrast to Wyatt's algorithm, where not only the locations of but also the ratio of trajectories in main and side maxima are reproduced correctly up to a small number and where a larger ensemble size does also reflect directly in an improvement of accuracy.

Now it is finally time to investigate the most interesting case of two Gaussians interfering destructively. Figures 4.13 and 4.14 contain the results for ψ_- . This case is interesting, because it makes all four approaches fail in one way or the other. The repulsive nature of the wave function node in the origin, which coincides with a diverging quantum potential there, is not at all reflected in numerical results for any of them. Wyatt's algorithm quickly becomes unstable after trajectories cross from one side of the node onto the other side. The many interacting worlds method remains stable, but its dynamics can at first glance not be distinguished from their counterpart in the constructive interference case and clearly do not match the expected interference pattern. The reason for this will be explained in the following subsection. The plain hybrid algorithm has its dynamics collapse quickly as well, so just as with the case of constructive interference before it is not saved by the external guiding of the outermost trajectories.

But what is interesting is the complex phase hybrid algorithm. It performs by far best on the integration time domain with most of the trajectories accurately reproducing the ones obtained from the explicit solution. Upon closer inspection however, one can see a few trajectories departing from the lower wave packet from the last quarter of the plot onward. Soon after, these will also cross through the node into the upper packet and eventually the dynamics will also break down in a way similar to Wyatt's algorithm. With a focus on the algorithms dealt with in this section, the following subsection presents a short discussion of this issue which always arises when ψ is zero somewhere on configuration space.

4.2 Discussion of Results

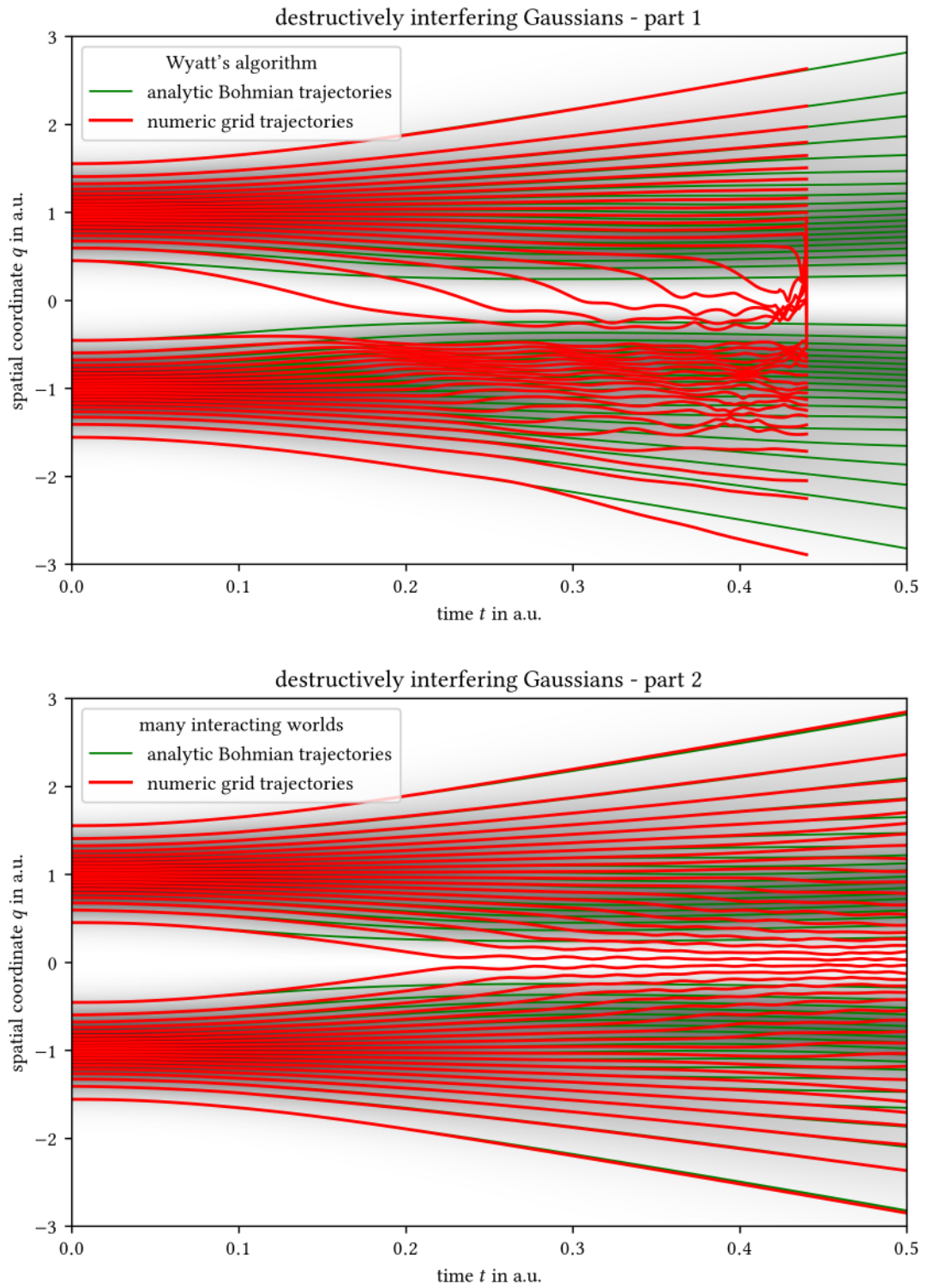


Figure 4.13: Comparison of the time evolution obtained from Wyatt's (top) and the many interacting worlds method (bottom) for two destructively interfering Gaussian wave functions. Background again shaded with the probability density of the analytic solution.

4. Employing Bohmian Trajectories in Quantum Numerics

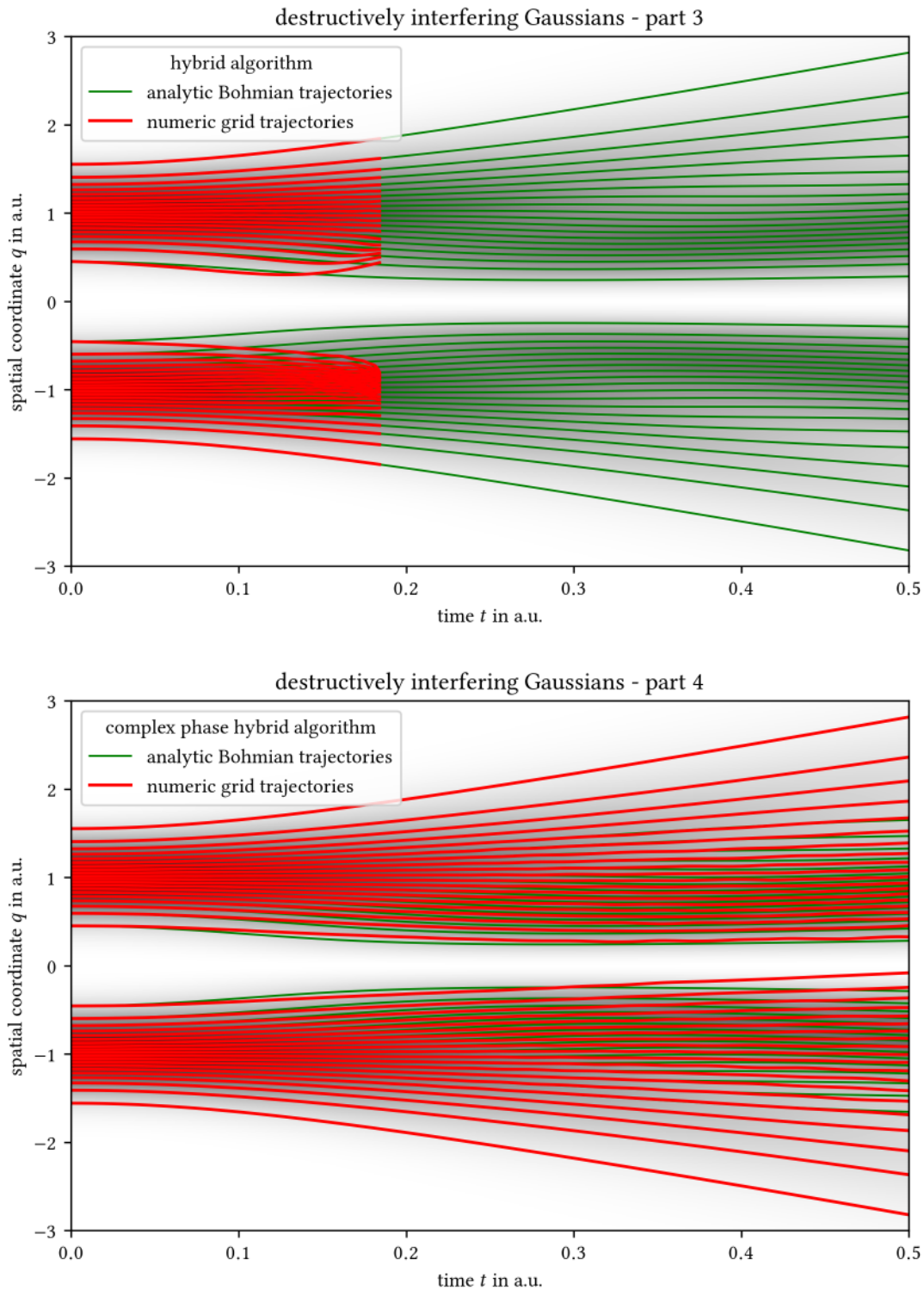


Figure 4.14: Comparison of the time evolution obtained from the hybrid algorithm (top) and its complex phase variant (bottom) for two destructively interfering Gaussian wave functions. Background again shaded with the probability density of the analytic solution.

4.2 Discussion of Results

4.2.3 The Node Problem

The difficulty which adaptive grid algorithms face with wave function interference is known as the *node problem* in the literature. It is caused by the discontinuity in the phase when the wave function passes through zero, which poses a problem to evaluating the derivatives on the unstructured grid. Because wave function nodes are a very general feature, for example in a scattering scenario or with any excited state in a potential, the general applicability of these algorithms is severely limited without further modifications.

As mentioned before, when comparing Wyatt's algorithm to the complex phase hybrid method at a node, the phase jumps by a smaller amount when integrating the complex phase function e^{iS} . This may explain why in the presence of a node the complex phase hybrid algorithm works best out of the three approaches which explicitly integrate the phase. The discontinuity only being less severe but not completely removed leaves little hope that this approach can be used to fix the node problem in general, though.

By construction, the many interacting worlds algorithm is very robust and its numeric time evolution does not easily come to a halt with the adaptive stepsize Runge–Kutta integrator. Nonetheless, the dynamics completely fail to acknowledge the presence of a node in the bot-

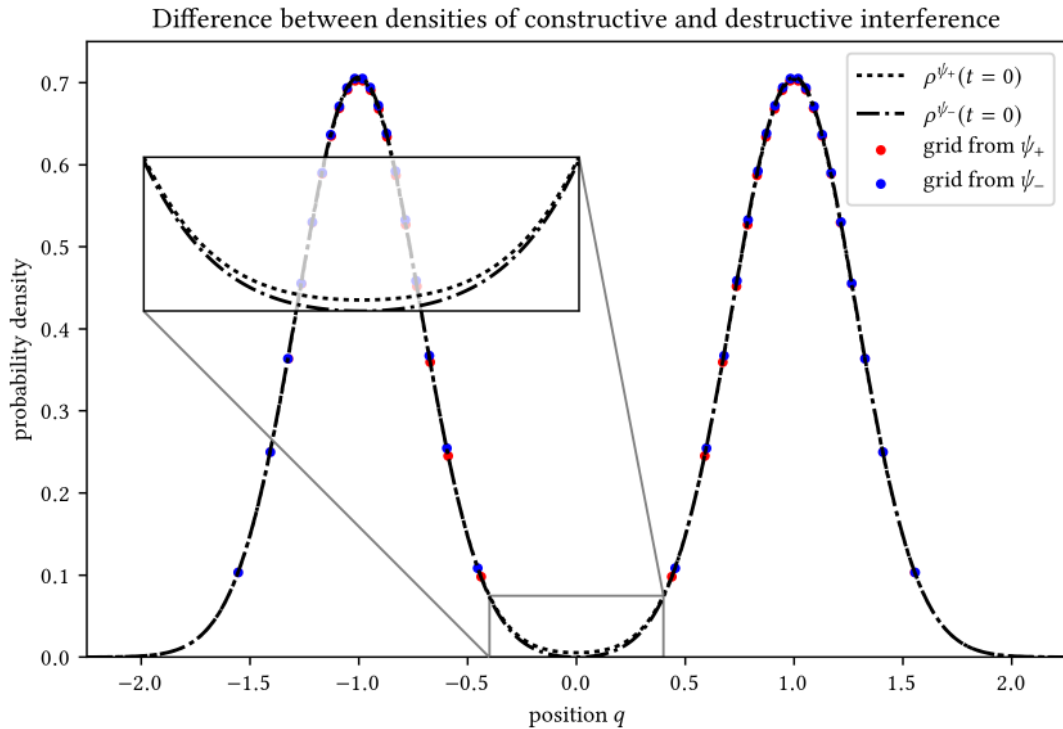


Figure 4.15: Comparison of the initial probability densities and world distributions in the two cases of constructive and destructive interference when parametrizing ψ_{\pm} with $d = 2$ and the values of table 4.1 as used in figures 4.10 to 4.14.

4. Employing Bohmian Trajectories in Quantum Numerics

tom plot of figure 4.13. Instead, when compared to figure 4.10, the trajectories look very similar. To understand how this comes about, it is important to realize that the choice of parameters to equation (4.47) lead to initial conditions in all the figures 4.10 to 4.14 which make it particularly tricky to distinguish between constructive and destructive interference by looking at the density only. Figure 4.15 illustrates the initial distributions obtained from ψ_+ for constructive and from ψ_- for destructive interference. With $d = 2$ a.u. and the parameters of table 4.1, the distribution of worlds is almost identical in both cases. This follows from the probability densities being almost indistinguishable, with the difference only becoming visible when zooming in.

Here, in the easiest case of perfect symmetry around the node, in order to distinguish between constructive and destructive interference the algorithm must be able to tell apart a density that is quadratic⁵ at first order around and touches zero at a node from a density whose first nonzero terms upon expansion are a constant and a polynomial of order four. With five world positions contributing to the interworld interaction force for each world, this does not pose a problem in principle. The sole reason why it does not work here, is that the number of worlds is too small to be able to sense the difference. Unfortunately, when increasing N , the majority of additional worlds will end up within the peaks of the density. For an increase near the node, a disproportionately large number of worlds need to be added.

In this way, the Bohmian grid, on which all four algorithms in this section operate, turns out to be blessing and curse simultaneously. The advantage of reducing the total number of grid points by distributing them according the probability density backfires by leaving some important domain of configuration space underrepresented and it turns out that good resolution there is essential. For Wyatt's algorithm, several strategies for dealing with this problem are known [3]. Some of them exploit the linearity of the Schrödinger equation. Examples would be the *covering function method* [52] and *bipolar decomposition* [53]. The former successively overlays the wave function by another one whenever a node forms somewhere, so that the node is covered up. The original part of the superposition is reconstructed afterwards. The latter decomposes the wave function into counterpropagating parts, a special carrier wave and a node-free component which are propagated separately. Unlike with Wyatt's algorithm, for which the adaptive grid is not required to be Bohmian, the application of versions of these methods adapted to the many interacting worlds or hybrid methods requires a redistribution of the grid points. Also, these strategies require a technique to detect nodes as they are forming. As figure 4.15 has shown, solely making use of the grid point distribution on a Bohmian grid turns it into a very hard task to distinguish a node from a legitimate dip in the density. All that prevents those strategies from being used with the three new algorithms in this chapter.

Another property of Wyatt's approach is, that not only are the grid points not required to be distributed according to the density, but the velocity of the grid points does not even need to be given by the Bohmian guiding law itself. Using an arbitrary Lagrangian–Eulerian grid, c.f. equations (4.11) and (4.12), instead of a Bohmian one, the grid points can be directed purposefully towards nodal regions, where they are needed. This solution to the node problem

⁵Recall that the density is the square of the wave function, so ψ linearly passing through the zero axis becomes a polynomial of second order in the density.

4.3 Conclusions

is of course also not applicable to the many interacting worlds and hybrid methods, because those rely on the grid being Bohmian in order to dispose of integrating the magnitude of the wave function explicitly.

A last resort is to redistribute the regions containing nodes onto a traditional uniform grid, which also has been done successfully with Wyatt's method [54]. Difficulties at the boundaries between the Bohmian adaptive and the stationary grid with equal spacing between grid points arise when trying to do the same with the other algorithms in this section, though. In summary, this means that none of the techniques, which were developed to cope with the node problem within the broad picture of Wyatt's algorithm are straightforwardly applicable to the other approaches analyzed in this chapter. Within the scopes of these, the only promising way of dealing with the node problem is to redistribute the entire integrated quantities onto a static grid and continuing the time evolution using the tools available there as soon as a node starts developing. In case all nodes vanish again after a while, it may then be possible to redistribute back to an adaptive grid.

4.3 Conclusions

Starting off from the established adaptive grid algorithm of Wyatt, which is particularly useful for long-time numeric integration of the Schrödinger equation, this chapter constitutes an analysis of how it compares to three other algorithms, and how reliable their results are. Those other ones, one that directly arises from the many interacting worlds description of quantum mechanics and two algorithms, which rely on Gaussian kernel density estimation, attempt to simplify Wyatt's method by means of getting rid of all of but at most one of the derivatives, which are hard to evaluate on the non-uniform grid. To the knowledge of the author, the last two approaches, one being a direct hybrid between Wyatt and many interacting worlds, the other one differing by integrating the phase as a complex variable, have not been proposed before in their specific implementation. The simplification is always accomplished by disposing of the information about the wave function's magnitude, which is available redundantly if Wyatt's algorithm is used on a Bohmian grid. Doing this gives rise to approximate dynamics, which reproduce Bohmian trajectories in the limit of a large number of grid points by inferring that information on the fly from the configuration of grid points at each integration step. In this way the computational complexity is reduced significantly, particularly when also dropping the explicit phase information as in the many interacting worlds case.

The analysis of how the algorithms perform, divided into an investigation of the correct reproduction of wave packet dispersion and interference effects, ultimately highlights the limitations of the different methods. The many interacting worlds algorithm features robust dynamics that correctly reproduce the dispersion of a Gaussian wave packet even if the number of worlds is relatively small. This requires the worlds being correctly distributed initially and in fact the numerical data proves to be quite sensitive to this initial distribution. The one used here arguably is an improvement over the distribution used in the original publication of the algorithm. When testing constructive interference of two Gaussians, the resulting set of trajectories is qualitatively correct. Quantitative deviations however do not seem to be easily fixed by increasing

4. Employing Bohmian Trajectories in Quantum Numerics

the number of worlds, despite the many interacting worlds theory exactly reproducing the dynamics of Bohmian mechanics in the continuum limit. For destructive interference, almost identical dynamics as in the constructive case are produced, which is obviously incorrect. The many interacting worlds paradigm works entirely without the notions of quantum potential and even wave functions in the equations of motion. Without these quantities, it does hence not seem to be easy to distinguish between a wave function node and a simple dent in the density caused by overlapping wave packet tails, at least for the parameters chosen here.

Both hybrid methods have problems with stability, caused by an inaccuracy of the density estimation at the outermost grid points. Theoretically it should be possible to fix this issue by guiding those grid points using the interworld interaction force, which has proven to yield correct results at the tails of wave packets, at least if the worlds are distributed initially in the appropriate way as mentioned above. Here however, the explicit solution of the Schrödinger equation to be solved numerically for benchmarking the algorithms is known anyway. So using this wave function directly to guide the outermost trajectories eliminated the need for such a modification. With this fix in place, the plain hybrid algorithm still remains unstable when wave packets interfere, so that this direct hybridization attempt turns out to be unsuccessful. The particular implementation of the idea here, using $N - 1$ Gaussians to interpolate the density estimate on a grid of size N , thus proves to be completely inferior to the related algorithm independently proposed by Garashchuk and Rassolov. Using a different fitting procedure and restricting to a smaller number of fitting functions, their implementation reproduces the dynamics of a coherent state in the harmonic oscillator potential at least. They have not presented calculations involving interference, though.

The combination of Wyatt and many interacting worlds into a hybrid algorithm simplifies the set of equations in a way that allows for a variant, in which the complex exponential e^{iS} instead of the real-valued phase S is integrated. This complex phase hybrid method suffers from the same problem of instability unless its outermost trajectories are held in place externally. With that done, this algorithm does however perform best out of the whole set tested here, when two Gaussians interfere destructively. In particular, its results are better than Wyatt's algorithm, which otherwise works extremely well as long as wave function nodes are absent. However, the complex phase hybrid variant is also not able to distinguish between constructively and destructively interfering Gaussians by solely looking at the density of grid points. This manifests in qualitatively incorrect dynamics in the constructive case.

The only algorithm that can essentially tell these two cases apart is Wyatt's algorithm on a Bohmian grid, whose dynamics rapidly collapse for destructive interference, though. Nodes do thus present a fundamental problem to all these algorithms operating on adaptive Bohmian grids. Even with the complex phase hybrid algorithm, along the grid there is still a discontinuous jump in the integrated variable, which impedes the derivative evaluation on the non-structured grid and eventually leads to a collapse of its dynamics. The many interacting worlds method does not need to evaluate any spatial derivative explicitly and thus its dynamics never break down, even if nodes are present. It does however illustrate how a Bohmian adaptive grid is blessing and curse at the same time. On the one hand, the total number of grid points reduces, because only those parts of configuration space are covered, where a wave function is currently present. On the other hand, regions around nodes, where a good grid resolution

4.3 Conclusions

is essential, are undersampled. When the grid points are distributed according to the probability density, most of them are placed in regions where there are already many and only a sub-proportionate part ends up where they are needed most.

Since all four algorithms in this section use a Bohmian adaptive grid, each one is affected by this problem. However, by disposing of the density information redundantly contained in Wyatt's algorithm, the Bohmian grid becomes fundamental to the three other ones. Wyatt's algorithm however can also be formulated with respect to any other distribution and dynamics of grid points. This ultimately prevents the strategies of dealing with the node problem in Wyatt's approach from being adapted to the other algorithms. The only possibly useful application worth being investigated in a further study would be combining the many interacting worlds algorithm with a more general variant of Wyatt's method on an arbitrary Lagrangian–Eulerian grid. Since the many interacting worlds algorithm features stable dynamics, but is not sensitive to nodes, even more, by construction covers nodal regions with trajectories for any manageable number of worlds, one could use these trajectories to guide the grid on which Wyatt's equation of motion are integrated. This may or may not provide a remedy to the burden that when using arbitrary Lagrangian–Eulerian grids to cope with the node problem, they need to be controlled and guided manually after identifying problematic regions by inspection. The property of not wasting grid points in large areas, where the wave function is nearly zero at times and does not change much, would of course be retained.

Finally, it should be pointed out, that the usefulness of the new algorithms discussed in this chapter is further limited by the lack of a straightforward answer to the question of how to generalize these methods to a configuration space with dimension greater than one. For the toy model here, in which a wave function describes a single particle in one spatial dimension, the problematic scaling behavior in the number of grid points on a uniform, static grid does of course not pose an actual practical problem with modern computing technology. So far, an interworld interaction potential for more than one dimension has not been proposed yet. In his master's thesis, H. Herrmann attempted to generalize the dissipative many interacting worlds algorithm for finding stationary states by using a two-dimensional version of Gaussian kernel density estimation, similar to what is used in the hybrid algorithm here. Even for the simplest cases, this has proved to be challenging and the problems with boundary worlds encountered there are likely going to have much worse consequences when trying to solve the time-dependent Schrödinger equation instead of the time-independent one, because errors in the dynamics accumulate over time. So for now, the question of efficient algorithms of the kind discussed in this chapter for more than one spatial dimension remains open.

5 Employing Bohmian Trajectories in Semiclassical Numerics

This chapter continues in the spirit of Dirac’s quote on page 35, but the approach here is fundamentally different from chapter 4. It heads more into the direction of what Dirac probably had in mind, when he suggested the development of “approximate practical methods of applying quantum mechanics” in order to obtain “an explanation of the main features of complex atomic systems without too much computation”. This is exactly this chapter’s paradigm. Just like Wyatt’s quantum trajectory method, the mixed quantum–classical Bohmian method presented here also relies on Bohmian trajectories as a numerical tool. Another similarity to Wyatt’s approach is that not too long ago it was developed to overcome difficulties in computational quantum chemistry, but in this case it was proposed twice independently, by E. Gindensperger, C. Meier and J. Beswick [6] as well as by O. Prezhdo and C. Brooksby [5].

As the former group puts it in their introductory article, with molecular dynamics or processes involving for example liquids, interfaces or biological systems as well as interactions of atoms/molecules with surfaces, a fully quantum treatment of multidimensional, anharmonic, large-amplitude problems is not possible. Thus, for dealing with problems of such kind it is required to rest on hybrid quantum/classical schemes¹. In these, only essential subsets of degrees of freedom are treated quantum mechanically, while the rest can more easily be dealt with by using the much more efficient Newtonian formalism. Making a classical subsystem affect a quantum subsystem’s time evolution is straightforward via incorporation of a suitable potential term into the Hamiltonian. However, in certain situations it may be required to not limit the interaction between subsystems to only one direction, but to also have a quantum subsystem backreact on a classical one.

Unfortunately, to achieve this, no method is currently known, which works well independently of the particular physical situation of interest. In the mean field approach, the most commonly used scheme, an average force is derived from the wave function’s probability density and then plugged into the classical equations of motion. This approach likely yields incorrect results when the wave function is a superposition of separated states, such that its mean does not properly represent the overall shape. One attempt to overcome this problem is the so-called surface hopping trajectory technique [10], where basically only one of the superposed states is considered for the evolution, but at each step there is a probability amplitude for jumping from one of these states to another. This method comes with its own limitations though, and will not be considered in this thesis. Instead, this chapter will focus on a relatively new, promising

¹ The computational chemistry literature distinguishes between the terms *semiclassical* and *mixed quantum–classical*, but for the course of this chapter there is no ambiguity, so here the terms will be used interchangeably.

5.1 The Backreaction Problem

variant of implementing backreaction onto the classical subsystem, one that employs Bohmian trajectories. It has been applied very successfully in a model of O_2 interacting with a Pt surface [5] and with advantageous observables chosen has also proven to be useful in some scattering toy models.

After introducing the algorithm's foundations and workings, this chapter will add to these scattering results and finally apply the method to a new kind of interaction, which has not been tested before. The model of interest originates from cavity quantum electrodynamics and is one of the few actually solvable models of its kind. It is the hydrogen atom in the Jaynes–Cummings model, which is of simple nature but still displays a very important, genuinely quantum effect. Under the rotating wave approximation, the model is explicitly solvable, both semiclassically and in its fully quantum formulation. There is a vast number of reports about experimental implementations in the regime where the approximation holds, but even more interestingly, recent advances in the area of circuit quantum electrodynamics made experiments possible, which violate the rotating wave approximation in semiconductors with Josephson junctions [55]. Fortunately, a couple of years ago, also a numerical solution beyond the rotating wave approximation was published by Y.-Y. Zhang, Q.-H. Chen and S.-Y. Zhu [56]. The author is not aware so far of any reports comparing this solution to the results obtained from semiclassical, numeric treatment, which would be interesting, because the rotating wave approximation is absent in the numerical schemes. So this comparison will be presented as well.

A recent proposal to apply the Bohmian backreaction approach to semiclassical quantum gravity [57], where a fully quantum theory is completely lacking, provides additional motivation for investigating how well this semiclassical method works compared to the explicitly quantum results in this nontrivial model. The proposal was put forward by one of the thesis advisors, W. Struyve, and the idea of benchmarking the Bohmian backreaction method via this particular physical system should also be credited to him.

5.1 The Backreaction Problem

Consider the following problem: given an interaction Hamiltonian and an initial wave function for a (possibly large²) number of particles, the dynamics of these particles is to be computed, but computational resources are too sparse to numerically solve the Schrödinger equation on the dimensional configuration space. As already mentioned, the obvious way is to treat only part of the ensemble quantum, be it on a lattice or maybe using something like Wyatt's trajectory method from the previous chapter, if applicable. For those particles, whose quantum nature might not be that important, e.g. heavy particles with internal degrees of freedom that are unlikely to play an important role, the much more efficient Newtonian mechanics can be used instead.

To compute statistics over several runs, the initial positions of the classical particles can be sampled from the initial wave function. It is usually straightforward to incorporate the interaction between the classical particles and the quantum ones into the modified Hamiltonians

²A number of 10 can already be considered large in the context of a quantum description of molecular dynamics [58].

acting on the restricted wave functions. How to do it the other way round is not that easy, however. For best accuracy of the results, the classical particles should be able to react to changes in the state of the quantum subsystems, of course. This issue, i.e. that not only the evolution of quantum mechanical degrees of freedom under the influence of the surrounding classical motions must reflect the correct physical behavior, but also the other way round, goes by the name of *self-consistency* [58].

For now, assume that the ensemble consists of only two particles, one with mass m and the other one with mass M , where $m \leq M$. Then the system simply splits up into a one-particle quantum and a one-particle classical system. This keeps the equations simpler, but of course the generalization to many more particles is straightforward. As before, the symbol \mathbf{q} denotes a vector in configuration space, but now only for that part which continues to be treated quantum mechanically, and similarly \mathbf{x} is used in the context of Bohmian trajectories. Furthermore, \mathbf{Q} stands for the counterpart of configuration space, which is going to become classical. Finally, \mathbf{X} now denotes the classical trajectories, not, as one might expect from the previous notation, the Bohmian ones. The Bohmian ones, the solutions of equation (2.9), are written as $\check{\mathbf{X}}$ and hopefully will be approximated by the classical ones.

The full wave function is written as $\Psi(\mathbf{q}, \mathbf{Q}, t)$, and the Hamiltonian governing its time evolution can be written as, again in atomic units,

$$\hat{H}(\mathbf{q}, \mathbf{Q}) = \frac{1}{2m} \Delta_{\mathbf{q}} + \frac{1}{2M} \Delta_{\mathbf{Q}} + V_{\mathbf{q}}(\mathbf{q}) + V_{\mathbf{c}}(\mathbf{Q}) + V_{\text{int}}(\mathbf{q}, \mathbf{Q}), \quad (5.1)$$

where the total potential has already been split up into to-remain quantum and to-become classical parts as well as an interaction part. Making the usual quantum–classical split now leads to an explicitly time dependent Hamiltonian

$$\hat{h}(t) = \frac{1}{2m} \Delta_{\mathbf{q}} + V_{\mathbf{q}}(\mathbf{q}) + V_{\text{int}}(\mathbf{q}, \mathbf{X}(t)), \quad (5.2)$$

which acts on a restricted wave function $\psi(\mathbf{q}, t)$. The time dependence arises from the interaction potential now depending on the current position $\mathbf{X}(t)$ of the classical particle, whose equation of motion is given by

$$M\ddot{\mathbf{X}}(t) = -\nabla_{\mathbf{Q}} V_{\mathbf{c}}(\mathbf{Q})|_{\mathbf{Q}=\mathbf{X}(t)} + \mathbf{F}_{\text{br}}. \quad (5.3)$$

Here the term \mathbf{F}_{br} is a placeholder for what to do about V_{int} . It represents the influence exerted by the quantum system to establish self-consistency. Now two mechanisms for implementing this backreaction term are going to be introduced.

5.1.1 The Mean Field Method

The first one is called the mean field method or Ehrenfest method and is the most commonly used one. As backreaction term it uses the classical force derived from the interaction potential, which gets averaged over the quantum part's probability density

$$\mathbf{F}_{\text{br}}(t) = - \int d\mathbf{q} |\psi(\mathbf{q}, t)|^2 \nabla_{\mathbf{Q}} V_{\text{int}}(\mathbf{q}, \mathbf{Q})|_{\mathbf{Q}=\mathbf{X}(t)}. \quad (5.4)$$

5.1 The Backreaction Problem

Again, this force obtains its time dependence by being evaluated along the path of the classical particle. Equations (5.2) to (5.4) are the working equations of this scheme. The backreaction term can be viewed as a consequence of the Ehrenfest theorem [59]. Equation (5.4) is not going to be derived explicitly in this paper. A detailed and instructive derivation of it as the classical limit of the so-called time-dependent self-consistent field method has been given by J. Tully [58]. Total energy is a conserved quantity within this scheme, a statement which ultimately results from a time-dependent variant of the Hellman-Feynman theorem [60].

5.1.2 The Bohmian Method

The Bohmian backreaction approach is of different nature. It is a relatively new method and was independently proposed twice, with the same final result for \mathbf{F}_{br} , but different ways of arriving there. In a sense, the averaged force is also the starting point in the derivation given by Prezhdo and Brooksby [5], but the average is to be understood in a different way, because it is moved out of each time step. On the other hand, the route chosen by Gindensperger, Meier and Beswick [6] starts from Madelung's polar decomposition of the wave function, which has already shown up as equation (4.1) in the previous chapter. It is then followed by a series of explicit approximations. Here, neither of these will be followed. Instead, the derivation will be along the lines of the one recently given by Struyve [57].

Starting point is the conditional wave function $\tilde{\psi}$, which simply is the conditional wave function with respect to the to-be classical but currently still Bohmian particle. Its definition reads

$$\tilde{\psi}(\mathbf{q}, t) := \Psi(\mathbf{q}, \tilde{\mathbf{X}}(t), t), \quad (5.5)$$

where the Bohmian trajectory $\tilde{\mathbf{X}}(t)$ first arises from and then is plugged into the solution wave function $\Psi(\mathbf{q}, \mathbf{Q}, t)$ of the Schrödinger equation associated with the full quantum description of equation (5.1). For this conditional wave function, it is possible to find the following equation of motion from the chain rule and application of the Schrödinger equation via

$$i \frac{\partial}{\partial t} \tilde{\psi}(\mathbf{q}, t) = i \left(\frac{\partial \Psi(\mathbf{q}, \mathbf{Q}, t)}{\partial t} \Big|_{\mathbf{Q}=\tilde{\mathbf{X}}(t)} + \dot{\tilde{\mathbf{X}}}(t) \cdot \nabla_{\mathbf{Q}} \Psi(\mathbf{q}, \mathbf{Q}, t) \Big|_{\mathbf{Q}=\tilde{\mathbf{X}}(t)} \right) \quad (5.6)$$

$$= \left[\left(-\frac{1}{2m} \Delta_{\mathbf{q}} + V_{\mathbf{q}}(\mathbf{q}) + V_{\text{int}}(\mathbf{q}, \mathbf{Q}) \right) \Psi(\mathbf{q}, \mathbf{Q}, t) + \left(-\frac{1}{2M} \Delta_{\mathbf{Q}} + V_{\mathbf{c}}(\mathbf{Q}) \right) \Psi(\mathbf{q}, \mathbf{Q}, t) + i \dot{\tilde{\mathbf{X}}}(t) \cdot \nabla_{\mathbf{Q}} \Psi(\mathbf{q}, \mathbf{Q}, t) \right] \Big|_{\mathbf{Q}=\tilde{\mathbf{X}}(t)} \quad (5.7)$$

$$=: \hat{h}(t) \tilde{\psi}(\mathbf{q}, t) + \mathcal{R}(\mathbf{q}, t), \quad (5.8)$$

where \mathcal{R} denotes the terms in the second row of the middle step.

For the Bohmian trajectory of the particle which is soon going to become classical, the classical-looking formulation of Bohmian theory, equation (2.10) can be employed:

$$M \ddot{\tilde{\mathbf{X}}} = -\nabla_{\mathbf{Q}} \left[V_{\mathbf{q}}(\mathbf{q}) + V_{\mathbf{c}}(\mathbf{Q}) + V_{\text{int}}(\mathbf{q}, \mathbf{Q}) + Q \Psi(\mathbf{q}, \mathbf{Q}, t) \right]_{\mathbf{q}=\mathbf{x}(t), \mathbf{Q}=\tilde{\mathbf{X}}(t)}. \quad (5.9)$$

5. Employing Bohmian Trajectories in Semiclassical Numerics

It contains the quantum potential Q^Ψ , which is to be computed from the full wave function Ψ via equation (2.11). The first term in the sum vanishes of course when the derivative is taken.

Now it is time to split off the classical part. Neglecting \mathcal{R} in equation (5.8) in many cases amounts to just neglecting the dispersion of the wave packet with respect to the heavier particle, c.f. [6]. For a classical particle with $M \gg m$, this should not hurt much. However, that alone is not enough. Evaluating equation (5.9) still requires the full quantum solution, so Q^Ψ needs to be removed from that equation, too, in order to turn the scheme into a computationally useful one. For a heavy particle, the motion should mainly be guided by the gradient of the classical potential anyway, since Q^Ψ is inversely proportional to M . In a study [6] by Gindensperger et. al., it was found that doing so did not change the dynamics significantly for them. Equation (5.9) then becomes the Newtonian equation (5.3) for the classical trajectory \mathbf{X} . However, it did of course not completely get rid of all quantum influence, because the backreaction term

$$\mathbf{F}_{\text{br}}(t) = -\nabla_{\mathbf{Q}} V_{\text{int}}(\mathbf{q}, \mathbf{Q}) \Big|_{\mathbf{q}=\mathbf{x}(t), \mathbf{Q}=\tilde{\mathbf{X}}(t)} \quad (5.10)$$

still depends on the position \mathbf{x} of the leftover Bohmian particle. Even after dropping \mathcal{R} from equation (5.8), this position still depends on the full quantum solution, but it should be understood as a solution of equation (5.2). Only after replacing $\tilde{\mathbf{X}}$ by the classical solution \mathbf{X} , i.e. evaluating the interaction potential in \hat{h} at the position of the classical particle, equation (5.8) turns precisely into equation (5.2). When making the step from $\tilde{\psi}$ to ψ , the latter should be normalized to be interpreted as a wave function.

So now the working equations of the Bohmian scheme have been derived, they are equations (5.2) and (5.3) with the backreaction term given by equation (5.10), and they differ from the mean field approach only in the latter. The Bohmian particle in the quantum subsystem is of course guided by ψ via the Bohmian guiding law (2.9). This is however not yet the full method. Even if only one Bohmian trajectory of a quantum system might be realized in nature, which initial condition should be chosen for computational purposes? Different ones will result in different dynamics of both ψ and \mathbf{X} . The algorithm is described by Prezhdo and Brooksby as follows [5]:

1. Initial conditions are chosen in the usual manner with positions \mathbf{x} sampled from the initial distribution $|\psi_0|^2$. This way, an ensemble of quantum–classical systems is generated, each with a different initial position of the Bohmian particle, but the same initial condition for the wave function and the classical particle.
2. For each instance of the system, the time dependent Schrödinger equation is solved for the restricted wave function ψ , the motion of the Bohmian particle \mathbf{x} is derived from it. The trajectory \mathbf{X} is computed from the classical equation using the respective backreaction term. Because of the coupling between the equations, simultaneous integration is necessary. Finish at the desired time t .
3. After having integrated the whole ensemble up to time t , the results are averaged over the Bohmian ensemble.

In this thesis, the prescription is taken even one step further. The ensemble is not only formed over the quantum coordinate, but also the classical one, so the initial conditions are directly sampled from $|\Psi_0|^2$.

5.2 Application to Different Toy Models

As was pointed out in a comment by L. Salcedo, the total energy is not conserved in this approach [61]. Also, despite the microscopic equations remaining invariant under time reversal, applying the entire algorithm backwards in time will not yield the exact reverse dynamics when the new initial ensemble is derived again from the full quantum wave function at a different time. Thus the initial time is distinguished, because due to the approximate nature of the algorithm, the full quantum wave function is typically not known at any time other than initial time. This may be unsatisfactory from a theoretical point of view, but has not posed any problem in practical applications of the numeric scheme so far. In many physically relevant situations, the initial state is either a known asymptotic state like in all collisional processes or an eigenfunction anyway [62].

At the end of the day, one is left with a highly nonlinear set of partial differential equations, coupled in both directions, that approximate the full quantum behavior in one way or the other, both here and in the mean field case. Note that for the Bohmian backreaction approach described above, there is no concept of equivariance like in the Bohmian description of quantum theory. Because of the different particle initial conditions, the time evolutions of the restricted wave functions ψ differ among the ensemble, so it does not even make sense to talk about the Bohmian particles being distributed according to the associated probability density ρ^ψ .

5.2 Application to Different Toy Models

Now the two methods are to be evaluated on different toy models. The mean field method has been around in the literature for quite a while and has been tested extensively already. So this section has its focus on how well the Bohmian backreaction works in comparison. The first application will be an example scattering situation of two one-dimensional particles. The interaction between them is designed to put the mean field approach at disadvantage. After confirming that the Bohmian approach does not suffer from the same problem, the Jaynes–Cummings model will be introduced. The interaction in this model is then also subject to the investigation of how well the two semiclassical, numerical methods reproduce the fully quantum solution and whether or not they fail in similar ways. In all applications, the quantum part is not going to be integrated with the trajectory methods from the previous chapter, so the node problem identified there does not pose a problem here.

5.2.1 One-dimensional Scattering

Try to come up with an example situation in which the mixed quantum–classical dynamics with the traditional mean field backreaction does not work well. How could the setup be designed to make the mean field approach fail? One way might be to exploit the exact form of the backreaction term. Because the essence of mean field is to average the backreaction force over the quantum subsystem, a suitable superposition of quantum states will ensure that the mean does not properly represent what is going on on the quantum side. With Bohmian backreaction, the force is evaluated at one particular point rather than taking the average. So despite

5. Employing Bohmian Trajectories in Semiclassical Numerics

using the exact same equations apart from the backreaction term, qualitatively different results can be expected in the Bohmian case.

To implement this idea, the following suffices: two one-dimensional particles with a repelling interaction between them, the lighter particle of mass m being treated quantum and evolving freely ($V_q \equiv 0$) apart from the interaction, the other particle additionally being bound to an external potential. For the heavier particle having enough mass $M \gg m$, treating it classically seems appropriate, but the mass should not be large enough to justify replacing this particle itself by a static, external potential. Choosing an interaction potential which gives rise to an antisymmetric force makes sure that the mean field backreaction yields only a small value as long as the wave function is symmetric about the classical particle. This could be achieved for example by the quantum particle, represented by a Gaussian wave function traveling with group velocity k , passing through a beam splitter and then traveling along wave guides arranged such that it ends up approaching the classical particle from both, left and right symmetrically before scattering takes place, i.e.

$$\psi(q, t = 0) = \frac{1}{\sqrt{2\sqrt{2\pi}\sigma_q}} \left[\exp\left(-ikq - \frac{(q - q_0)^2}{4\sigma_q^2}\right) + \exp\left(ikq - \frac{(q + q_0)^2}{4\sigma_q^2}\right) \right]. \quad (5.11)$$

It is actually possible to make the total force acting on the classical particle vanish almost completely at all times at which the wave function is sufficiently symmetric. When choosing the harmonic oscillator with eigenfrequency ω as the external potential in which the classical particle is bound,

$$V_c(Q) = \frac{1}{2}\omega Q^2, \quad (5.12)$$

then the initial positions of the classical part can be sampled from its ground state for example. The full quantum initial wave function then reads

$$\Psi(q, Q, t = 0) = \psi(q, 0) \left(\frac{M\omega}{\pi}\right)^{\frac{1}{4}} e^{-\frac{1}{2}M\omega Q^2}. \quad (5.13)$$

i.e. initially the classical part is also distributed Gaussian, centered about the origin and with variance $\sigma_c^2 = \frac{1}{2M\omega}$. Figure 5.1 contains a visualization of the description so far.

Now taking the interaction potential between the particles to be also harmonic³, but repelling as in

$$V_{\text{int}}(q, Q) = -\frac{1}{2}\omega(q - Q)^2, \quad (5.14)$$

then the total mean field backreaction force in equation (5.3) acting on the classical particle reduces to

$$M\ddot{X} = \underbrace{-\omega X}_{F_c} - \underbrace{\langle \omega(q - X) \rangle_\psi}_{F_{\text{br}}} = -\omega \langle q \rangle_\psi \quad (5.15)$$

³This is of course physically rather absurd, but it is an excellent choice here to engineer a setup which demonstrates both the shortcomings of the mean-field approach and how the Bohmian approach is not affected.

5.2 Application to Different Toy Models

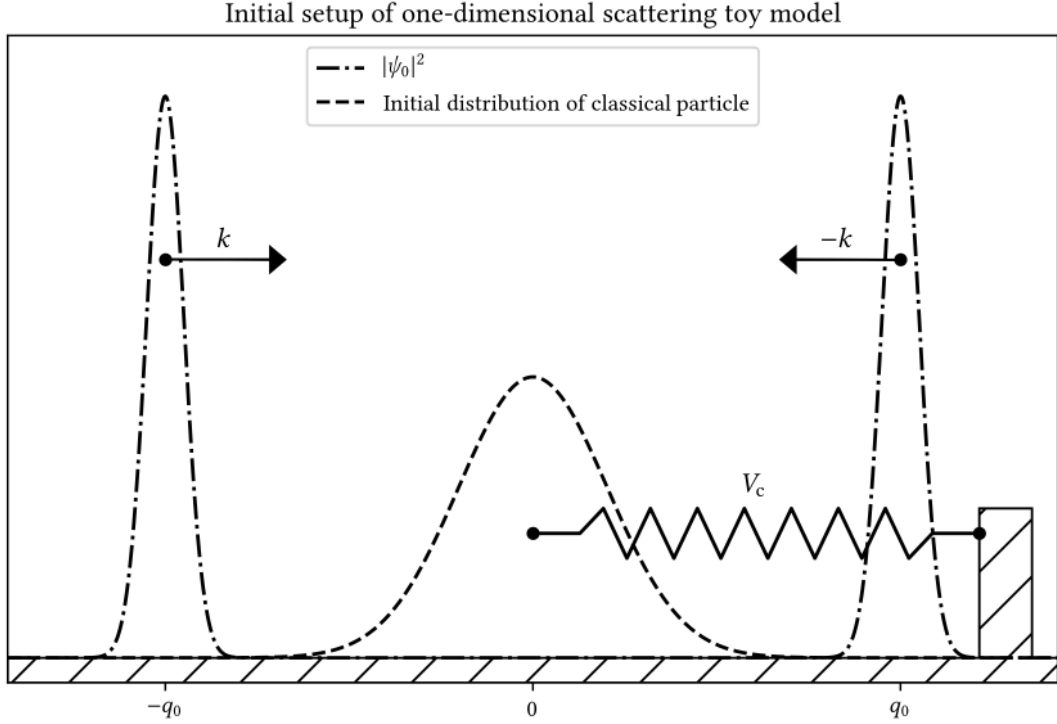


Figure 5.1: Sketch of the toy scattering setup, i.e. a superposition of the quantum part hitting the bound classical particle from left and right. The spring, attached to a pole, just illustrates the potential. Interaction between quantum and classical subsystems not depicted.

which, for symmetric $|\psi|^2$ is zero. The total force in the Bohmian approach

$$M\ddot{X} = -\omega X - \omega(x - X) = -\omega x \quad (5.16)$$

however is clearly nonvanishing unless the Bohmian particle's position x happens to be at the origin. For a numerical comparison of the two methods, the classical particle's final position variance over many runs with different initial conditions, $(\Delta X)^2$, is an observable which can be expected to reflect the differences between the approaches. In the fully quantum case, the quantity is readily obtained from the numerical wave function⁴ while for the semiclassical approaches the usual discrete formula can be applied to the finite ensemble of classical trajectories.

The Runge-Kutta solver from chapter 3 was used here once more to compute the time evolution of the fully quantum wave function Ψ on a two-dimensional lattice. The semiclassical dynamics were computed applying the same method for ψ and by extending the code to also integrate equation (5.3) for Bohmian and mean field backreaction, respectively. The numerical values of the other parameters which were used are summarized in table 5.1.

⁴Strictly speaking, it should be written $(\Delta Q)^2$ in the fully quantum case, but for simplicity that is not done. One could think of this quantity as the variance among the different possible Bohmian trajectories \tilde{X}_t .

5. Employing Bohmian Trajectories in Semiclassical Numerics

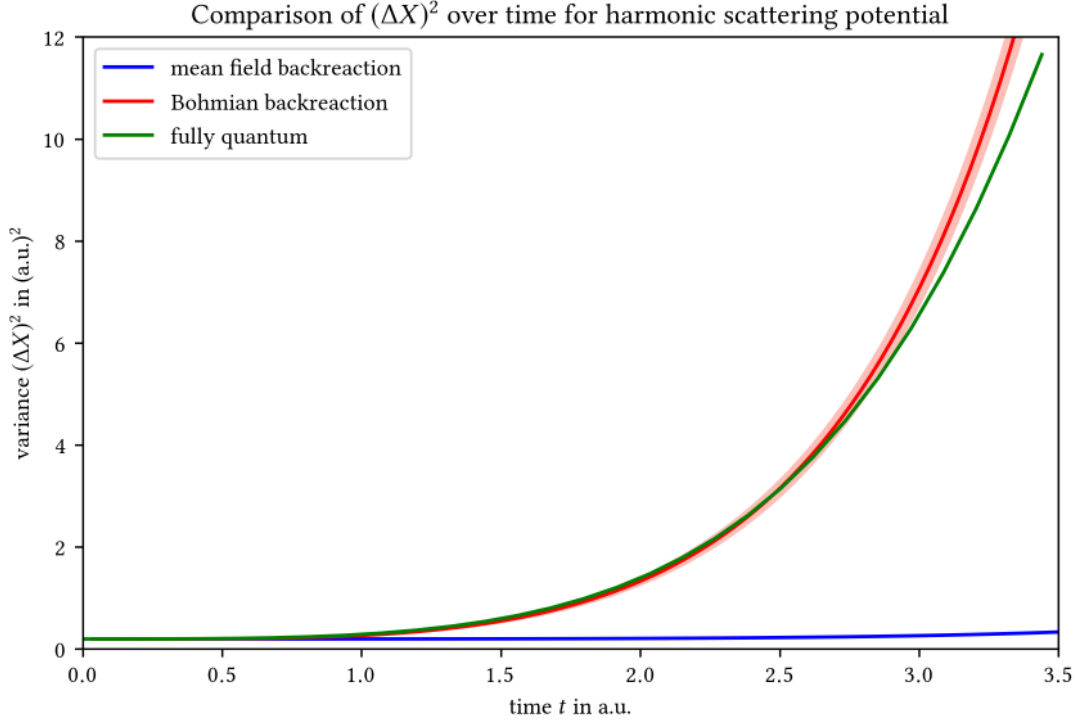


Figure 5.2: Variances $(\Delta X)^2$ over time for the harmonic potentials as obtained from the different approaches and compared to the full quantum solution. The light red area is the $2\text{-}\sigma$ confidence interval of the Bohmian method, the light blue counterpart for the mean field case is too small to be visible. Semiclassical results computed from five batches with 500 different initial conditions each.

A sample size of 500 initial conditions turned out to suffice for convergence. To get a grip on the statistical significance, five batches of these 500 samples of initial conditions were computed with the results presented in figure 5.2. The red and blue lines are the mean of the variances of the classical trajectories for Bohmian and mean field backreaction respectively, while the confidence intervals depicted around them are two standard deviations among these five batches.

parameters of equation (5.11)		additional parameters of equation (5.13)	
m	1	M	10
σ_q	1.5	ω	0.25
k	5		
q_0	10		

Table 5.1: Chosen values of the parameters in the equations above for the harmonic potential. All numbers are given in their respective atomic unit.

5.2 Application to Different Toy Models

The numerical data shows that the backreaction in the mean field case almost completely cancels the gradient of the external potential, so that the classical particle does almost not move at all. With the classical particle not, or only at very late times, reacting to the incoming wave packet, its behavior totally differs from the time evolution of the full quantum wave function. The Bohmian backreaction term on the other hand leads to a qualitatively and quantitatively much better behavior. With this approximation, the curve initially follows the correct one very closely up to $t \approx 2.5$ a.u., but eventually overshoots in the asymptotics.

One can see from the plot that taking the potentials to be harmonic is the most extreme case of disadvantaging the mean field approach over the Bohmian one. The choice however is problematic not only from a physical but also from a computational point of view. Because the repelling interaction is not bounded and grows stronger and stronger as the particles separate after scattering, the wave function soon leaves the grid and thus integration to longer times becomes exceedingly demanding on computational resources. Fortunately, there is a whole class of symmetric potentials, which are approximately harmonic around the origin, but do not suffer from this issue. For these, the Schrödinger equation also can be still be solved explicitly.

For positive integer λ , the *Pöschl–Teller potential* [63]

$$V(q) = -\frac{\lambda(\lambda+1)}{2M} \frac{1}{\cosh(q)^2} \quad (5.17)$$

has λ bound states of energy $E = -\frac{\mu^2}{2}$ where $\mu = 1, 2, \dots, \lambda$. The eigenstates are simply given by the normalized, associated Legendre–Polynomials $\mathcal{P}_\lambda^\mu(\tanh(q))$.

Using the Pöschl–Teller potential with $\lambda = 2$ as a substitute for the harmonic potential makes the interaction essentially finite-ranged and enables the bound particle to escape from its trapping potential in principle. Also, the backreaction term and the classical force do no longer cancel like they did before in equations (5.15) and (5.16). The full initial wave function, whose to-be classical factor now becomes the ground state of the new potential, is given by

$$\Psi(q, Q, t = 0) = \psi(q, 0) \frac{\sqrt{3}}{2} \frac{1}{\cosh(Q)^2}. \quad (5.18)$$

For the choice $\lambda = 2$ and M from table 5.2, the potential, its energy eigenstates and its ground state wave function are depicted in figure 5.3. Some of the previously used parameters also need to be changed to account for the change of potential. They are listed in table 5.2.

For this potential, figure 5.4 contains the result of the two algorithms, again obtained from five batches of 500 different initial conditions. The first thing hitting the eye is that the confidence

parameters that changed with respect to table 5.1	
k	1
M	5
ω	no longer needed

Table 5.2: Choice of parameters for the Pöschl–Teller potential. All numbers given in a.u.

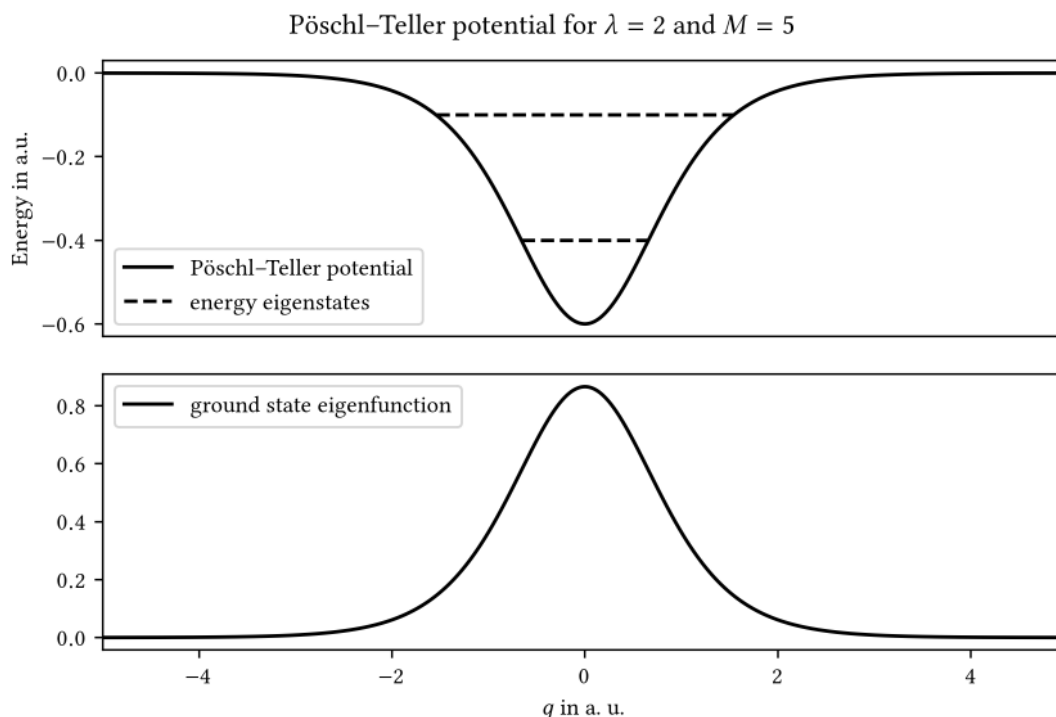


Figure 5.3: Top: Pöschl–Teller potential with parameters $\lambda = 2$ and $M = 5$. Bottom: ground state eigenfunction for this choice of parameters.

intervals look much wider than before. This is less an effect of changing the initial quantum state for the classically approximated particle, but rather results from a change of scale on the vertical axis because the dispersion is much less pronounced for the Pöschl–Teller potentials. Nonetheless, the amount of samples is still large enough to properly separate the results of the different approaches from each other. The Bohmian approach has the initial position of the Bohmian particle as an additional random initial parameter, so one might expect that this method’s confidence interval eventually becomes bigger than the mean field one. But interestingly that is not the case.

Both semiclassical methods feature a dip right after starting the simulation. This is an artifact of neglecting the quantum wave packet dispersion in the approximations, which for an eigenstate exactly balances the effect of the external potential in a quantum treatment. For most⁵ particles the external potential still looks very similar to a harmonic one. Thus, what basically happens here is that particles falling towards the bottom of the potential arrive there at the same time more or less, resulting in the pronounced dip. This behavior was absent in the harmonic interaction case before, because the respective terms from external potential and backreaction happened to cancel at all times, whereas now the interaction is limited in range.

⁵Apart from the ones towards the outsides of the potential. But as can be seen from figure 5.3, sampling these is less likely than close to the center.

5.2 Application to Different Toy Models

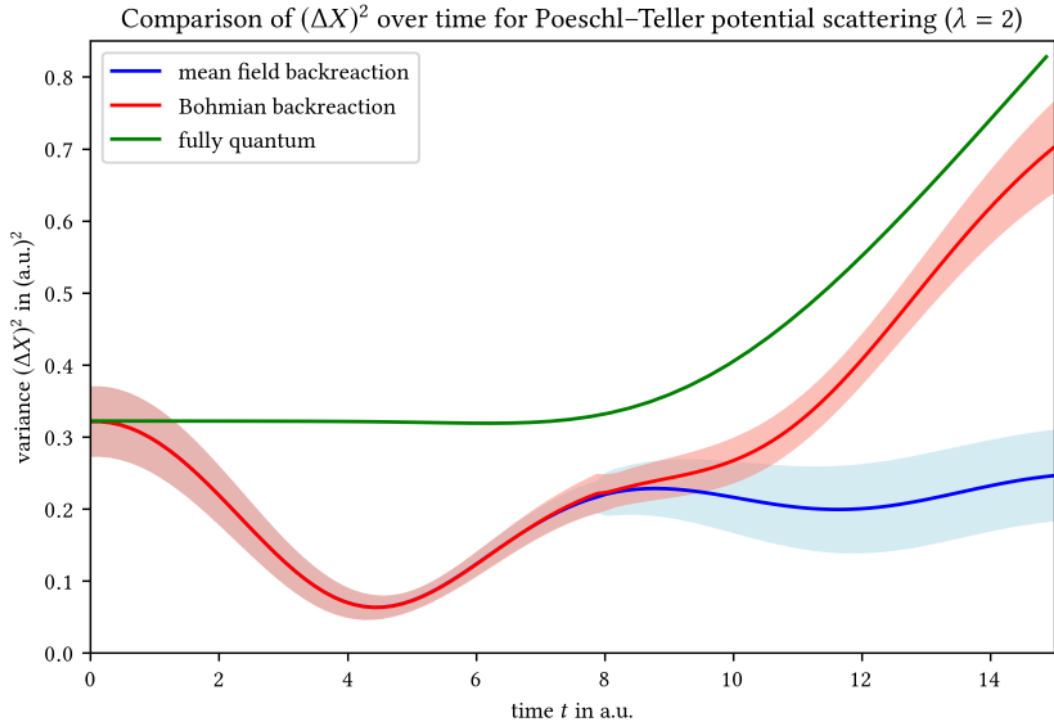


Figure 5.4: Variances $(\Delta X)^2$ over time for the Pöschl–Teller potentials as obtained from the different approaches and compared to the full quantum solution. The shaded areas are again the $2\text{-}\sigma$ confidence intervals. Semiclassical results computed from five batches with 500 different initial conditions each.

As soon as the quantum wave packets come together close enough at $t \approx 8$ a.u., the heavier particle no longer completely remains in the ground state of the potential. At about the same time as the quantum curve, the Bohmian backreaction one also starts rising up. It does not exactly reproduce the quantum result towards the end of the simulation, but qualitatively the behavior seems correct. The mean field result on the other hand remains largely unaffected by the scattering in this scenario as well. When the wave packet of the lighter particle eventually loses its symmetry⁶, it is already too late.

So the upshot of this section is, that it is at least possible to construct scenarios in which the mixed quantum–classical dynamics with Bohmian backreaction approximates the full quantum solution much better than the traditional mean field approach. The examples here were purposefully engineered to explicitly demonstrate this, but in the literature some realistic models of chemical processes have been identified where the Bohmian results were comparable or even better than the usual approach [6, 5, 62, 64, 65, 66]. In terms of computational effort, the Bohmian method is also a bit more efficient, because determining the Bohmian velocity is

⁶That happens because its Hamiltonian is parametrized on the location of the classical particle, which is initially sampled slightly off-center.

faster than integrating $|\psi|^2$ along the grid for the mean field backreaction estimate. But with respect to wall clock time the difference is small. In a different setup, the classical particle might be well localized in its binding potential and the symmetry of the interaction need not be as elaborate as here. In such a case it might be possible to get away with only one classical trajectory in the mean field approach, rather than averaging over many initial conditions for the classical particle as done here. Then the Bohmian method would be at disadvantage from a computational resources point of view, because forming the ensemble with many different initial positions for the Bohmian particle would still be required.

5.2.2 The Hydrogen Atom in the Jaynes–Cummings Model

As the previous section showed, the Bohmian method is able to produce better results than the mean field approach for certain superpositions of wave functions. With this the back of the mind, it is now interesting to see how well the two approaches compete in a physically more relevant model system, for which the superposition principle is fundamental, but with a different type of interaction. To the knowledge of the author, no applications of the Bohmian backreaction approach to anything even remotely similar to this model or interaction have been reported in the literature yet.

The Jaynes–Cummings model, originally proposed in 1963 [67], is the simplest model that describes the interaction of a quantum system with a quantized electromagnetic field. It consists of a two-level system, which is placed in a cavity containing a single field mode. As was discovered later, its explicit solution displays genuinely quantum effects such as photon antibunching and photon reabsorption after emission. These make it similarly important to the field of quantum optics as the Ising model is in statistical physics. Experimental verification of one of these effects, the phenomenon of collapse and revival, was first achieved in the microwave regime in a maser [68] by G. Rempe, H. Walther and N. Klein. In the years after that, a series of astonishing experiments based on this model earned S. Haroche the Nobel prize in 2012.

Theory

The description here is just one possible way⁷ of implementing the idea of Jaynes and Cummings. A hydrogen atom placed inside the cavity behaves essentially like a two-level system when the field frequency ν matches⁸ the energy difference between states. In this case, resonance screens out all other excited states and as long as the hydrogen selection rules are obeyed, any two states can be used. The theory allows for a small detuning between field frequency and atomic transition, but for simplicity perfect resonance is assumed here.

The following derivation of the equations is mainly adapted from chapters 5 and 6 of the textbook by Scully and Zubairy [69]. The full quantum theory is introduced first before proceeding

⁷Another one would be talking about coupled spins for example.

⁸Still in atomic units.

5.2 Application to Different Toy Models

with the semiclassical equations. Starting point is the atom–field interaction Hamiltonian of the resonant system,

$$\hat{H} = \underbrace{-\Delta_{\mathbf{q}} + V(\mathbf{q})}_{=: \hat{H}_a} + \underbrace{\nu \left(\hat{a}^\dagger \hat{a} + \frac{1}{2} \right)}_{=: \hat{H}_f} - \underbrace{\mathbf{q} \cdot \mathbf{E}}_{=: \hat{H}_{\text{int}}}, \quad (5.19)$$

which consists of an atomic part \hat{H}_a containing the nucleus' Coulomb potential for the electron, a field part \hat{H}_f describing a single mode and the interaction term \hat{H}_{int} . Actually, the last one can also be written in terms of annihilation and creation operators via

$$\hat{H}_{\text{int}} = -\mathbf{q} \cdot \mathbf{e}_p \mathcal{E} \left(\hat{a} + \hat{a}^\dagger \right) \quad \text{w. } \mathcal{E} = \sqrt{\frac{4\pi\nu}{2\mathcal{V}}} \quad (5.20)$$

if the atom is stationary at the center of the cavity, coinciding with the origin of the coordinate system [69]. In this equation, \mathbf{e}_p denotes the unit polarization vector of the field mode and \mathcal{V} the mode volume.

The interaction here does not give the full physical picture, because the Hamiltonian assumes the validity of the *dipole approximation*. This approximation is valid for sufficiently weak fields and small enough transition frequency ν and neglects electric quadrupole and higher interactions as well as all magnetic phenomena. A derivation of the dipole Hamiltonian from the Pauli equation and a discussion of the dipole approximation in more generality can be found in standard textbooks, for example [70, p. 467ff].

In the next step, the Hamiltonian (5.19) reduces to a simpler expression by exploiting the fact that only two energy levels of the hydrogen atom ever become relevant. Calling the one with lower energy $|-\rangle$ and the more excited one $|+\rangle$, and their energies E_- , E_+ resp. results in

$$\hat{H} = E_+ |+\rangle\langle +| + E_- |-\rangle\langle -| + \nu \left(\hat{a}^\dagger \hat{a} + \frac{1}{2} \right) - (|+\rangle\langle +| + |-\rangle\langle -|) \mathbf{q} (|+\rangle\langle +| + |-\rangle\langle -|) \cdot \mathbf{e}_p \mathcal{E} \left(\hat{a} + \hat{a}^\dagger \right), \quad (5.21)$$

after also inserting two identities into the interaction term by suitable use of the completeness relation. Taking note of $\nu = E_+ - E_-$ and that the first terms can be split into $\frac{1}{2}\nu (|+\rangle\langle +| - |-\rangle\langle -|) + \frac{1}{2}(E_+ + E_-) \cdot 1$, this can then be rewritten to

$$\hat{H} = \frac{1}{2}\nu \hat{\sigma}_z + \nu \hat{a}^\dagger \hat{a} - \underbrace{\mathcal{P}_\pm \cdot \mathbf{e}_p \mathcal{E}}_{=: g} (\hat{\sigma}_+ + \hat{\sigma}_-) \left(\hat{a}^\dagger + \hat{a} \right) \quad (5.22)$$

by dropping the constant terms and using the abbreviations

$$\mathcal{P}_\pm := \langle +|\mathbf{q}|-\rangle \left(\stackrel{\in \mathbb{R}}{=} \langle -|\mathbf{q}|+\rangle \text{ here} \right), \quad (5.23)$$

5. Employing Bohmian Trajectories in Semiclassical Numerics

for the so-called *transition dipole moment*⁹ and

$$\hat{\sigma}_z = |+\rangle\langle+| - |-\rangle\langle-| \quad (5.24)$$

$$\hat{\sigma}_+ = |+\rangle\langle-| \quad (5.25)$$

$$\hat{\sigma}_- = |-\rangle\langle+|. \quad (5.26)$$

$$(5.27)$$

$\hat{\sigma}_z$ and $\hat{\sigma}_\pm = \frac{1}{2}(\hat{\sigma}_x \pm i\hat{\sigma}_y)$ satisfy the usual spin-half algebra of Pauli matrices. $\hat{\sigma}_\pm$ can be interpreted as respective annihilation and creation operators for the two-level atom, taking it from the ground state to the excited one or the other way round, while $\hat{\sigma}_z$ is in some way similar to the number operator $\hat{N} = \hat{a}^\dagger \hat{a}$. It preserves the current state, but yields ± 1 when applied to one of the eigenstates $|\pm\rangle$.

The generic two-level Hamiltonian (5.22) is not yet soluble explicitly. The last ingredient still missing is the *rotating wave approximation*. Multiplication of the last two parentheses in the expression gives rise to terms $\hat{\sigma}_+ \hat{a}$ and $\hat{\sigma}_- \hat{a}^\dagger$. Those represent either the destruction of a photon in the cavity while raising the atom from the lower to the excited state or the emission of a photon into the cavity while the atom becomes deexcited. However, there are also the terms $\hat{\sigma}_+ \hat{a}^\dagger$ and $\hat{\sigma}_- \hat{a}$. They violate energy conservation by an amount of 2ν , either absorbing a photon from the cavity and going from upper to lower level, or raising the atom's energy while at the same time creating a photon. It turns out that for small values of $g \ll \nu$, these last two processes are highly suppressed. The reason for this is that by analyzing the Hamiltonian in the interaction picture, the respective terms happen to carry a phase factor of $\exp(i(E_+ - E_- + \nu)t)$, which oscillates on time scales much shorter than the lifetimes of atomic excitations in the model. Because those lifetimes are usually the observable of interest in the model and by effect of those rapidly rotating terms, energy conserving fluctuations average to zero, only the energy-conserving terms are kept in the Jaynes–Cummings Hamiltonian (without detuning)

$$\hat{H} = \nu \left(\frac{1}{2} \hat{\sigma}_z + \hat{a}^\dagger \hat{a} \right) - g \left(\hat{\sigma}_+ \hat{a} + \hat{\sigma}_- \hat{a}^\dagger \right). \quad (5.28)$$

The two-level atom in the cavity containing a single mode is generally described by a wave function of the form

$$\Psi(t) = \sum_n (C_{+,n}(t)|+, n\rangle + C_{-,n}(t)|-, n\rangle) \quad (5.29)$$

where $C_{\pm,n}(t)$ are the weighting factors of each atomic state when n photons are present in the cavity. The observable

$$W(t) := \sum_n \left(|C_{+,n}|^2 - |C_{-,n}|^2 \right) \quad (5.30)$$

is constructed from these and $W(t) = \pm 1$ indicates whether the atom is entirely in the lower or excited state at time t or otherwise in a superposition in between.

⁹This constant of the eigenstates can be found tabulated in books and is a real vector only in the two-level case in the dipole approximation dealt with here!

5.2 Application to Different Toy Models

There are several possible routes towards finding an explicit expression for $W(t)$ under the time evolution of the Jaynes–Cummings Hamiltonian (5.28) [69]. For a general initial photon distribution $\rho_n(t=0)$ and the atom initially in the excited state, the solution is as simple as¹⁰

$$W(t) = \sum_n \rho_n(t=0) \cos(\Omega_n t), \quad (5.31)$$

where Ω_n is the Rabi frequency $2g$ scaled by a factor depending on the photon number

$$\Omega_n = 2g\sqrt{n+1}. \quad (5.32)$$

In particular, even placing an excited atom into the vacuum cavity, $\rho_n(t=0) = \delta_{n0}$, gives rise to an oscillation at the Rabi frequency. Those are shown in figure 5.5. The mechanism at work is the atom emitting the photon into the cavity by going into the ground state. Soon later, the photon, which remains trapped inside the cavity gets reabsorbed, exciting the atom again and so on.

More interesting is actually the behavior when the initial photon distribution in the cavity is in a so-called *coherent state* of parameter $\gamma \in \mathbb{C}$. A coherent state, sometimes also called Glauber

¹⁰If there is detuning between energy levels and field mode, i.e. $\nu \neq E_+ - E_-$, then the solution is still available, but more complicated.

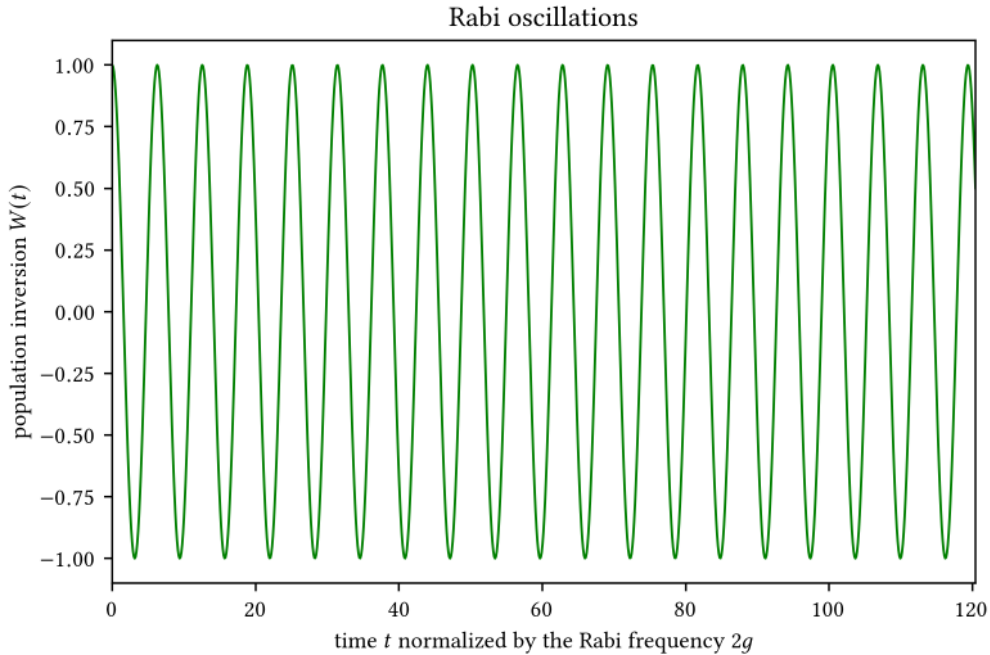


Figure 5.5: Population inversion of the initially excited hydrogen atom placed in an initially empty cavity as a function of $2gt$ displaying ordinary Rabi oscillations.

5. Employing Bohmian Trajectories in Semiclassical Numerics

state or displaced ground state is essentially a Gaussian wave function, shifted away from the origin by γ

$$\phi_\gamma(q) = \left(\frac{\nu}{2}\right)^{\frac{1}{4}} \exp\left[-\frac{\nu}{2}\left(q - \sqrt{\frac{2}{\nu}}\Re(\gamma)\right)^2 + i\sqrt{2\nu}\Im(\gamma)q\right]. \quad (5.33)$$

and it is an eigenstate of the annihilation operator. As already mentioned in chapter 4, it was initially discovered by Schrödinger looking for the quantum counterpart of the oscillatory behavior of a classical harmonic oscillator [51]. But it was R. Glauber, who later introduced the concept into quantum electrodynamics [71]. The term coherent is somewhat overused in physics, here it means that the wave function *coheres*, i.e. its shape does not change, while the packet oscillates back and forth in the harmonic potential [69].

A nice feature of coherent states is, that they are the most classical states in the sense that they minimize the uncertainty relation to $\frac{1}{2}$, so for large displacements $|\gamma|$, the relative uncertainty becomes tiny. Also, a coherent state's time evolution is concentrated along the classical trajectories. This will come in handy later during the semiclassical analysis of the model. In a coherent state of parameter γ , the expectation value of the number of photons present is given by

$$\langle \hat{N} \rangle = |\gamma|^2, \quad (5.34)$$

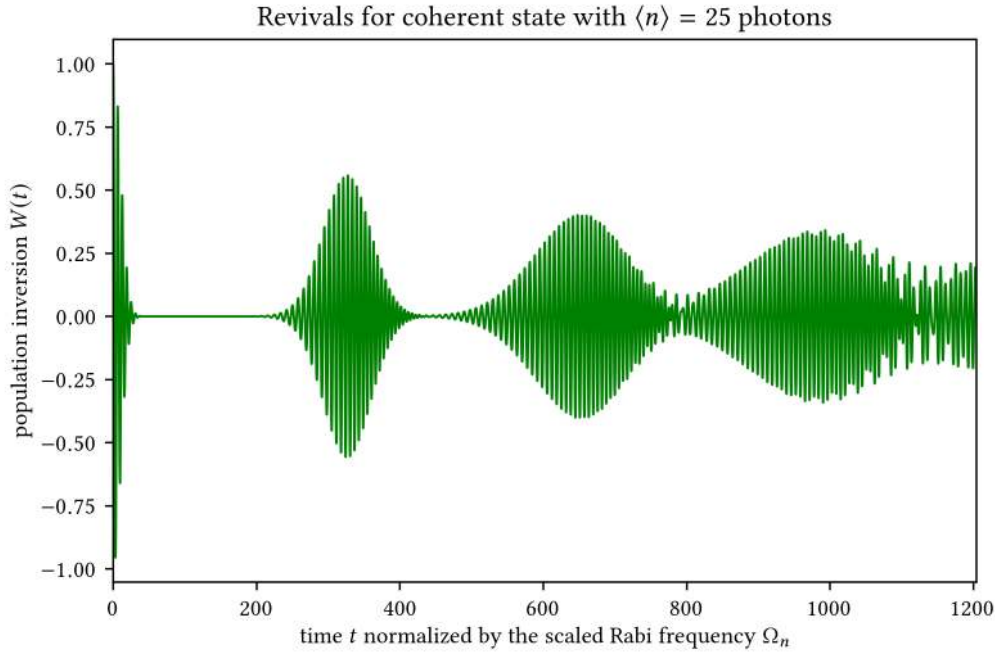


Figure 5.6: Population inversion of the initially excited hydrogen atom placed into a cavity initially containing an expected amount of 25 photons in a coherent state. As a function of $\Omega_n t$, the oscillations display the celebrated collapse and revival phenomenon.

5.2 Application to Different Toy Models

and the distribution is Poissonian in the number states,

$$\rho_n = \frac{\langle \hat{N} \rangle^n \exp(-\langle \hat{N} \rangle)}{n!}. \quad (5.35)$$

Figure 5.6 has the time evolution of the population inversion for this initial photon distribution with $\langle \hat{N} \rangle = 25$. At first, the oscillation dies off into a superposition of lower and upper atomic levels, but after a while the oscillation reappears. After this oscillation has also collapsed, a second revival becomes visible, whose tail already overlaps with a third one. Eventually, the widths of the envelopes will become large enough so that the overlap leads to highly irregular behavior.

After this short excursion illustrating the dynamics of the full quantum Jaynes–Cummings model, the semiclassical analysis will be prepared now. To this end, the initial Hamiltonian in the dipole approximation (5.19) is rewritten in position representation by substituting

$$\hat{a} \mapsto \sqrt{\frac{v}{2}} \left(Q + \frac{1}{v} \frac{\partial}{\partial Q} \right) \quad (5.36)$$

$$\hat{a}^\dagger \mapsto \sqrt{\frac{v}{2}} \left(Q - \frac{1}{v} \frac{\partial}{\partial Q} \right) \quad (5.37)$$

into equations (5.19) and (5.20). The result

$$\hat{H} = \hat{H}_a - \Delta_Q + \frac{v^2}{2} Q^2 - \underbrace{\sqrt{2v} \mathcal{E} \mathbf{q} \cdot \mathbf{e}_p}_{=: \alpha} Q \quad (5.38)$$

is expressed in terms of the mode coordinate Q and yet another coupling constant α to keep the following equations simpler. This coupling is related to the coupling g previously introduced in equation (5.22) via

$$g = \frac{\alpha}{\sqrt{2v}} \mathcal{P}_\pm \cdot \mathbf{e}_p \quad (5.39)$$

Now, the system can be split into a classical and a quantum part as suggested by W. Struyve. The atom inside the cavity, represented by

$$\hat{H}_q = \hat{H}_a + \alpha \mathbf{q} \cdot \mathbf{e}_p Q \quad (5.40)$$

acting on the wave function ψ becomes the quantum subsystem when replacing Q by the classical mode trajectory X . Analogously to going from the Hamiltonian (5.19) over (5.21) to (5.22), \hat{H}_q here can be rewritten as

$$\hat{H}_q = E_+ |+\rangle \langle +| + E_- |-\rangle \langle -| + \alpha X (|+\rangle \langle -| + |-\rangle \langle +|). \quad (5.41)$$

Making again an ansatz for the two-level wave function as a superposition of eigenstates $|\pm\rangle$,

$$\psi(t) = C_+(t) |+\rangle + C_-(t) |-\rangle \quad (5.42)$$

5. Employing Bohmian Trajectories in Semiclassical Numerics

and plugging that into the Schrödinger equation associated to (5.41) results in a set of coupled ordinary inhomogenous differential equations

$$\dot{C}_+(t) = -i \left(E_+ C_+(t) + \alpha \mathcal{P}_\pm \cdot \mathbf{e}_p C_-(t) X(t) \right), \quad (5.43)$$

$$\dot{C}_-(t) = -i \left(E_- C_-(t) + \alpha \mathcal{P}_\pm \cdot \mathbf{e}_p C_+(t) X(t) \right). \quad (5.44)$$

For the classical part of the scheme, the two expressions

$$V_c(Q) = \frac{v^2}{2} Q^2 \text{ and} \quad (5.45)$$

$$V_{\text{int}}(\mathbf{q}, Q, t) = \alpha \mathbf{q} \cdot \mathbf{e}_p Q \quad (5.46)$$

can be plugged into equation (5.3) with the backreaction terms evaluated via equation (5.4) and (5.10) for the mean field and the Bohmian approach. In the Bohmian case, the equation of motion for the classical particle solely depends on the position of the Bohmian particle \mathbf{x} projected onto the polarization of the field mode,

$$\ddot{X}(t) + v^2 X(t) + \alpha \mathbf{x} \cdot \mathbf{e}_p = 0. \quad (5.47)$$

The equation of motion for the Bohmian particle is of course given by the guidance law (2.9), which here simplifies to

$$\dot{\mathbf{x}}(t) = \Im \left(\frac{C_+(t) (\nabla|+\rangle) + C_-(t) (\nabla|-\rangle)}{C_+(t)|+\rangle + C_-(t)|-\rangle} \right) \quad (5.48)$$

On the other hand, the resulting equation of motion for the mean field method is

$$\ddot{X}(t) + v^2 X(t) - 2\alpha \mathcal{P}_\pm \cdot \mathbf{e}_p \Re \left(\overline{C_+(t)} C_-(t) \right) = 0, \quad (5.49)$$

which is nice because the integral over the wave function is hidden inside the transition dipole moment \mathcal{P}_\pm of (5.23), which is a known constant anyway. This translates directly into an advantage of this backreaction method in terms of computational effort. Unlike in the one-dimensional scattering examples of the previous section, where the mean field backreaction requires explicit integration over $|\psi|^2$, a classical trajectory here can be integrated even faster than in the Bohmian case.

The mean field approach suffers from a theoretical drawback in this semiclassical model however. When the initially excited atom in the cavity is placed into the *classical vacuum*, which means that $X(t=0) = \dot{X}(t=0) = 0$, while $C_-(t=0) = 0$, $C_+(t=0) = 1$, the energy is trapped in this excited state as the equations do not give rise to the Rabi oscillations which are present in the fully quantum treatment. For the Bohmian semiclassical approach on the other hand, which obtains its backreaction from the position of the Bohmian particle, the classical field's equation of motion typically is not trivially fulfilled for these initial conditions, so this is not an issue.

5.2 Application to Different Toy Models

The mean field equations for C_{\pm} and for the classical field can actually be solved explicitly, when applying the rotating wave approximation while deriving the solution. Here again, the rotating wave approximation amounts to neglecting terms which contain rapidly rotating expressions $\propto \exp(i2\nu t)$, as they oscillate much faster than the Rabi frequency $2g$. The excited atom placed into the cavity initially containing a nonzero classical field displays the usual Rabi oscillations as in figure 5.5 on page 86, because the explicit solution for the population inversion in this case reads

$$W(t) = \cos(2gt), \quad (5.50)$$

which is the same as equation (5.30) for $\rho_n(t=0) = \delta_{n0}$.

It is important to keep in mind that in the full quantum case and in the semiclassical mean field treatment, the rotating wave approximation, which ultimately permits an explicit solution, is applied in different places. As just mentioned, in the semiclassical mean field backreaction approach, the rapidly rotating terms are dropped while deriving the solutions for C_{\pm} from the equations. In particular, the working equations of both semiclassical schemes, (5.43), (5.44) and (5.49) for mean field, as well as (5.43), (5.44), (5.47) and (5.48) resp. in the Bohmian case, are not affected so that when integrating these equations numerically, those terms remain present. This is in contrast to the full quantum case, where the rotating wave approximation already enters into the Jaynes–Cummings Hamiltonian (5.28) which gives rise to the equation of motion of the full quantum wave function Ψ . Unfortunately, solving the full two-level Hamiltonian (5.22) without the approximation is anything but easy. This distinction will become important when the numerical results from the semiclassical treatment are compared to the full quantum solutions, because the former contain the counterrotating terms, while their analytic counterparts do not. This can also be seen from figure 5.7, which summarizes and the steps of the derivation above and visualizes their dependencies.

Implementation

Unlike with the semiclassical scattering examples in the first part of this chapter, an integration using grid methods is not necessary here at all. This is because the full quantum behavior is described by the explicit expression (5.31) and the wave function of the semiclassical scheme can be expanded into a two-dimensional basis, leading to the two equations (5.43) and (5.44) for the time evolution of C_{\pm} . Nonetheless, the same Runge–Kutta scheme, DOP853, as used for everything else so far in this theses, is employed here to directly integrate the working differential equations.

As with the one-dimensional scattering calculations before, initial conditions are sampled from the wave function. For the classical field coordinate X , this means drawing initial conditions from the density

$$\rho(X, \dot{X}) = \sqrt{\frac{\nu}{\pi}} e^{-\nu \left(X - \sqrt{\frac{2}{\nu}} \Re(\gamma) \right)^2} \delta \left(\dot{X} - \sqrt{2\nu} \Im(\gamma) \right), \quad (5.51)$$

which derives from the coherent state with complex parameter γ in equation (5.33). Unless otherwise mentioned, γ will be taken real and positive from now on. It is then possible to

5. Employing Bohmian Trajectories in Semiclassical Numerics

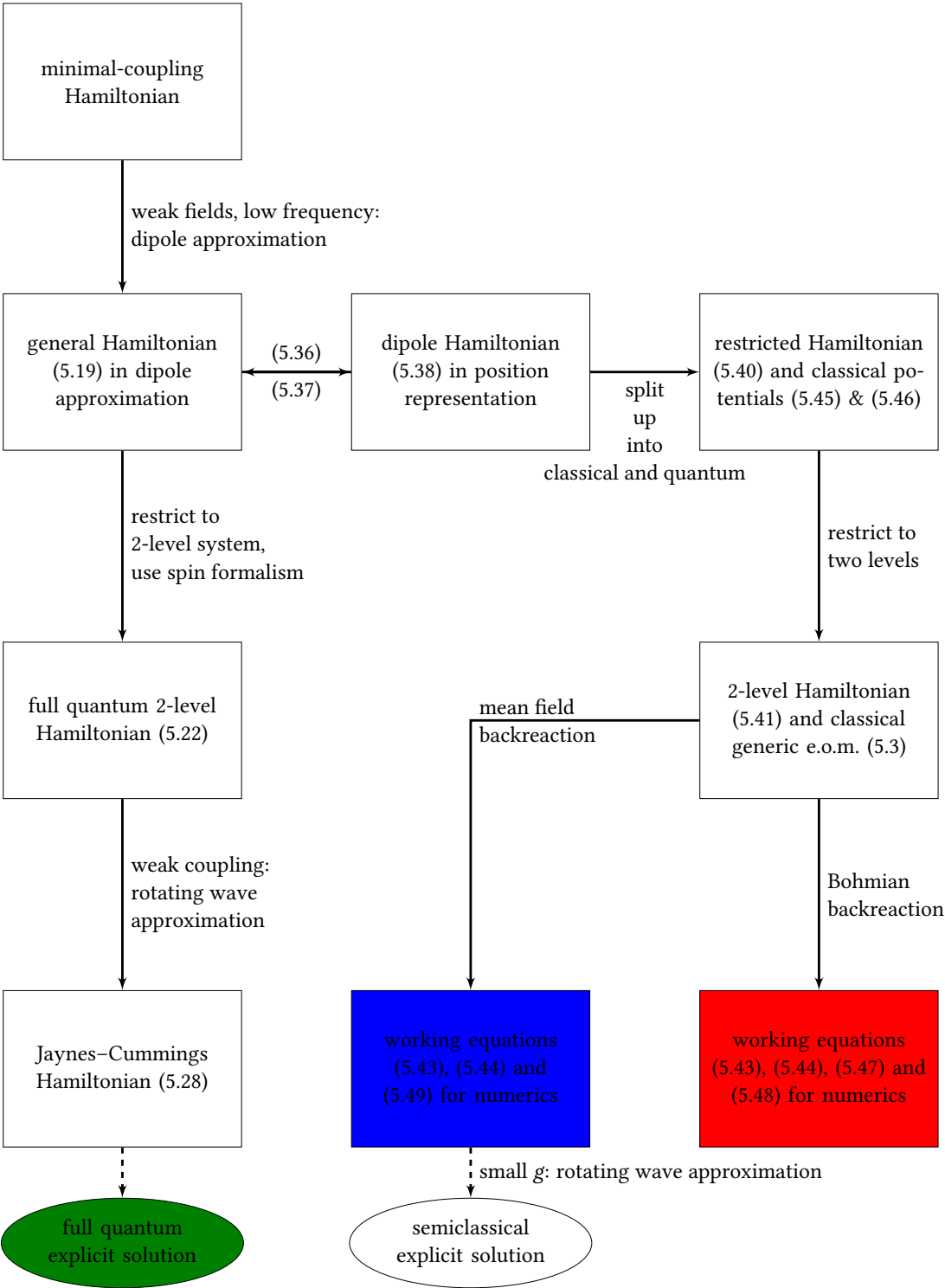


Figure 5.7: Overview of the course of derivation, the different steps involved and at which points approximations are made. Colors indicate which results will be compared to each other and match the colors in the plots of this section.

5.2 Application to Different Toy Models

directly compute its value from the expected number of photons in the coherent state by means of $\gamma = \sqrt{\langle \hat{N} \rangle}$.

For the Bohmian particle, an additional initial condition needs to be sampled from the linear combination of initial hydrogen atom eigenfunctions. These eigenstates are usually given in spherical coordinates in terms of $R_{nl}(r)Y_{lm}(\theta, \phi)$ where the radial part R_{nl} contains a generalized Laguerre polynomial and the spherical harmonic Y_{lm} is the phase factor $e^{im\phi}$ times an associated Legendre polynomial. The hydrogen quantum numbers $n = 1, 2, 3, \dots$, $l = 0, 1, 2, \dots, n - 1$ and $m = -l, \dots, l$ suffice to describe the eigenstate, because under the dipole approximation of Hamiltonian (5.19), spin is a conserved quantity in transitions between hydrogen states.

Despite the description of the hydrogen atom's eigenstates being very compact in spherical coordinates, for numerical purposes it is better to integrate the Bohmian trajectories in Cartesian ones. The reason is that as it turns out, the degeneracy of the origin causes problems when a particle has a trajectory passing by close to the origin. In such a situation, the value of the polar angle θ has to jump to $\pi - \theta$, but for values of θ close to zero or to π , numerical inaccuracies can lead to nonsensical descriptions like negative values of the radial coordinate r .

From a fundamental point of view, in Bohmian theory the outcome of any measurement of an observable should be described in terms of positions of Bohmian particles. A concrete analysis, possibly including the measurement apparatus, of how to obtain the population inversion from Bohmian coordinates for combinations of eigenstates with significant overlap would lead too far here, though. As the semiclassical treatment does not make this task easier, this would probably be material for a thesis of its own. So for simplicity, in this section the population inversion will just be read off from the wave function coefficients C_{\pm} for both semiclassical approaches, not just the mean field one. Aspects of the motion of the Bohmian particles in the ensemble can of course be discussed nonetheless.

Results and Discussion

The topical review paper on the Jaynes–Cummings model by B. Shore and W. Knight [72] has a nice series of plots on how the time evolution of the population inversion changes with increasing expected photon number in the cavity. Because the coherent state becomes more and more classical as $\langle \hat{N} \rangle$ increases, a comparison to this plot seems like a good starting point for investigating how well the semiclassical approximation works.

Figures 5.8 and 5.9 reproduce the plots of [72] together with the semiclassical numerical data. The confidence intervals are again the result of five batches of 500 trajectories each. The transition from the hydrogen atom's ground state to its first excited state is realized in the resonant two-level system with the coupling chosen in the range where the rotating wave approximation applies. The remaining parameters used are listed in table 5.3 on page 95.

The plots show, that indeed the semiclassical approaches describe the collapse better and better as the number of photons initially present in the cavity increases. The mechanism, which leads to the collapse in the semiclassical case is, that each single entity of the model system performs its Rabi oscillations with a slightly different frequency. Initially, the phases are still correlated,

5. Employing Bohmian Trajectories in Semiclassical Numerics

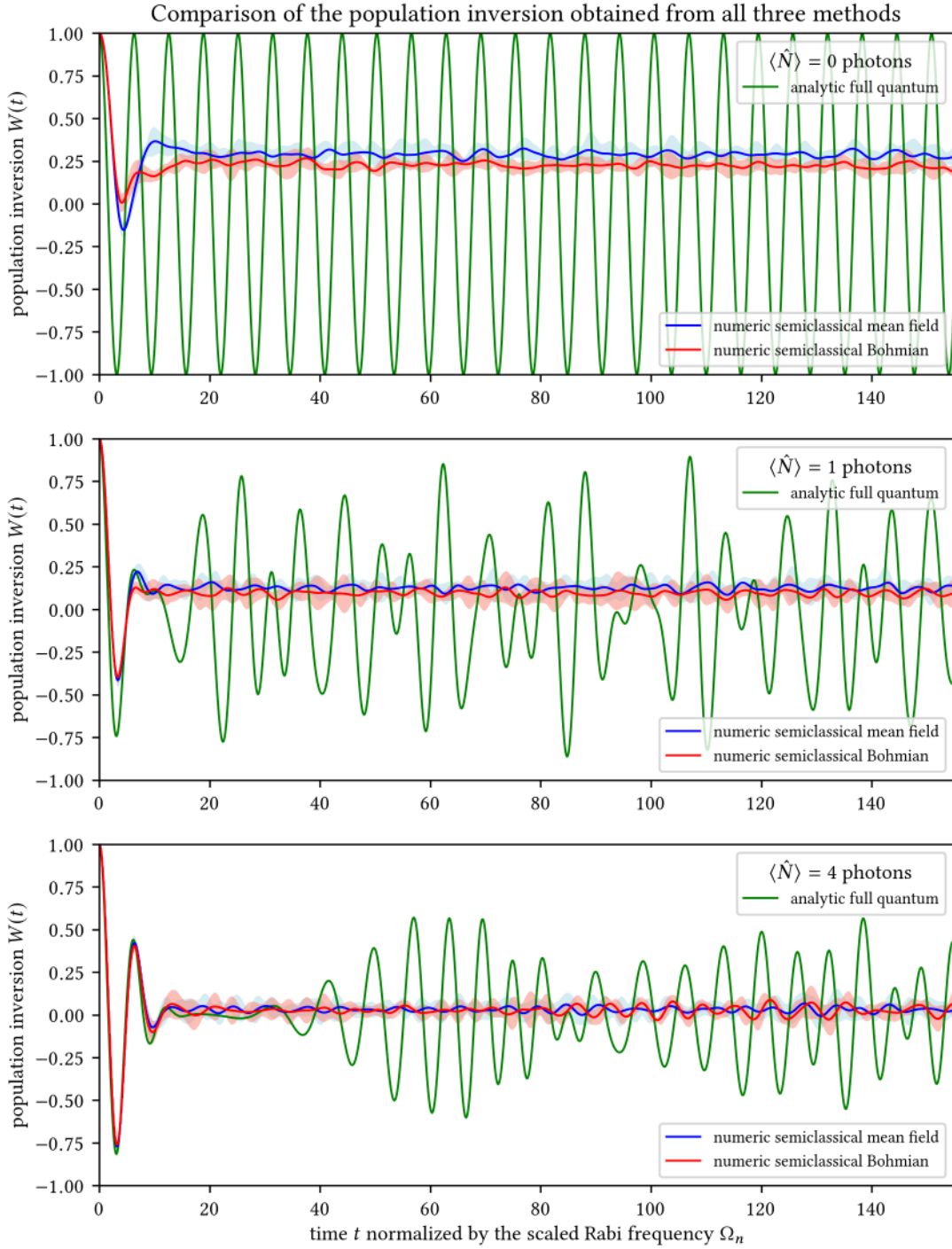


Figure 5.8: First part of the comparison between full quantum and semiclassical solutions in the rotating wave approximation for different expected photon numbers, here 0, 1 and 4. Again $2\text{-}\sigma$ confidence intervals for the numerical data.

5.2 Application to Different Toy Models

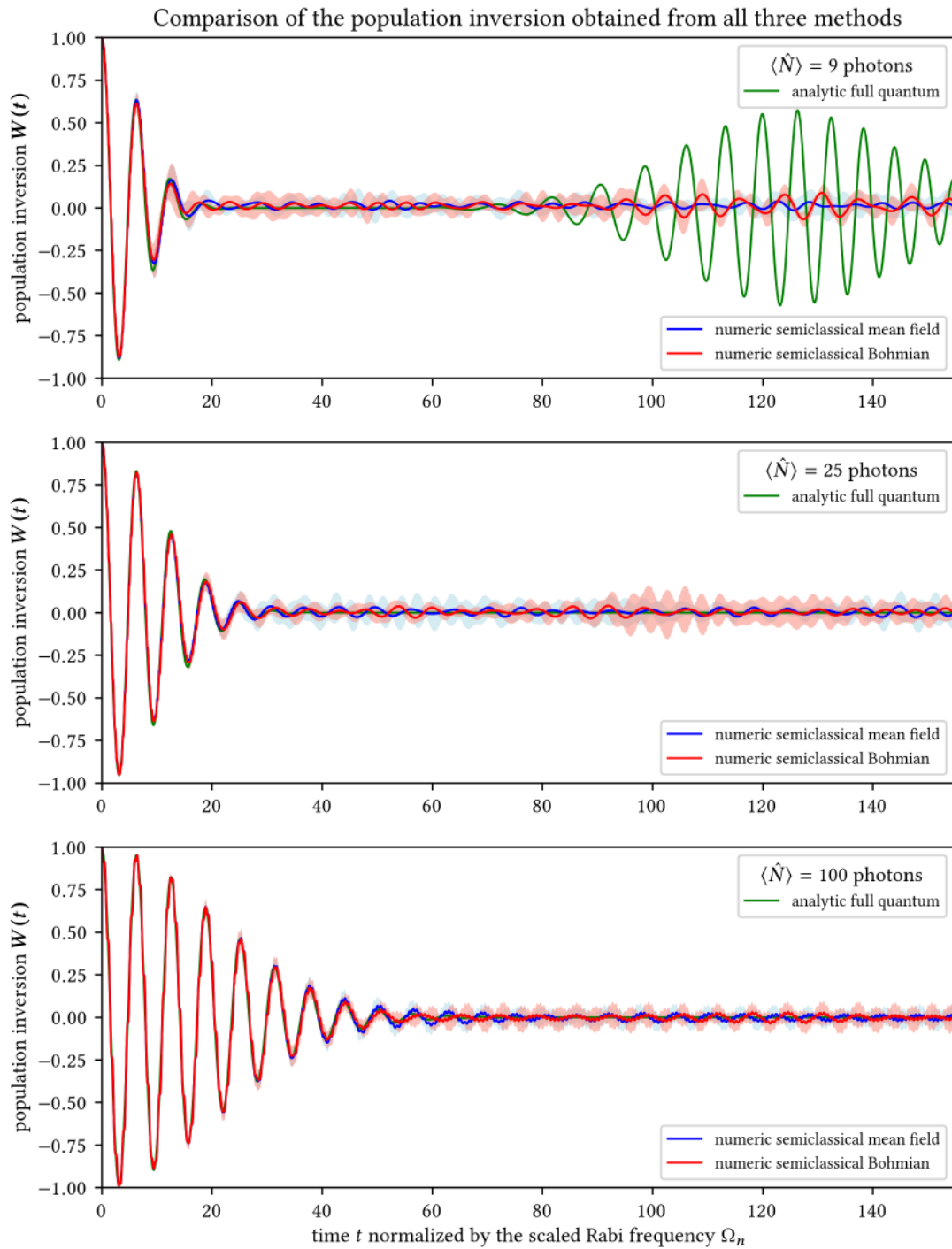


Figure 5.9: Second part of the comparison between full quantum and semiclassical solutions in the rotating wave approximation for different expected photon numbers, here 9, 25 and 100. Again 2- σ confidence intervals for the numerical data.

5. Employing Bohmian Trajectories in Semiclassical Numerics

fundamental parameters		derived parameters	
n_-, l_-, m_-	1, 0, 0	\mathcal{P}_\pm	≈ 0.745
n_+, l_+, m_+	2, 1, 0	ν	0.375
α	0.005	g	≈ 0.0043
\mathbf{e}_p	z-direction		
γ	0, 1, 2, 3, 5, 10		

Table 5.3: Choice of parameters for producing figures 5.8 and 5.9. Left: parameters fixed in the model, right: values of constants as a consequence of the choice on the left. All numbers are given in their respective atomic units.

but dispersion among them develops more or less quickly. Averaging the population inversion over the whole ensemble then leads to the collapse phenomenon. What both Bohmian and mean field backreaction fail to reproduce are the genuine quantum effects of vacuum Rabi oscillations and revivals after collapse. The absence of revivals is sometimes phrased as “semiclassical light is lost from the cavity” in the literature. In the quantum field description, the cavity is of course idealized in the sense that no photon ever escapes.

When inspecting the plot with $\langle \hat{N} \rangle = 100$ photons in the coherent state closely, small ripples in the semiclassical graphs catch the eye. Those are the oscillations that are neglected in the rotating wave approximation for small α . Because of the scaled Rabi frequency being proportional to $\sqrt{\langle \hat{N} \rangle + 1}$, they are visible in this plot only. The time along the horizontal axes is multiplied by Ω_n to normalize the oscillation periods among the plots, so this last one is stretched the most. This scaling is also responsible for creating the impression that the collapse of the oscillations happens more slowly as $\langle \hat{N} \rangle$ grows, but the opposite is actually true in terms of physical time. The presence of a large number of photons in the cavity actually makes emission of a photon from the atom a much more likely process.

From about $\langle \hat{N} \rangle = 4$ onward, the collapse is approximated very well by the semiclassical methods. For $\langle \hat{N} \rangle = 1$, the semiclassical solutions quickly differ quantitatively and later also qualitatively from the quantum solution, which displays a somewhat erratic behavior. In the $\langle \hat{N} \rangle = 0$ case, instead of Rabi oscillations, the population inversion not only rapidly drops down but also ends up slightly offset towards the excited state. The author has no explanation for a mechanism causing this offset. In all other plots, after the collapse, the semiclassical graphs drop down to about zero population inversion, which means that the atom is in the ground or first excited state with equal probability. There are still small, irregular residual oscillations, which are essentially a consequence of the random sampling of initial conditions and become smaller with increasing sample size.

It is also important to point out that the differences seen between the Bohmian backreaction curve and the mean field backreaction curve in figures 5.8 and 5.9 are solely caused by the initial conditions of X being randomly sampled individually in each approach. In fact, when looking at the dynamics resulting from using identical initial conditions for the field mode, the two semiclassical graphs are essentially identical and only show differences upon sufficiently strong magnification of the plots.

5.2 Application to Different Toy Models

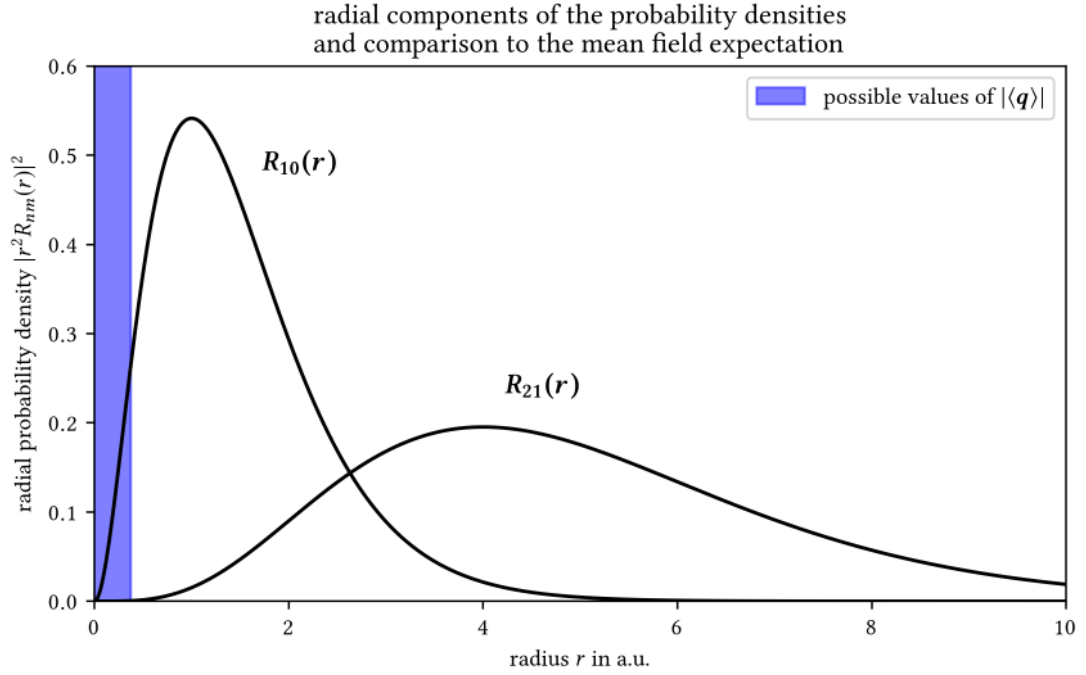


Figure 5.10: Visualization of the difference between backreaction terms. Radial probability densities of the distribution of a Bohmian particle in each state of the two-level hydrogen atom, which gets projected onto \mathbf{e}_p in the Bohmian backreaction term. The blue area represents the range on the horizontal axis where $|\langle \mathbf{q} \rangle|$, on which the mean field backreaction term depends linearly, can have values for the value of \mathcal{P}_\pm from table 5.3. Hence, the maximum absolute value of the Bohmian backreaction term is about an order of magnitude bigger than the mean field backreaction one.

This is surprising, because the two backreaction terms differ quite a lot, both conceptually and also potentially in magnitude as figure 5.10 clarifies. The only possible explanation for this behavior must hence be, that for weak coupling, where the rotating wave approximation is valid only, the effect of the backreaction term on the dynamics must somehow be suppressed almost completely.

A recent publication [56] fortunately contains exactly the information required to extend the comparison beyond the rotating wave approximation. The authors numerically computed $W(t)$ for a hydrogen atom in the Jaynes-Cummings model described by the general 2-level Hamiltonian (5.22) with the atom initially being in the ground state and the cavity containing $\langle \hat{N} \rangle = 10$ photons. Their data is compared to the semiclassical results in figure 5.11 below. Unlike it was the case with the previous plots, the results in this situation are not as clear any more now, but they finally constitute some examples where the semiclassical graphs significantly differ from each other.

Starting at a coupling $g = 0.0075$ in the top plot, the regime where the rotating wave approximation stops working is entered. Both semiclassical approaches again reproduce the collapse

5. Employing Bohmian Trajectories in Semiclassical Numerics

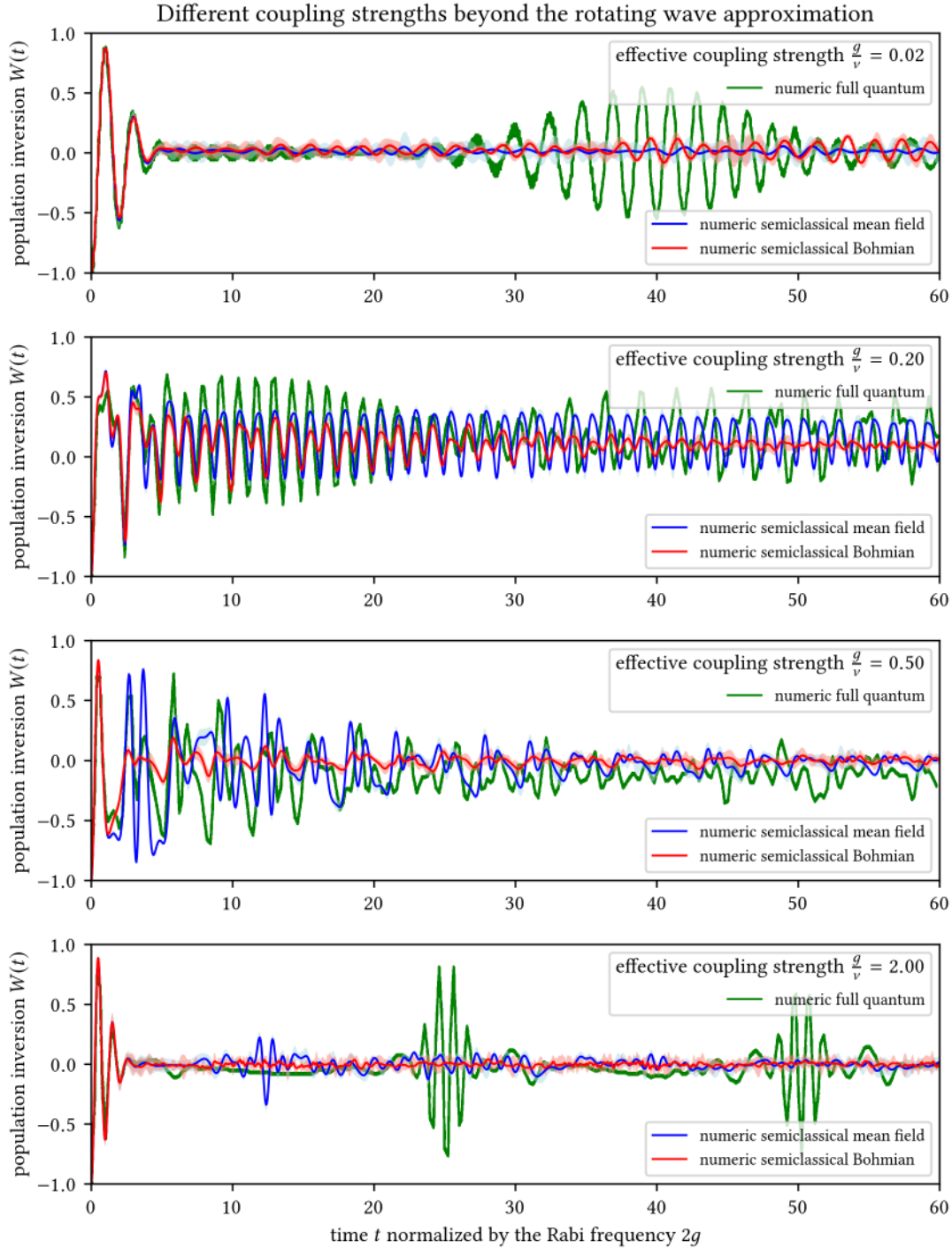


Figure 5.11: Direct comparison of the semiclassical results to the numerical data beyond the rotating wave approximation for a series of effective couplings. The green curves have been computed by Zhang, Chen and Zhu [56, fig. 3]. With kind permission of Yu-Yu Zhang and Chinese Physics Letters.

5.2 Application to Different Toy Models

well, but directly after that, the full quantum behavior displays some additional oscillations of very high frequency, which is absent for both backreactions.

Increasing the coupling to $g = 0.075$ makes the revival phenomenon disappear in the full quantum results. It gets replaced by an again very erratic behavior, which however still differs from the middle plot of figure 5.8. Both semiclassical graphs qualitatively follow the quantum solution up to $2gt \approx 5$. After that, all three curves separate. One could claim that the mean field solution approximates the full quantum case better than the Bohmian one, which also oscillates, but with an even lower amplitude, but the overall differences are still significant.

At $g = 0.1875$, where the Rabi frequency matches the counterrotating terms' frequency, the picture becomes even more jumbled. Despite quantitatively being completely off, the mean field method at least qualitatively follows the quantum result up to about the same time as before. The Bohmian one on the other hand rapidly collapses down around $2gt \approx 3$ already and then settles to small amplitude oscillations around zero, which eventually die off. Again, it is not easy to argue which semiclassical approach performs better.

Finally, the collapse and revival phenomenon returns for extremely strong coupling $g = 0.75$. As has been the case in the weak coupling regime of the rotating wave approximation, the semiclassical data accurately reproduces the collapse, but none of the revivals. In the mean field case however, at precisely half of the first revival time, there is a small, but statistically absolutely significant surge in oscillation amplitude, resulting in what looks like a small version of the first revival event.

Unfortunately, what one is ultimately left with is, that the analysis of the strong coupling regime is not at all conclusive when it comes to judging which backreaction method is better at approximating the full quantum behavior. There is however another way in which the quantitative difference between the two backreaction terms can be increased. This is done by changing the energy levels excited in the cavity, for example by starting with a highly excited Rydberg hydrogen atom in the cavity resonant with the transition to the ground state. For the mean field backreaction, this will reduce the contribution to almost zero because the eigenstates have only little overlap. The maximum magnitude of the Bohmian backreaction on the other hand gets boosted, as the position of a very far away electron directly enters equation (5.10).

fundamental parameters		derived parameters	
n_-, l_-, m_-	1, 0, 0	\mathcal{P}_\pm	≈ 0.047
n_+, l_+, m_+	9, 1, 0	v	≈ 0.494
α	0.1	g	≈ 0.005
\mathbf{e}_p	z-direction	$\langle \hat{N} \rangle$	100
γ	10		

Table 5.4: Choice of parameters for producing figure 5.12. Left: parameters fixed in the model, right: values of constants as a consequence of the choice on the left. All numbers given in their respective atomic units.

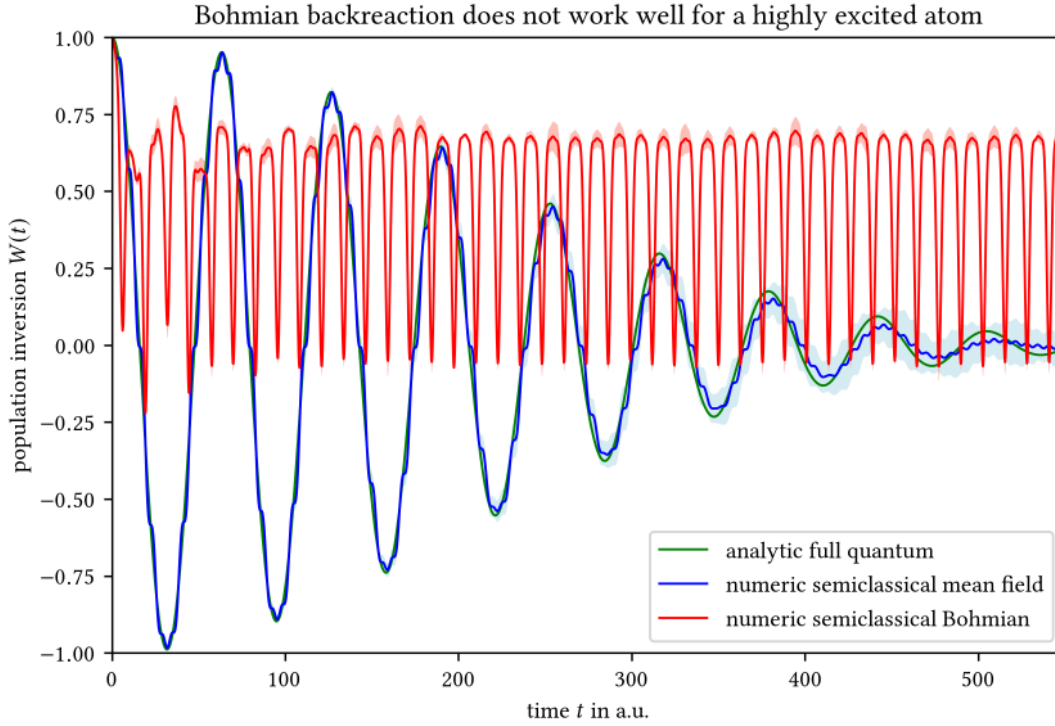


Figure 5.12: Comparison for a transition between ground state and a highly excited hydrogen eigenstate with $n=9$.

To investigate the behavior in this scenario, it is sufficient to return back into the realm of the rotating wave approximation and look at the collapse phase only. With the parameters of table 5.4, the scenario is very similar to the bottom plot of figure 5.9. The major change is that the excited state has been replaced by the one with $n_+ = 9$, which results in almost no overlap between the relevant eigenstates. The transition dipole moment, which contributes to the mean field backreaction term, is then very small, $\mathcal{P}_\pm \approx 0.05$ a.u., so that the mean field approach is essentially the same as having no backreaction present at all. The position of the Bohmian particles on the other hand becomes large with values of \mathbf{x} up to 250 a.u. establishing a much stronger backreaction in this particular case.

Figure 5.12 contains the numerical results from the semiclassical algorithms and the quantum solution of equation (5.31), so the counterrotating terms have again been neglected. The blue mean field graph almost perfectly reproduces the time evolution of the population inversion oscillations during the collapse phase up to small wiggles. These originate from the rotating wave approximation being absent in the numerical scheme. The Bohmian counterpart in red however strongly differs from both other curves. It features a pronounced, asymmetric oscillation between zero population inversion and the atom mostly being in the ground state at roughly the same frequency at which the field oscillates, i.e. half of the frequency of the counterrotating terms visible in the plot.

5.2 Application to Different Toy Models

In fact, in this case for some entities of the ensemble the anharmonic oscillation is directly reflected in the time evolution of the field coordinate trajectory X , which has mainly just been carrying out a plain harmonic oscillation in all other cases so far. Indeed, for the far-out Bohmian particles, the large backreaction term messes up the individual field time evolution and boosts the values of X up one order of magnitude over the typical value resulting from the choice of γ . Because of the symmetry properties of the model system, averaging X over the whole ensemble again cancels these strongly deviating time evolutions of the individual entities and results in a harmonic oscillation very similar to the mean field case. Interestingly, both the Bohmian as well as the mean field approaches produce similar results when starting with the atom initially in the ground state instead of the excited state.

One might wonder, whether or not it was possible to obtain the population inversion in a different way in the Bohmian semiclassical treatment. Instead of calculating the population inversion from the wave function's superposition coefficients, the state in which a particular atom in the ensemble of system copies is currently in should be indicated by the position of its Bohmian particle. This approach of course requires that the two eigenstates $|\pm\rangle$, between which the transition happens, are sufficiently separated in terms of $|\langle - | + \rangle|^2 \approx 0$ whenever $|\langle + | + \rangle|^2$ is not approximately zero and the other way round.

The picture to have in mind is the following. The electron, represented as a Bohmian particle, is likely going to be at a location initially, where the probability density associated to the initial state is large. During the transition to the other state, the probability density at this location decreases, so the particle moves over to a region, where the other state's probability density sufficiently differs from zero. As the population inversion oscillates back and forth, so does the Bohmian particle. In a full quantum Bohmian version of the system, this expectation is certainly justified and in fact required by equivariance. However, when splitting it up into a classical and a quantum part, quantum correlations between the subsystems are not necessarily preserved when the residual term in equation (5.8) is neglected. And in fact, in the semiclassical model here, the picture of the Bohmian particle moving back and forth between eigenstate supports guided by the wave function restricted to the quantum subsystem is not justified.

To support this claim, figure 5.13 contrasts the time evolution of the radial component of a Bohmian particle's position with the time evolution of the population inversion obtained in the usual way. This is done for four different entities of the Bohmian ensemble with randomly sampled initial conditions. The situation is again a very weakly coupled transition between hydrogen ground and first excited state with 100 photons initially in the cavity, but the precise parameters are not really important, because the qualitative behavior is universal. Starting with describing the bottom plot, the population inversion performs the usual Rabi oscillations starting in the excited state, but each one has a slightly different frequency, depending on the respective field initial conditions. This dispersion of course accounts for the collapse of the population inversion oscillations when averaging over the ensemble.

Now, compare the population inversions of the lower plot to the radial component of the Bohmian particles' positions in the upper plot. It becomes apparent that the state, which the atom is in according to the restricted wave function ψ , does not reflect in the position of the particle. The expectation would be, that the radial component has a smaller value when $W(t) = -1$,

5. Employing Bohmian Trajectories in Semiclassical Numerics

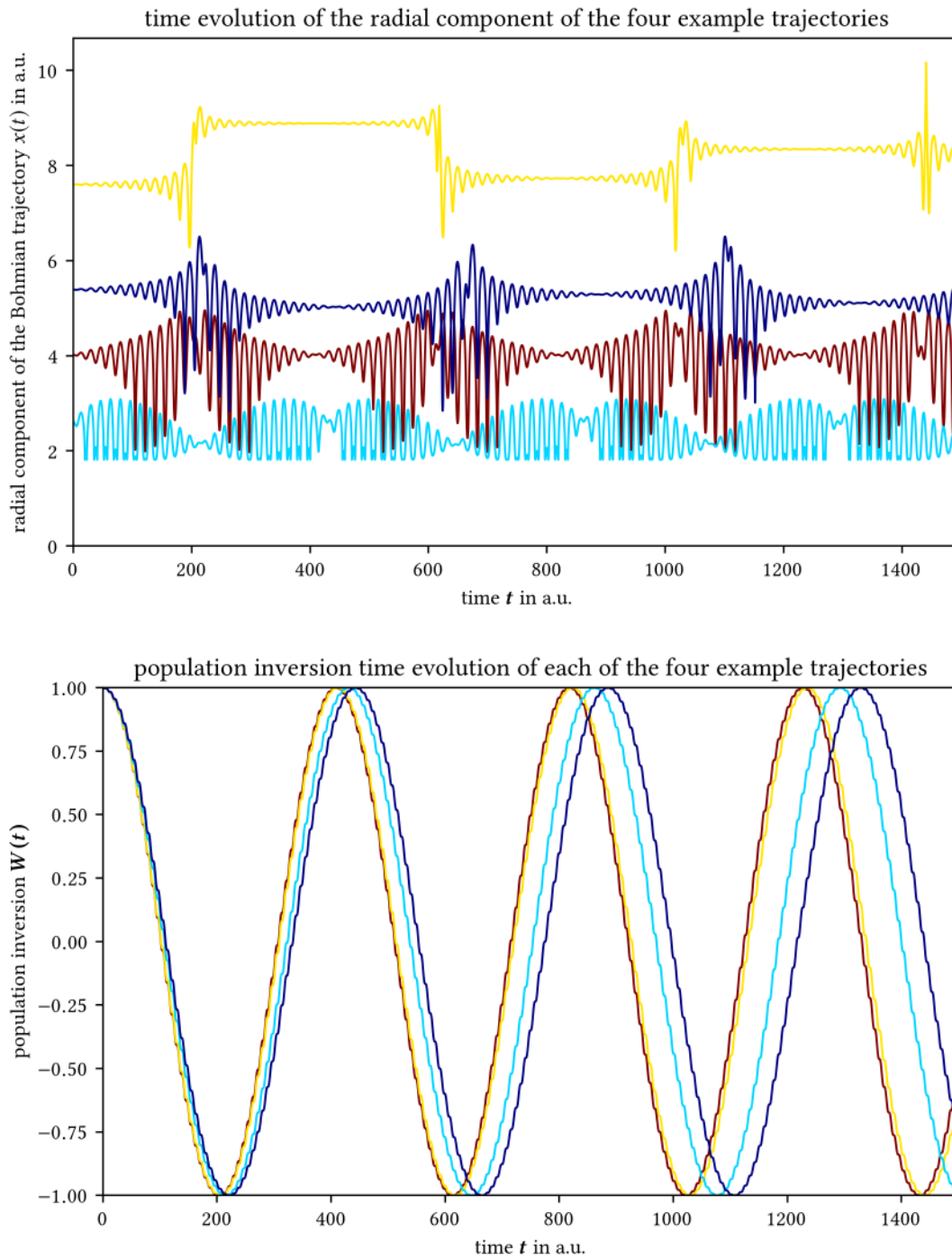


Figure 5.13: Four different examples of the Bohmian ensemble showing why obtaining the population inversion from the Bohmian position does not work. Top: radial part of the Bohmian particles' positions over time; bottom: corresponding time evolution of the population inversion obtained from the restricted wave function. Colors refer to the same ensemble entities across both plots.

5.2 Application to Different Toy Models

i.e. the atom is in the ground state and analogously, that all particles are further away from the nucleus when the atom is excited and $W(t) = 1$, c.f. the radial distributions of the two states in figure 5.10. But instead of moving closer towards and away from the origin at about the Rabi frequency, the Bohmian particles mostly remain over long time scales where they had initially started. There is however some dynamics going on by means of the particle performing oscillations about its original position with the frequency of the field whenever the atom is in the “opposite” state, i.e. when the value of $|\psi|^2$ at the location of the particle becomes small. That is, the particles further away from the nucleus wiggle most when the particles close to the nucleus remain basically stationary and the other way round. Nonetheless, ensemble entities with the particle far out can have population inversion frequencies very similar to those with the particle on the inner side, as the yellow and reddish brown graphs exemplify.

The oscillations in the radial component of the Bohmian particle’s positions in the upper plot of figure 5.13 feature some sudden changes in amplitude at times, like for example the reddish brown curve at $t \approx 100$ a.u.. A thorough analysis of the precise dynamics in this case shows that this effect is a consequence of nodes forming and moving around under the time evolutions of the complex coefficients of the superposed eigenstates, so that effectively the particle is being locked into particular regions of configuration space at times. In fact, the choice of eigenstates used in figure 5.13 is optimal in the sense that the eigenstates themselves have no radial nodes as can be seen from figure 5.10, too. A general hydrogen eigenstate with quantum numbers n and l has $n - l - 1$ radial nodes in addition, which makes the situation even worse for transitions between such eigenstates, because then the Bohmian particle has no chance at all to cross this obstacle in the semiclassical case.

Hence, within the realm of the semiclassical approximation here, counting Bohmian particles with positions within one of the atomic orbitals does not constitute a practically useful method of obtaining information about the population inversion of the ensemble. This may seem surprising at first glance, because from a fundamental point of view, in Bohmian theory the outcome of measuring any observable, such as the population inversion, should be described in terms of locations of Bohmian particles.

But this does not reveal an inconsistency of the scheme by itself, because there is no notion of equivariance in the semiclassical Bohmian treatment. Ultimately, the quantum subsystem of each copy of the model evolves independently from all others through the coupling to its field coordinate, whose trajectory also differs from the ones in other ensemble entities, so $|\psi|^2$ cannot be a measure of typicality. Thus, it is not even possible to speak of the single particle having a distribution related to its guiding wave function, because each such distribution would be unique in the ensemble and thus cannot be verified by only looking at that single particle each time.

Before concluding the chapter, the reader may argue that the choice of eigenstates in the preceding discussion always had zero angular momentum. Nonzero angular momentum would alter the trajectories of the Bohmian particle and thus the backreaction term. A quantum number $m \neq 0$ leads to a term $\propto \frac{m}{r^2} \mathbf{e}_\phi$ in the guiding law, i.e. the Bohmian particle follows a circular orbit around the nucleus. This is of course a valid objection and has thus been investigated with the result being that the computational effort increases significantly when trajectories

rapidly¹¹ rotating around the origin need to be followed in the integration, while qualitatively there is no change to the results presented here. Some features become a bit less pronounced, like the improper oscillations of the Bohmian graph in figure 5.12, but that is about it. The relevant dynamics of the Bohmian particle arise from the time dependence of the coefficients C_{\pm} in the guiding law and not from its angular momentum term.

Also, one may wonder why the electron has been treated as a spinless particle, despite a physical electron clearly having nonzero spin. The reason for that is also, that starting in a spin eigenstate \mathbf{s} collinear with the polarization vector \mathbf{e}_p only marginally affects the numerical results, but not significantly. There is in fact a theoretical explanation for this. Everything in this section has made use of the dipole approximation. It was already contained in Hamiltonian (5.19) from which the derivation initially started. Within the dipole approximation, spin is a conserved quantity and thus the atom always remains in the initial spin eigenstate. In this case, spin can be incorporated into Bohmian mechanics by adding the term $\nabla \ln(\rho^{\psi}) \times \mathbf{s}$ to the guidance law.

Furthermore, C. Colijn and E. Vrscaj have shown [73], that under the dipole approximation, a hydrogen atom's electron subjected to semiclassical radiation is confined to a motion on invariant hyperboloid surfaces for the transition between ground and first excited state which has also been examined here. By visual inspection of the trajectories, this still seems to hold largely true when the Bohmian backreaction term is added to the equations. This means that the Bohmian trajectories continue revolving around the z-axis on these surfaces and do not start off to explore other parts of configuration space in the semiclassical treatment when the spin term is present.

So after all, equipping the electron with angular momentum or spin does not qualitatively change the results that have been presented here. In particular, even combined together they do not constitute a remedy for the lack of being able to deduce the population inversion in an alternative fashion here, namely from the position of the Bohmian particles in the Bohmian backreaction approach.

5.3 Conclusions

The results of benchmarking the mean field versus the Bohmian backreaction approaches to mixed quantum–classical dynamics in order to determine their ability to approximate the full quantum behavior do not lead to a clear winner in the toy model considered here. With the motivation provided by the successful application of the Bohmian method in different publications as a starting point, the expectation that the Bohmian method works better in certain cases, where a superposition of wave functions poses problems to the mean field method, was confirmed first.

This raised hope, that the Bohmian backreaction approach would perform nicely in a semiclassical version of the Jaynes–Cummings model, which builds on such a superposition. Apart from that, there is no theoretical reason why one should expect that for this type of interaction

¹¹At least when r is tiny.

5.3 Conclusions

in one of the most important model systems in physics, the Bohmian approach approximates the full quantum solution better or worse than the traditional mean field approach.

For the two-level atom in a cavity, S. Haroche predicts [74], that an external “noisy classical field” leads to collapse, but not revival of the population inversion oscillations. The revival phenomenon requires a discrete distribution of field frequencies and can thus not be observed when treating the electromagnetic part of the system classically. Indeed, when splitting the system into a classical and a quantum part as in the preceding section, the statement is confirmed by both semiclassical approaches, provided that dipole and rotating wave approximations hold, the two-level system does not involve hydrogenic Rydberg states and the number of photons initially present in the cavity is sufficiently large.

However, in this case the backreaction terms play no significant role for the overall dynamics. So to discern their effects, it is necessary to violate some of these prerequisites. Beyond the rotating wave approximation, none of the approaches properly approximates the features found in the numerical data of the full quantum case. It remains unclear, which approach should be considered better in this regime of strong coupling. When returning to the realm of the rotating wave approximation but increasing the Bohmian backreaction term by considering a Rydberg state of the hydrogen atom, the backreaction onto the field leads to a qualitatively incorrect description of the collapse, while mean field or even no backreaction at all work very well.

While the mean field backreaction is computationally more efficient in this particular model, the Bohmian approach could have given rise to an alternative way of obtaining the population inversion, namely by looking at the position of the Bohmian particles in the ensemble. At least for the hydrogen atom in the Jaynes–Cummings model, this turned out not to work, because the numerical scheme does not come with the equivariance property, which holds in actual Bohmian mechanics. The formation of nodes in the wave function of the quantum subsystem prevents the Bohmian particles from moving between the supports of separated eigenstates. This shows that the entanglement between the atomic and the field part, which is neglected in the Bohmian mixed quantum–classical treatment of the model system, is fundamental to the correct microscopic dynamics. It is thus questionable whether sampling the initial velocity of the classical particle from the Wigner or¹² Husimi distribution of the coherent state instead of assigning the Bohmian velocity to it, as was done here, would have an impact on the results.

Nonetheless, it has been demonstrated that the Bohmian semiclassical approach does actually sometimes give rise to predictions, which approximate the full quantum solutions well. This is remarkable, because the scheme is essentially a set of highly nonlinear and backcoupled equations, in which the backreaction originates from the actual position of the Bohmian particle so that properties like charge are thus attributed to the particle. This presents a significant shift away from the Bohmian paradigm in quantum mechanics, where the linear Schrödinger equation contains these parameters and governs the time evolution of the wave function, which in turn guides the otherwise totally passive Bohmian particles, described by nothing but a position in configuration space. In particular, a Bohmian particle does not backreact on the time evolution of the wave function at all in the proper theory.

¹²For a coherent state, both coincide anyway.

5. Employing Bohmian Trajectories in Semiclassical Numerics

At the end of the day, different backreaction schemes in mixed quantum–classical dynamics simply perform better or worse for different computational quantum problems and for sufficiently complicated ones, there is not necessarily a way of telling a priori which one will work best. So this chapter confirms once more, that tailoring a solver to the particular problem at hand unfortunately remains an essential task in fields like computational chemistry.

6 Summary, Concluding Remarks and Future Directions

The number of particles, for which the time-dependent Schrödinger equation can be solved numerically on a fixed grid for general wave functions, is inherently limited. This is because when not sacrificing on grid resolution, the amount of grid points grows exponentially in the number of degrees of freedom. As of today, still only a handful of interacting particles can be handled in this way in a fully quantum manner unless special wave function properties can be exploited in fortunate circumstances. Without any strategies explicitly attacking the exponential scaling, this situation is not going to change significantly by the growth of computational power alone.

Of course, many approximate strategies for dealing with this fundamental problem exist. In this thesis, several methods have been analyzed, which turn Bohmian trajectories into a numerical tool for achieving this goal in various ways. Some very recent ones and also one newly proposed here were compared to more established algorithms in view of the quality of their predictions. The approaches can generally be divided into two categories:

- Using adaptive Bohmian grids instead of a stationary one, the basis of the exponential scaling can be reduced. Wyatt's algorithm does this, but seemed to exhibit potential for simplification and speedup. This is leveraged by the many interacting worlds method of Hall, Deckert and Wiseman and to a limited extent also by a new hybrid method, via trading accuracy for less computational effort when approximating the Bohmian dynamics, from which the wave function time evolution can be restored. How well this approximate procedure ultimately works out and what the limitations are, was analyzed in the context of simple explicit solutions of the Schrödinger equation.
- The exponent itself can be reduced by only considering those degrees of freedom as quantum, for which classical treatment is not justified, and applying Newtonian mechanics to the rest. To account for self-consistency, a backreaction from the quantum onto the classical subsystems needs to be implemented in this approximation. The traditional way of doing this, the mean field or Ehrenfest approach, was recently challenged by a Bohmian method. Both seem to have advantages every now and then, depending on the properties of the quantum system under consideration, as was confirmed by a preliminary analysis in a specific scattering scenario. They were then put to test against each other in an application of real-world relevance, the hydrogen atom in the Jaynes-Cummings model.

In the first case, all of the algorithms face trouble dealing with nodes in the wave function, which severely limits the set of admissible wave functions. The problem with Bohmian grids is, that reducing the total number of grid points by distributing them according to the probability

density backfires. The domain of configuration space around nodes is left underrepresented and it turns out that good resolution there is essential to all the algorithms under investigation. An increase of the number of grid points will first and foremost improve the resolution in the peaks of the wave function. For a similar one near a node, a disproportionately large number is required, which reduces the primary advantage *ad absurdum*. Wyatt's algorithm also suffers from this, but strategies to cope with it by making use of more advanced grids exist. These can, however, not be applied to the more efficient methods, because disposing of the information about the density and solely inferring it from the $|\psi|^2$ -distributed grid points makes the Bohmian grid fundamental to them.

Furthermore, the applicability of the new algorithms is currently limited to one-dimensional configuration space, where the static grid's scaling problem is insignificant. In future work, still striving for the goal of not wasting grid points in areas where the wave function nearly vanishes at times and does not change much, a prospective combination of the stable many interacting worlds dynamics with the flexibility of Wyatt's method on an Eulerian–Lagrangian grid guided by the former could be investigated. For any practical relevance, a generalization of the many interacting worlds dynamics to multidimensional configuration space per world featuring the same robustness under time evolution and retaining the properties of covering nodal areas with trajectories and complying with the inverse-square scaling law would need to be attained first, though.

The hybrid algorithm presented in this thesis is likely running into a dead end, however. This is not because of its issues with stability arising from an inaccuracy in the adaptive Gaussian kernel density estimation at the fringe of the wave packet. How to fix this by guiding those trajectories with the interworld interaction force has been outlined. But even the complex phase variant of the approach has to eventually collapse when a node is present, despite a respectable result with the parameters used here. The problem with the discontinuity in the spatial derivative along the unstructured grid caused by a node seems only alleviated, but not remedied.

In the second category, mixed quantum–classical dynamics, the Bohmian backreaction algorithm proved to be superior over the mean field approach in a specific scattering scenario, where the wave function superposition in the quantum subsystem was not properly reflected in the mean field backreaction term. For the hydrogen atom in the Jaynes–Cummings model, which also builds on a superposition, parameters can be chosen, so that on bounded time scales the time dependence of the population inversion in the rotating wave approximation is reproduced with great accuracy by a semiclassical description of the light field. But for these parameters, the particular type of backreaction had no effect distinguishable from no backreaction at all. As expected from treating the atom quantum-mechanically and the light field classically, the backreaction term in neither of the two semiclassical methods gave rise to the eventual revival of oscillations in a lossless cavity.

Deviations of the semiclassical results from the full quantum behavior were observed for a coupling strength beyond the rotating wave approximation. Both methods resulted in different dynamics each, but none prevailed as preferable to the other in terms of an accurate description of the dynamics. In the regime of extremely strong coupling, both approaches did

6. Summary, Concluding Remarks and Future Directions

correctly reproduce the collapse of population inversion oscillations again. After that, looking at the transition between the ground and a Rydberg state back in the rotating wave approximation in order to provoke a difference in the maximal magnitude of the backreaction terms finally provided a clear picture. The distortion of the field oscillations caused by the artificially increased Bohmian backreaction resulted in a nonsensical time evolution of the population inversion. With the mean field backreaction term having been brought down to a negligible magnitude on the other hand, the collapse was again very accurate for this method.

The ensembles of trajectories of the Bohmian particles describing the electron in the orbitals were analyzed, too. The reduction of configuration space down to the atomic subsystem seems to significantly alter their dynamics, because without a quantum description of the photons in the cavity, it is no longer possible to move around certain wave function nodes. Due to this, the electron could end up locked within one of the orbitals. Unfortunately, obtaining the population inversion from looking at the particle position for wave functions with little overlap is prohibited in consequence.

The semiclassical Bohmian backreaction method is an approximation to Bohmian mechanics, but many features of the theory are not preserved. For example, with an ensemble of differently evolving wave functions, there cannot be a notion of equivariance. Unlike the quantum version of the theory, where Bohmian particles never exert any influence onto the time evolution of the wave function guiding them, the equations of motion in the semiclassical method are coupled in both directions in a highly nonlinear way. The approach departs from the Bohmian description of nature even more by explicitly assigning properties, such as charge, directly to the Bohmian particle instead of just letting it be a parameter to the Schrödinger equation. It is thus remarkable that in specific situations the values of observables are predicted in good agreement with the results of a fully quantum treatment.

On top of Bohmian trajectories being eligible as a building block in algorithms computing the wave function time evolution in quantum systems or mixed quantum–classical dynamics, they can also be used to numerically obtain time of arrival statistics. The time, at which a measurement device detects a particle, can be measured in the lab, but predicting the statistics, by which it happens, from textbook quantum mechanics is cumbersome. A complete quantum description of the measurement apparatus and its interaction with the particle is required. Without it, the quantum flux into the detector cannot be interpreted as the detection probability rate for wave functions, which violate the current positivity condition. Within Bohmian mechanics it is however straightforward to compute an approximation to the empirical probability rate, provided that the detector is sufficiently simple and its interaction is well localized, so that it can be assumed to not significantly change the Bohmian trajectories before they arrive. Backflow through the detector is a very common phenomenon even for simple wave functions. For such cases, one can argue that the probability current should be replaced by a quantity without an obvious correspondent in textbook quantum mechanics. This so-called truncated current is then proportional to the rate of detection events.

The double slit experiment is discussed in the literature on Bohmian mechanics in essentially only one dimension, and at best uses plane waves when referring to higher-dimensional configuration space. Here, the wave function time evolution, its Bohmian trajectories and time of

arrival statistics were computed for a two-dimensional, localized and normalizable Gaussian describing an electron hitting a screen after passing through a double slit. The insight obtained from the resulting data was, that the trajectory plots in such a case differ from the ones in textbooks, which show a set of disjoint graphs, and also that the interference pattern can no longer remain completely static in time. The latter was recognized as a consequence of wave packet dispersion, which leads to somewhat washed out minima on the screen.

The time of arrival statistics in this double slit scenario were most interesting when being compared to the ones arising from a modified double slit, where one of the slits closes while the wave packet has only halfway passed through, but with the remaining setup unchanged. Bohmian trajectories through each slit could then be followed to plot their first arrival time and position on the screen in order to compare this distribution to what would be expected from a semiclassical geometric optics estimate.

In the near field, both showed a qualitatively similar behavior, but with quantitative agreement heavily depending on the precise manner, in which the slit was being closed. Another finding was that in the closing slit scenario, the first particles could be detected earlier than in the one with the slits constantly open. The mechanism behind this was identified as the cut off wave function relaxing faster than its undisturbed counterpart from the open slit, eventually overtaking the wave packet and on its way accelerating Bohmian particles, which had already passed through the slit before closing. With shorter slit-closing time scales resulting in a sharper cutoff, the effect became more pronounced. Finally, the probability current turned out to not violate the positivity condition in any of the cases, so that the flux into the screen was directly proportional to the probability rate which would have been measured in a hypothetical experimental realization, barring effects resulting from neglecting the effects of the detector onto the particle dynamics.

Accessing the near field experimentally is hard, so the double slit setup analyzed here merely demonstrates the principles at work. Even if the time of arrival statistics from the truncated current were to differ from the unmodified current in the scenario here, it would not have been a good candidate for verifying the additional predictions of Bohmian mechanics with respect to time of arrival statistics. It would be wise to select a different proposal for this purpose, one which has been designed to better suit this task. These proposals are still difficult enough to implement, so that no such experiment could be performed yet. This is part of the reason why experimentally checking the geometric optics arrival time estimate against the Bohmian prediction in this dynamic double slit setup seems unfeasible. The main reason however is, that in Bohmian theory a detector simply cannot discriminate between particles having passed through one or the other slit, because the wave function cut off by the closing slit still deflects the motion of a particle already having passed through prior to that. As has been seen, possibly even into the domain, in which only particles from the open slit would be expected.

As a final remark, the Bohmian interpretation of quantum mechanics and the use of Bohmian vocabulary is not required for most of what has been computed in this thesis. Technically, the whole discussion about using trajectories to facilitate numerical integration of the dynamics could have revolved around flow lines of the quantum flux, as that is essentially what the Bohmian trajectories are. This also applies to the chapter on time of arrival statistics, provided

6. Summary, Concluding Remarks and Future Directions

that one is able to motivate in textbook quantum mechanics why the probability current should be replaced by the truncated current. Since the current positivity condition turned out not to be violated even in the case of closing slits, invoking the Bohmian interpretation would actually not even have been needed there at all. But as most of the concepts discussed in thesis rely on groundwork laid by members of the Bohmian mechanics community, it seems only fair to also use their language.

Appendix

The following pages contain the counterparts of figures 3.3 to 3.5 for the rapidly and the slowly closing lower slit. The resulting dynamics differ from the scenario, in which the slits are constantly open by the wave packets behind the screen somehow twisting after cutting off half of the wave function passing through the lower slit. Remarkably though, no significant backflow is encountered anywhere on the screen, so that the quantum flux into the screen in figures A.3 and A.6 is proportional to the detection probability rate along the screen (barring deviations from neglecting interactions between electron and screen and the quantum nature of the latter). In the same sense, the integral of the flux component into the screen then is proportional to the interference pattern that assembles on the screen when repeating the experiment sufficiently often. Thus, cuts along the yellow lines in these plots are essentially scaled versions of the graphs in figure 3.8.

The rapidly and the slowly closing case differ from each other with respect to certain details, such as the amount, by which the interference patterns become washed out. The differences in the trajectory arrival times of figure 3.10 between these two cases can not that easily be read off from the snapshots of the dynamics here, though. But what can be spotted, particularly well in the rapidly closing case in figure A.1, is the effect of part of the wave packet overtaking the rest as a result of the cutoff. At $t = 0.35$ a.u., there is still a dark vertical shape indicating a relatively large probability density in the rear part of the truncated packet following closely behind a front of ripples. Later at $t = 0.54$ a.u., this pattern has already moved forward to the front of the propagating wave. In contrast, this is no longer visible when looking at the density in the plots after those. Only in the wave function pictures of A.2, this pattern can still be seen, where it leads the way ahead of the wave packets. A similar effect is present in the slowly closing slit counterparts, although much less pronounced.

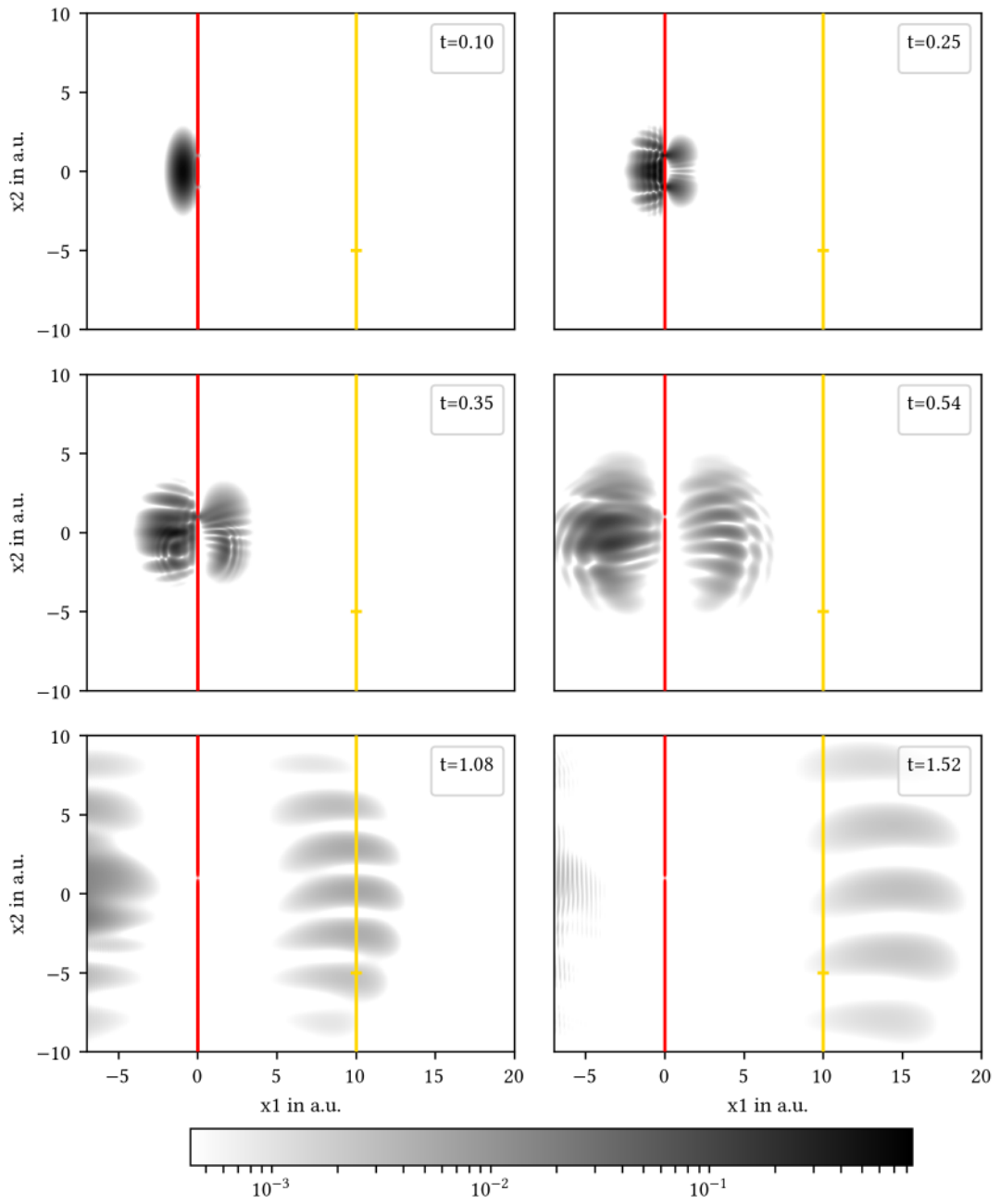


Figure A.1: Same as figure 3.3, i.e. samples from the time evolution of the probability density $|\psi|^2$ but this time for the bottom slit rapidly closing at $t_c = 0.25$ with closing parameter $\tau = 0.01$. Logarithmic scale in the intensity, same scale in all snapshots. The vertical red line is the double slit, the yellow one the screen with its marked position.

6. Summary, Concluding Remarks and Future Directions

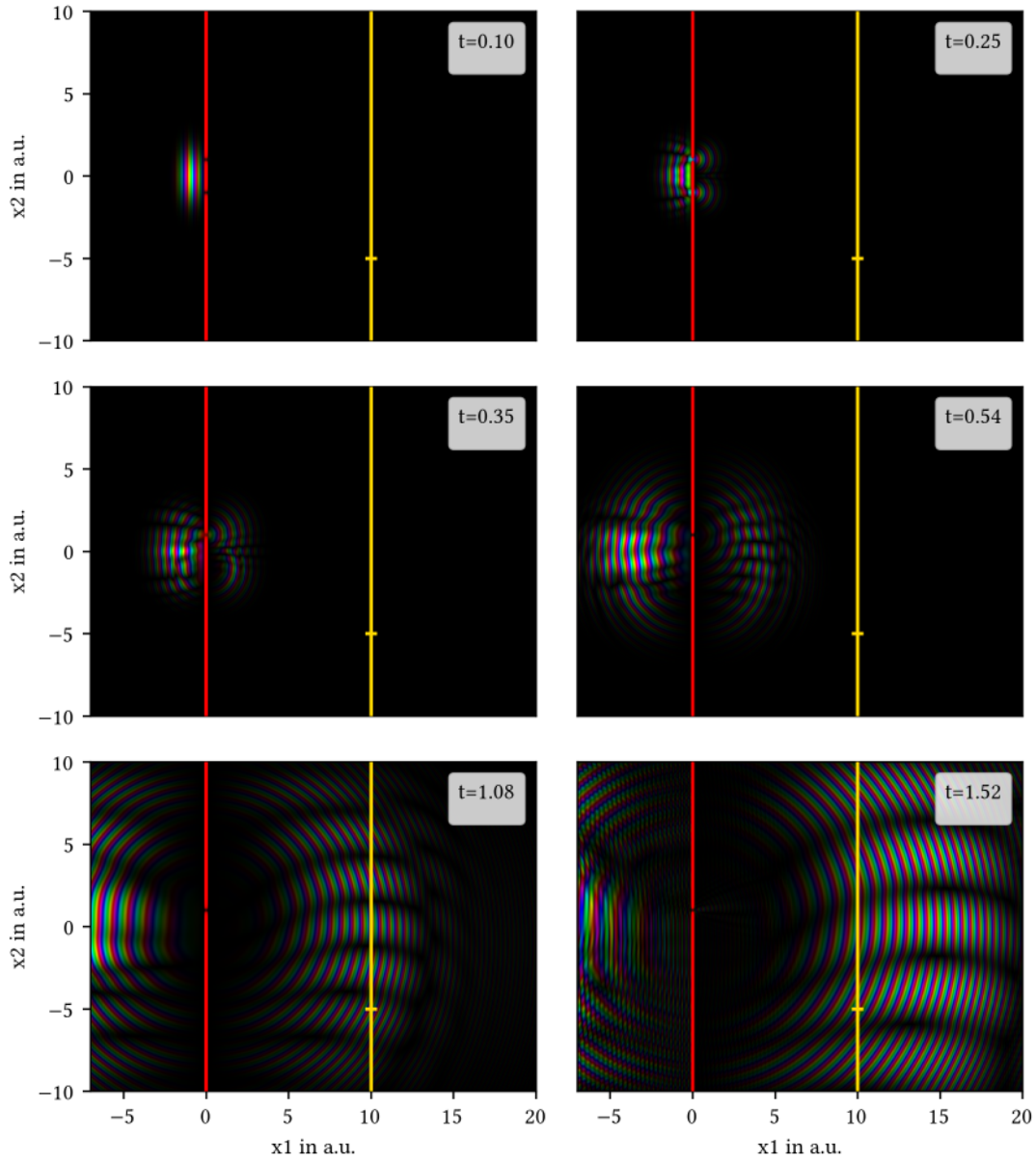


Figure A.2: Same as figure 3.4, i.e. samples from the time evolution of the wave function ψ but this time for the bottom slit rapidly closing at $t_c = 0.25$ with closing parameter $\tau = 0.01$. The color of each pixel represents the phase while the brightness is a measure for the amplitude $|\psi|$ on a linear scale. The amplitude is normalized to its maximum value in each snapshot. The vertical red line is the double slit, the yellow one the screen with its marked position.

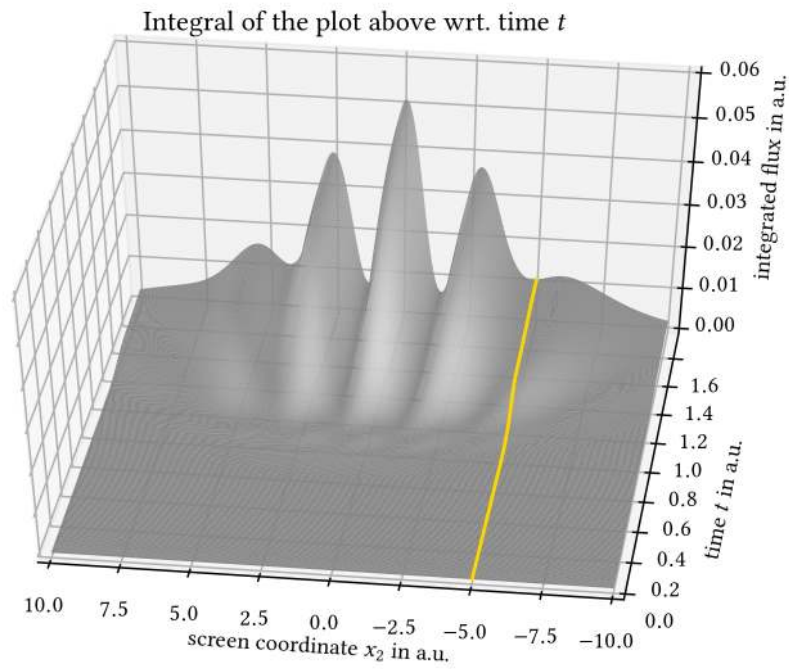
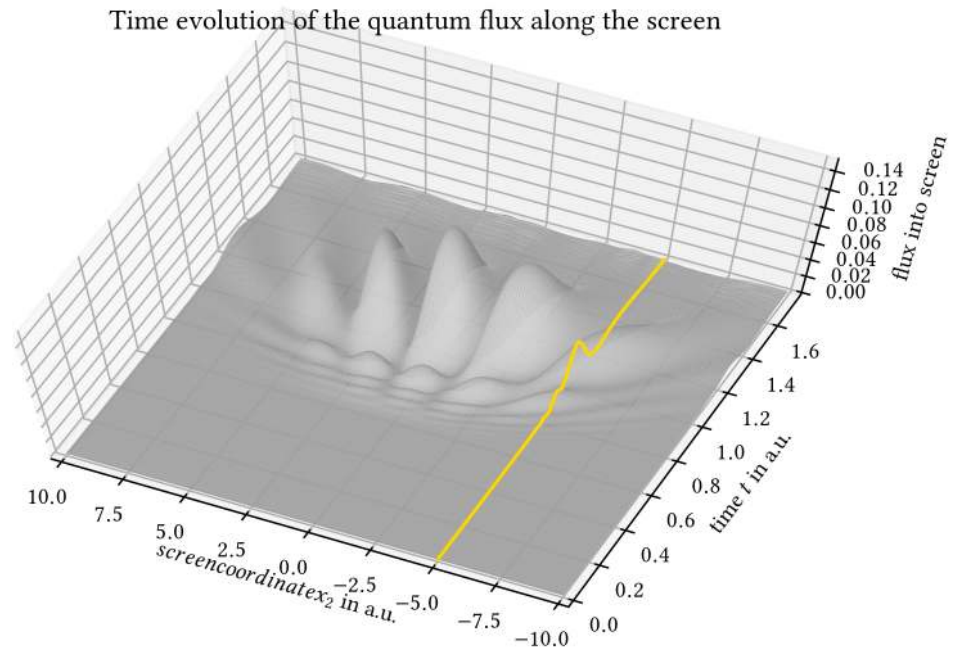


Figure A.3: Same as figure 3.4, but this time for the bottom slit rapidly closing at $t_c = 0.25$ with closing parameter $\tau = 0.01$. Top: the probability current $\mathbf{j}^\psi \cdot \mathbf{e}_1$ into the screen. Bottom: Integrated flux $\int_0^t \mathbf{j}(t')^\psi \cdot \mathbf{e}_1 dt'$, proportional to the interference pattern that would be observed on the screen. The marked position is indicated by the yellow line.

6. Summary, Concluding Remarks and Future Directions

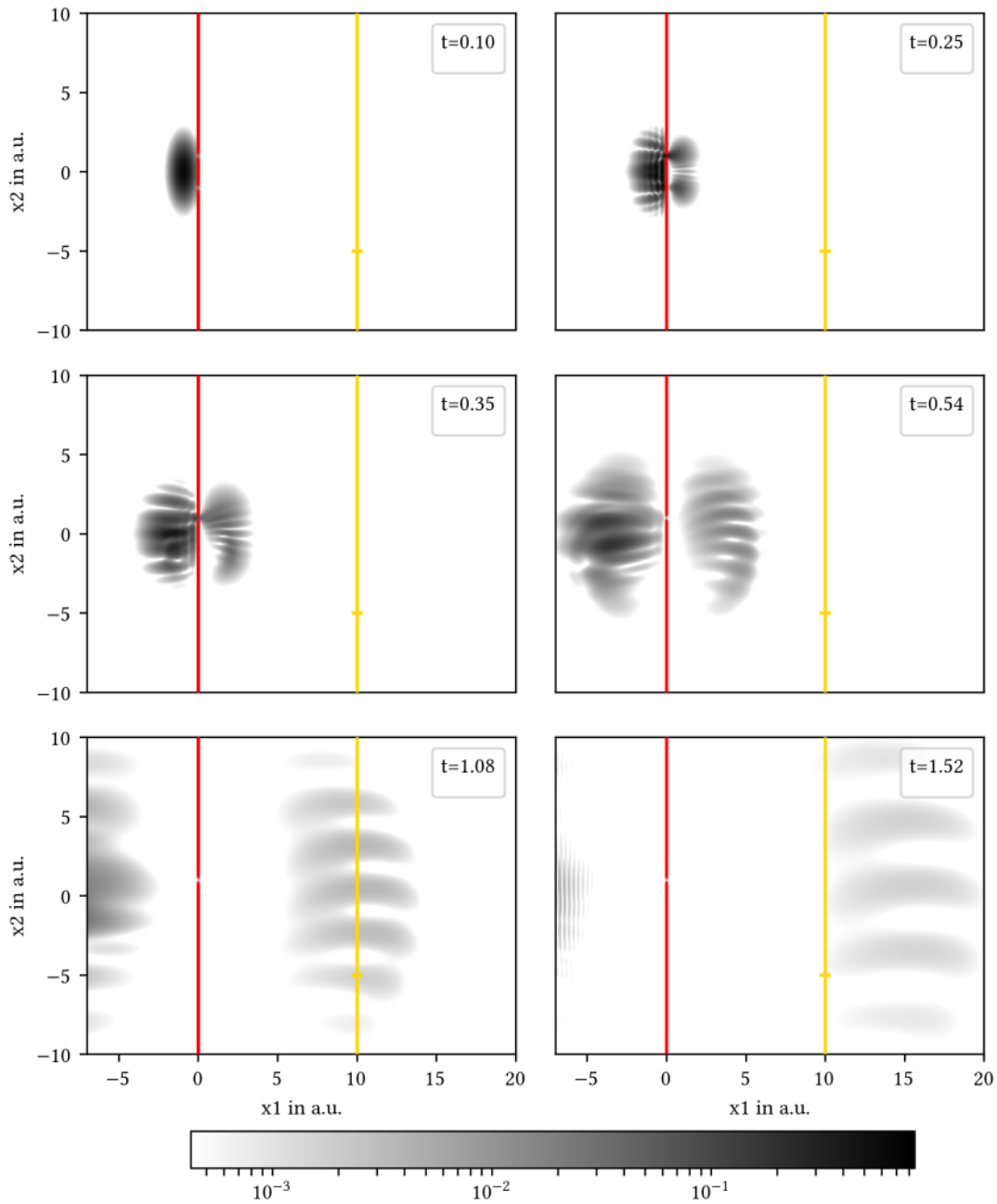


Figure A.4: Same as figure 3.3, i.e. samples from the time evolution of the probability density $|\psi|^2$ but this time for the bottom slit slowly closing at $t_c = 0.25$ with closing parameter $\tau = 0.05$. Logarithmic scale in the intensity, same scale in all snapshots. The vertical red line is the double slit, the yellow one the screen with its marked position.

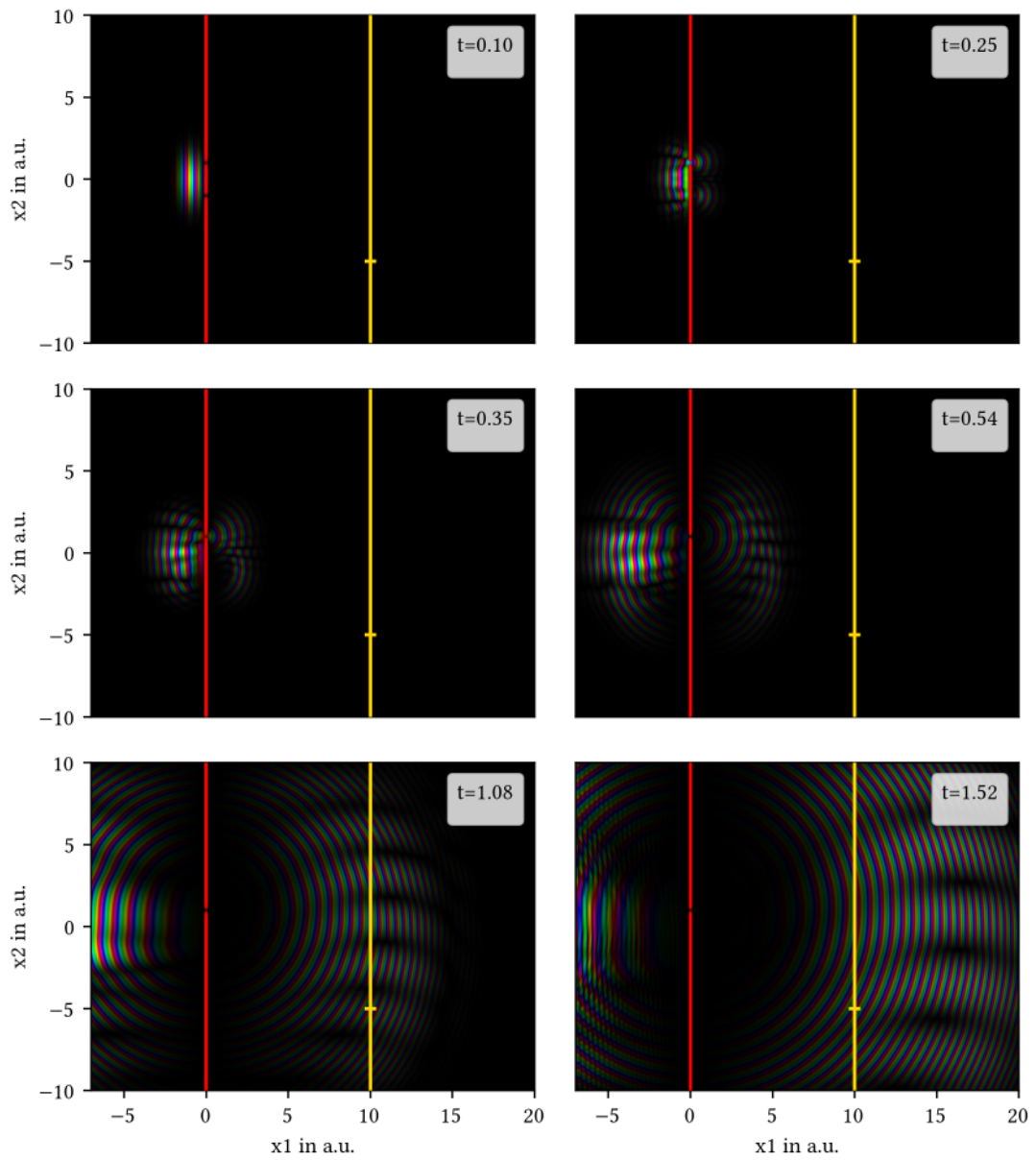


Figure A.5: Same as figure 3.4, i.e. samples from the time evolution of the wave function ψ but this time for the bottom slit slowly closing at $t_c = 0.25$ with closing parameter $\tau = 0.05$. The color of each pixel represents the phase while the brightness is a measure for the amplitude $|\psi|$ on a linear scale. The amplitude is normalized to its maximum value in each snapshot. The vertical red line is the double slit, the yellow one the screen with its marked position.

6. Summary, Concluding Remarks and Future Directions

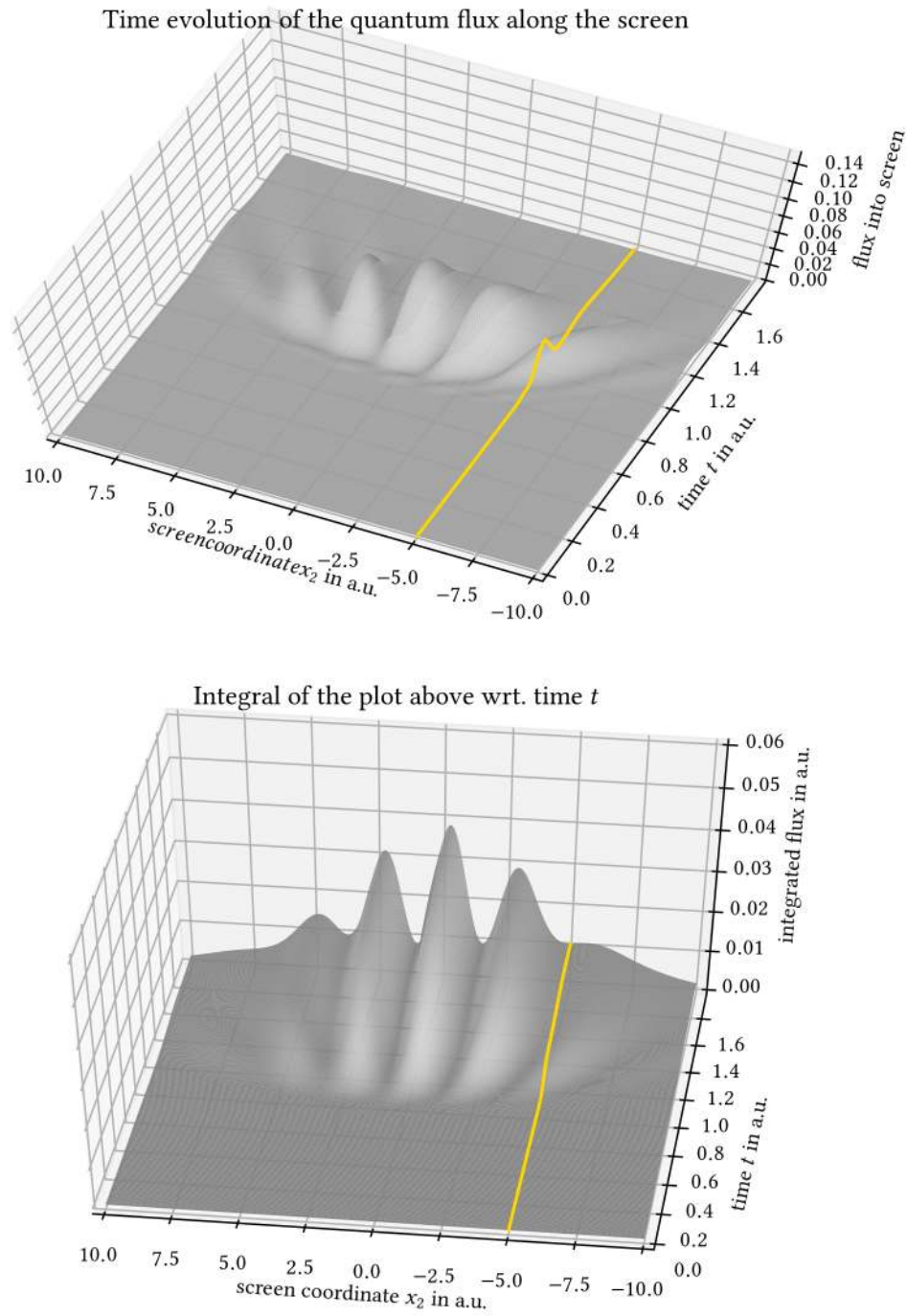


Figure A.6: Same as figure 3.4, but this time for the bottom slit slowly closing at $t_c = 0.25$ with closing parameter $\tau = 0.05$. Top: the probability current $\mathbf{j}^\psi \cdot \mathbf{e}_1$ into the screen. Bottom: Integrated flux $\int_0^t \mathbf{j}(t')^\psi \cdot \mathbf{e}_1 dt'$, proportional to the interference pattern that would be observed on the screen. The marked position is indicated by the yellow line.

Bibliography

- [1] J. Crank and P. Nicolson. A practical method for numerical evaluation of solutions of partial differential equations of the heat-conduction type. *Mathematical Proceedings of the Cambridge Philosophical Society*, 43(1):50–67, 1947.
- [2] A. D. Bandrauk and H. Shen. Improved exponential split operator method for solving the time-dependent schrödinger equation. *Chemical Physics Letters*, 176(5):428 – 432, 1991.
- [3] C.J. Trahan and R.E. Wyatt. *Quantum Dynamics with Trajectories: Introduction to Quantum Hydrodynamics*. Interdisciplinary Applied Mathematics. Springer New York, 2005.
- [4] M. J. W. Hall, D.-A. Deckert, and H. M. Wiseman. Quantum Phenomena Modeled by Interactions between Many Classical Worlds. *Phys. Rev. X*, 4:041013, Oct 2014.
- [5] O. V. Prezhdo and C. Brooksby. Quantum Backreaction through the Bohmian Particle. *Phys. Rev. Lett.*, 86:3215–3219, Apr 2001.
- [6] E. Gindensperger, C. Meier, and J. A. Beswick. Mixing quantum and classical dynamics using Bohmian trajectories. *The Journal of Chemical Physics*, 113(21):9369–9372, 2000.
- [7] B. Poirier. Bohmian mechanics without pilot waves. *Chemical Physics*, 370(1–3):4 – 14, 2010.
- [8] M. V. John. Modified de Broglie-Bohm Approach to Quantum Mechanics. *Foundations of Physics Letters*, 15(329):329–343, 2002.
- [9] I. Burghardt and G. Parlant. On the dynamics of coupled Bohmian and phase-space variables: A new hybrid quantum-classical approach. *The Journal of Chemical Physics*, 120(7):3055–3058, 2004.
- [10] D. S. Sholl and J. C. Tully. A generalized surface hopping method. *The Journal of Chemical Physics*, 109(18):7702–7710, 1998.
- [11] D. Dürr and S. Teufel. *Bohmian Mechanics: The Physics and Mathematics of Quantum Theory*. Springer Verlag Berlin Heidelberg, 2009.
- [12] P. R. Holland. *The Quantum Theory of Motion: An Account of the de Broglie-Bohm Causal Interpretation of Quantum Mechanics*. Cambridge University Press, 1995.
- [13] J. S. Bell. *Speakable and Unspeakable in Quantum Mechanics*. Collected papers on quantum philosophy. Cambridge University Press, 2004.
- [14] K. Berndl, D. Dürr, S. Goldstein, G. Peruzzi, and N. Zanghì. On the global existence of Bohmian mechanics. *Communications in Mathematical Physics*, 173(3):647–673, 1995.
- [15] Hannes Hermann. Finding Stationary States by Interacting Quantum Worlds. Master’s thesis, Ludwig-Maximilians-Universität München, December 2016.

Bibliography

- [16] C. Philippidis, C. Dewdney, and B. J. Hiley. Quantum interference and the quantum potential. *Il Nuovo Cimento B (1971-1996)*, 52(1):15–28, 1979.
- [17] Wikimedia Commons. <https://commons.wikimedia.org/w/index.php?title=File:Doppelspalt.jpg&oldid=145587846>, 2015. Online; accessed 05/05/2017.
- [18] R. P. Feynman and A. R. Hibbs. *Quantum mechanics and path integrals*. International series in pure and applied physics. McGraw-Hill, 1965.
- [19] A. Valentini and H. Westman. Dynamical origin of quantum probabilities. *Proc. Roy. Soc. Lond.*, A461:253–272, 2005.
- [20] C. Jönsson. Elektroneninterferenzen an mehreren künstlich hergestellten Feinspalten. *Zeitschrift für Physik*, 161(4):454–474, 1961.
- [21] P. Chen and H. Kleinert. Deficiencies of Bohm Trajectories in View of Basic Quantum Principles. *Electronic Journal of Theoretical Physics*, 12(35):1–11, 2016.
- [22] E. Deotto and G. C. Ghirardi. Bohmian Mechanics Revisited. *Foundations of Physics*, 28(1):1–30, 1998.
- [23] C. Colijn and E. R. Vrscaj. Spin-dependent Bohm trajectories for hydrogen eigenstates. *Physics Letters A*, 300(4):334 – 340, 2002.
- [24] L. Pauling and E. B. Wilson. *Introduction to Quantum Mechanics: With Applications to Chemistry*. International Student Edition. McGraw-Hill, 1935.
- [25] B. J. Hiley, R. E. Callaghan, and O. Maroney. Quantum trajectories, real, surreal or an approximation to a deeper process?, 2000. arXiv:quant-ph/0010020.
- [26] D. H. Mahler, L. Rozema, K. Fisher, L. Vermeyden, K. J. Resch, H. M. Wiseman, and A. Steinberg. Experimental nonlocal and surreal Bohmian trajectories. *Science Advances*, 2(2), 2016.
- [27] V. Allori, D. Dürr, S. Goldstein, and N. Zanghí. Seven steps towards the classical world. *Journal of Optics B: Quantum and Semiclassical Optics*, 4(4):S482, 2002.
- [28] M. Bauer. On time and space double-slit experiments. *American Journal of Physics*, 82(11):1087–1092, 2014.
- [29] W. Pauli. Die allgemeinen Prinzipien der Wellenmechanik. Number v. 5, pt. 1 in *Handbuch der Physik*. Springer, 1958.
- [30] N. Vona, G. Hinrichs, and D. Dürr. What does one measure when one measures the arrival time of a quantum particle? *Phys. Rev. Lett.*, 111:220404, Nov 2013.
- [31] N. Vona. *On Time in Quantum Mechanics*. PhD thesis, Ludwig-Maximilians-Universität München, 2014. <https://arxiv.org/abs/1403.2496>.
- [32] N. Vona and D. Dürr. The Role of the Probability Current for Time Measurements. In P. Blanchard and J. Fröhlich, editors, *The Message of Quantum Science: Attempts Towards a Synthesis*, pages 95–112. Springer Berlin Heidelberg, 2015.
- [33] R. Tumulka. Distribution of the Time at Which an Ideal Detector Clicks. Jan. 2016. <https://arxiv.org/abs/1601.03715>.

- [34] G. Grübl and K. Rheinberger. Time of arrival from Bohmian flow. *Journal of Physics A: Mathematical and General*, 35(12):2907, 2002.
- [35] M. Daumer, D. Dürr, S. Goldstein, and N. Zanghi. On the Quantum Probability Flux Through Surfaces. *Journal of Statistical Physics*, 88(3):967–977, 1997.
- [36] H. Weinfurter. private communications.
- [37] E. Hairer and G. Wanner. <http://www.unige.ch/~hairer/prog/nonstiff/dop853.f>, 2009. Online; accessed 05/05/2017.
- [38] E. Hairer, S. P. Nørsett, and G. Wanner. *Solving Ordinary Differential Equations I: Nonstiff Problems*. Springer Series in Computational Mathematics. Springer-Verlag New York, Inc., 2nd edition, 1993.
- [39] P. A. M. Dirac. Quantum Mechanics of Many-Electron Systems. *Proceedings of the Royal Society of London. Series A, Containing Papers of a Mathematical and Physical Character*, 123(792):714–733, 1929.
- [40] S. Goldstein, R. Tumulka, and N. Zanghi. In P. K. Chattaraj, editor, *Quantum Trajectories, Atom, Molecules and Clusters: Structure, Reactivity and Dynamics*, chapter Bohmian Trajectories as the Foundation of Quantum Mechanics, pages 1–15. CRC Press, 2010.
- [41] E. Madelung. Quantentheorie in hydrodynamischer Form. *Zeitschrift für Physik*, 40(3):322–326, Mar 1927.
- [42] D. Babyuk and R. E. Wyatt. Multidimensional reactive scattering with quantum trajectories: Dynamics with 50–200 vibrational modes. *The Journal of Chemical Physics*, 124(21):214109, 2006.
- [43] D.-A. Deckert, D. Dürr, and P. Pickl. In P. K. Chattaraj, editor, *Quantum Trajectories, Atom, Molecules and Clusters: Structure, Reactivity and Dynamics*, chapter Bohmian Grids and the Numerics of Schrödinger Evolutions, pages 345–360. CRC Press, 2010.
- [44] D.-A. Deckert, D. Dürr, and P. Pickl. Quantum Dynamics with Bohmian Trajectories. *The Journal of Physical Chemistry A*, 111(41):10325–10330, October 2007. Source code available at <https://arxiv.org/pdf/quant-ph/0701190v2.pdf>.
- [45] J. Schiff and B. Poirier. Communication: Quantum mechanics without wavefunctions. *The Journal of Chemical Physics*, 136(3):031102, 2012.
- [46] C. T. Sebens. Quantum Mechanics as Classical Physics. *Philosophy of Science*, 82(2):266–291, 2015.
- [47] J. B. Maddox and E. R. Bittner. Estimating Bohm’s quantum force using Bayesian statistics. *The Journal of Chemical Physics*, 119(13):6465–6474, 2003.
- [48] S. Garashchuk and V. A. Rassolov. Semiclassical dynamics with quantum trajectories: Formulation and comparison with the semiclassical initial value representation propagator. *The Journal of Chemical Physics*, 118(6):2482–2490, 2003.
- [49] H. Herrmann. private communications.
- [50] S. Goldstein and W. Struyve. On quantum potential dynamics. *Journal of Physics A: Mathematical and Theoretical*, 48(2):025303, 2015.

Bibliography

- [51] E. Schrödinger. Der stetige Übergang von der Mikro- zur Makromechanik. *Naturwiss.*, 14:664–666, 1926.
- [52] D. Babyuk and R. E. Wyatt. Coping with the node problem in quantum hydrodynamics: The covering function method. *The Journal of Chemical Physics*, 121(19):9230–9238, 2004.
- [53] B. Poirier. Reconciling semiclassical and Bohmian mechanics. I. Stationary states. *The Journal of Chemical Physics*, 121(10):4501–4515, 2004.
- [54] D. Babyuk and R. E. Wyatt. Hybrid adaptive grid algorithm for wave packet propagation. *Chemical Physics Letters*, 387(4):227 – 232, 2004.
- [55] A. Baust, E. Hoffmann, M. Haeberlein, M. J. Schwarz, P. Eder, J. Goetz, F. Wulschner, E. Xie, L. Zhong, F. Quijandría, D. Zueco, J.-J. García Ripoll, L. García-Álvarez, G. Romero, E. Solano, K. G. Fedorov, E. P. Menzel, F. Deppe, A. Marx, and R. Gross. Ultrastrong coupling in two-resonator circuit QED. *Phys. Rev. B*, 93:214501, Jun 2016.
- [56] Y.-Y. Zhang, Q.-H. Chen, and S.-Y. Zhu. Vacuum Rabi Splitting and Dynamics of the Jaynes–Cummings Model for Arbitrary Coupling. *Chinese Physics Letters*, 30(11):114203, 2013.
- [57] W. Struyve. Semi-classical approximations based on Bohmian mechanics. Jul. 2015. <https://arxiv.org/abs/1507.04771>.
- [58] J. C. Tully. Mixed quantum-classical dynamics. *Faraday Discuss.*, 110:407–419, 1998.
- [59] P. Ehrenfest. Bemerkung über die angenäherte Gültigkeit der klassischen Mechanik innerhalb der Quantenmechanik. *Zeitschrift für Physik*, 45(7):455–457, Jul 1927.
- [60] J. C. Tully. Nonadiabatic dynamics. In *Modern Methods for Multidimensional Dynamics Computations in Chemistry*, pages 34–72. WORLD SCIENTIFIC, 2011.
- [61] L. L. Salcedo. Comment on “Quantum Backreaction through the Bohmian Particle”. *Phys. Rev. Lett.*, 90:118901, Mar 2003.
- [62] C. Meier and J. A. Beswick. Hybrid Quantum/Classical Dynamics Using Bohmian Trajectories. In David A. Micha and Irene Burghardt, editors, *Quantum Dynamics of Complex Molecular Systems*, pages 369–390. Springer Berlin Heidelberg, Berlin, Heidelberg, 2007.
- [63] G. Pöschl and E. Teller. Bemerkungen zur Quantenmechanik des anharmonischen Oszillators. *Zeitschrift für Physik*, 83(3):143–151, Mar 1933.
- [64] E. Gindensperger, C. Meier, and J. A. Beswick. Quantum-classical dynamics including continuum states using quantum trajectories. *The Journal of Chemical Physics*, 116(1):8–13, 2002.
- [65] E. Gindensperger, C. Meier, J. A. Beswick, and M.-C. Heitz. Quantum-classical description of rotational diffractive scattering using bohmian trajectories: Comparison with full quantum wave packet results. *The Journal of Chemical Physics*, 116(23):10051–10059, 2002.
- [66] C. Meier. Mixed Quantum-Classical Treatment of Vibrational Decoherence. *Phys. Rev. Lett.*, 93:173003, Oct 2004.

- [67] E. T. Jaynes and F. W. Cummings. Comparison of quantum and semiclassical radiation theories with application to the beam maser. *Proceedings of the IEEE*, 51(1):89–109, Jan 1963.
- [68] G. Rempe, H. Walther, and N. Klein. Observation of quantum collapse and revival in a one-atom maser. *Phys. Rev. Lett.*, 58:353–356, Jan 1987.
- [69] M. O. Scully and M. S. Zubairy. *Quantum Optics*. Cambridge University Press, 1997.
- [70] C. Cohen-Tannoudji, B. Diu, F. Laloë, and J. Streubel. *Quantenmechanik*. Number Bd. 2 in *Quantenmechanik*. de Gruyter, 2010.
- [71] R. J. Glauber. Coherent and incoherent states of the radiation field. *Phys. Rev.*, 131:2766–2788, 1963.
- [72] B. W. Shore and P. L. Knight. Topical review: the Jaynes-Cummings model. *Journal of Modern Optics*, 40(7):1195–1238, 1993.
- [73] C. Colijn and E. R. Vrscaj. Spin-dependent Bohm trajectories associated with an electronic transition in hydrogen. *Journal of Physics A: Mathematical and General*, 36(16):4689, 2003.
- [74] S. Haroche and J. M. Raimond. *Exploring the Quantum: Atoms, Cavities, and Photons*. Oxford Graduate Texts. Oxford University Press, 2006.

Ich versichere, dass ich die vorliegende Arbeit mit dem Titel

Making Use of Quantum Trajectories for Numerical Purposes

selbständig verfasst habe, und dass ich keine anderen Quellen und Hilfsmittel als die angegebenen benutzt habe und dass die Stellen der Arbeit, die anderen Werken – auch elektronischen Medien – dem Wortlaut oder Sinn nach entnommen wurden, auf jeden Fall unter Angabe der Quelle als Entlehnung kenntlich gemacht worden sind.

Datum, Ort

Leopold Kellers